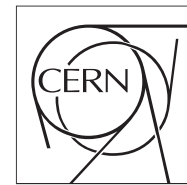




The Compact Muon Solenoid Experiment  
**CMS Note**

Mailing address: CMS CERN, CH-1211 GENEVA 23, Switzerland



2017/05/10

## Search for tHq production in multilepton final states at 13 TeV

Jose Monroy<sup>1</sup>, Pallabi Das<sup>2</sup>, Benjamin Stieger<sup>1</sup>, Sandhya Jain<sup>2</sup>, Ken Bloom<sup>1</sup>, and Kajari Mazumdar<sup>2</sup>

<sup>1</sup> University of Nebraska-Lincoln

<sup>2</sup> Tata Institute for Fundamental Research, Mumbai

### Abstract

This note presents a search for the associated production of a Higgs boson with a single top quark in multilepton (same-sign dilepton or three leptons) final states, targeting Higgs decay modes to WW, ZZ, and  $\tau\tau$ . The full 2016 LHC dataset at 13 TeV is used. Limits are evaluated as a function of the Higgs couplings to vector bosons and top quarks.



## Contents

|     |  |    |
|-----|--|----|
| 1   | Introduction . . . . .                                       | 2  |
| 2   | Data and MC Samples . . . . .                                | 3  |
| 2.1 | Full 2016 dataset and MC samples . . . . .                   | 3  |
| 2.2 | Triggers . . . . .   | 3  |
| 3   | Object identification and event selection . . . . .          | 8  |
| 3.1 | Jets and b tagging . . . . .                                 | 8  |
| 3.2 | Lepton selection . . . . .                                   | 8  |
| 3.3 | Lepton selection efficiency . . . . .                        | 10 |
| 3.4 | Event selection . . . . .                                    | 10 |
| 4   | Background predictions . . . . .                             | 12 |
| 5   | Signal discrimination . . . . .                              | 17 |
| 5.1 | Classifiers response . . . . .                               | 18 |
| 6   | Additional discriminating variables . . . . .                | 18 |
| 7   | Signal extraction . . . . .                                  | 27 |
| 7.1 | Signal extraction procedure . . . . .                        | 27 |
| 7.2 | Signal model . . . . .                                       | 27 |
| 7.3 | Binning and selection optimization . . . . .                 | 29 |
| 7.4 | Other binning strategies . . . . .                           | 31 |
| 8   | Systematics . . . . .  | 34 |
| 9   | Results . . . . .  | 38 |
| A   | Control region plots . . . . .                               | 51 |
| A.1 | Same-sign dilepton control plots . . . . .                   | 51 |
| A.2 | Three lepton control plots . . . . .                         | 51 |
| A.3 | Opposite-sign $e\mu$ control region . . . . .                | 51 |
| B   | BDT output change with varying $\kappa_V/\kappa_t$ . . . . . | 58 |
| C   | Further channel categorization . . . . .                     | 59 |
| D   | Cross section times BR scalings . . . . .                    | 60 |
| E   | $tHq$ - $t\bar{t}H$ overlap . . . . .                        | 67 |

## 1 Introduction

This note describes a search for the associated production of a Higgs boson and a single top quark, events with two same-sign leptons or three leptons, targeting Higgs decay modes to  $WW$ ,  $ZZ$ , and  $\tau\tau$ . The analysis uses the 13 TeV dataset produced in 2016, corresponding to an integrated luminosity of  $35.9 \text{ fb}^{-1}$ . It is based on and expands previous analyses at 8 TeV [1, 2] and searches for associated production of  $t\bar{t}$  and Higgs in the same channels [3], and complements searches in other decay channels targeting  $H \rightarrow b\bar{b}$  [4].

The production cross section of the single top plus Higgs boson ( $tHq$ ) process is driven by a destructive interference of two main diagrams (see Fig. 1), where the Higgs couples to either the  $W$  boson or the top quark. Any deviation from the standard model (SM) in the Higgs coupling structure could therefore lead to a large enhancement of the cross section, making the analysis sensitive to such deviations. A second process, where the Higgs and top quark are accompanied by a  $W$  boson ( $tHW$ ) has similar behavior, albeit with a weaker interference pattern.

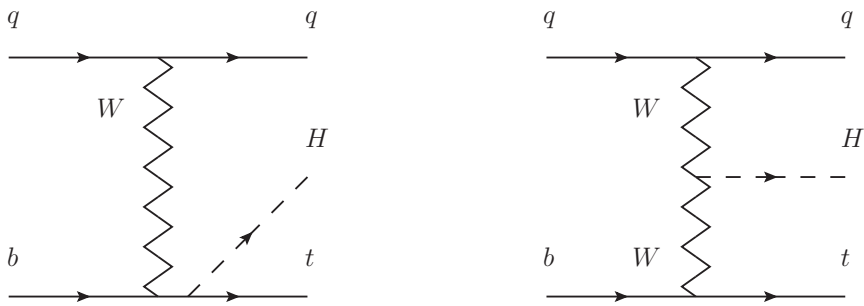


Figure 1: The two leading-order diagrams of  $tHq$  production.

The analysis selects events with either a pair of leptons of equal charge, or with three leptons, as well as  $b$  tagged jets. The  $tHq$  signal contribution is then determined in a fit of the observed data to two multivariate classifier outputs, each trained to discriminate against one of the two dominant backgrounds of events with non-prompt leptons from  $t\bar{t}$  and of associated production of  $t\bar{t}$  and vector bosons ( $t\bar{t}W$ ,  $t\bar{t}Z$ ). The fit result is then used to set an upper limit on the combined  $tHq$  and  $tHW$  production cross section, as a function of the relative coupling strengths of Higgs and top quark and Higgs and  $W$  boson, respectively.

### Related presentations in CMS meetings

- Top Higgs Forum, Hamed Bakhshiansohi, Sep. 13<sup>rd</sup>, 2016 [agenda](#)
- HWW Meeting, Jose Monroy, Oct. 19<sup>th</sup>, 2016 [agenda](#)
- HWW Meeting, Jose Monroy, Dec. 14<sup>th</sup>, 2016 [agenda](#)
- HWW Meeting, Pallabi Das, Dec. 16<sup>th</sup>, 2016 [agenda](#)
- ttH Leptonic Meeting, Pallabi Das, Jan. 19<sup>th</sup>, 2017 [agenda](#)
- Pre-approval, Jose Monroy, Feb. 7<sup>th</sup>, 2017 [agenda](#)

## 2 Data and MC Samples

### 2.1 Full 2016 dataset and MC samples

The data considered in this analysis were collected by the CMS experiment during 2016 and correspond to a total integrated luminosity of  $35.9 \text{ fb}^{-1}$ . The data used were collected only in periods when the CMS magnet was on. We use the 23 Sep 2016 (Run B to G) and PromptReco (Run H) versions of the datasets.

The MC samples used in this analysis correspond to the RunIISummer16MiniAODv2 campaign produced with CMSSW 80X.

The two signal samples (for tHq and tHW) were produced with MG5\_aMC@NLO (version 5.222), in leading-order order mode, and are normalized to next-to-leading-order cross sections, see Tab. 1. Each sample is generated with a set of event weights corresponding to different values of  $\kappa_t$  and  $\kappa_V$  couplings, see Tab. 2.

| Sample  | $\sigma [\text{pb}]$ | BF    |
|---|----------------------|-------|
| /THQ_Hincl_13TeV-madgraph-pythia8_TuneCUETP8M1/ | 0.7927               | 0.324 |
| /THW_Hincl_13TeV-madgraph-pythia8_TuneCUETP8M1/ | 0.1472               | 1.0   |

Table 1: Signal samples and their cross section and branching fraction used in this analysis. See Ref. [5] for more details.

Different MC generators were used to generate the background processes. The dominant sources ( $t\bar{t}$ ,  $t\bar{t}W$ ,  $t\bar{t}Z$ ,  $t\bar{t}H$ ) were produced using AMC@NLO interfaced to PYTHIA 8, and are scaled to NLO cross sections. Other processes are simulated using POWHEG interfaced to PYTHIA, or bare PYTHIA. See table 3 for more details. See also AN-2016-211 (Ref. [3]) for more details.

### 2.2 Triggers

We consider online-reconstructed events triggered by one, two, or three leptons. Single-lepton triggers are included to boost the acceptance of events where the  $p_T$  of the sub-leading lepton falls below the threshold of the double-lepton triggers. Additionally, by including double-lepton triggers in the  $\geq 3$  lepton category, as well as single-lepton triggers in all categories, we increase the efficiency, considering the logical “or” of the trigger decisions of all the individual triggers in a given category. Tab. 5 shows the lowest-threshold non-prescaled triggers present in the High-Level Trigger (HLT) menus for both Monte-Carlo and data in 2016.

#### 2.2.1 Trigger efficiency scale factors

The efficiency of events to pass the trigger is measured in simulation (trivially using generator information) and in the data (using event collected by an uncorrelated MET trigger). Small differences between the data and MC efficiencies are corrected by applying scale factors as shown in Tab. 6. The exact procedure and control plots are documented in Refs [3] (for the ICHEP dataset), and in [6] for the current analysis.

|            |            | tHq            |                    | tHW            |                    |                    |
|------------|------------|----------------|--------------------|----------------|--------------------|--------------------|
| $\kappa_V$ | $\kappa_t$ | sum of weights | cross section [pb] | sum of weights | cross section [pb] | LHE weights        |
| 1.0        | -3.0       | 35.700022      | 2.991              | 11.030445      | 0.6409             | LHEweight_wgt[446] |
| 1.0        | -2.0       | 20.124298      | 1.706              | 5.967205       | 0.3458             | LHEweight_wgt[447] |
| 1.0        | -1.5       | 14.043198      | 1.205              | 4.029093       | 0.2353             | LHEweight_wgt[448] |
| 1.0        | -1.25      | 11.429338      | 0.9869             | 3.208415       | 0.1876             | LHEweight_wgt[449] |
| 1.0        | -1.0       |                | 0.7927             |                | 0.1472             |                    |
| 1.0        | -0.75      | 7.054998       | 0.6212             | 1.863811       | 0.1102             | LHEweight_wgt[450] |
| 1.0        | -0.5       | 5.294518       | 0.4723             | 1.339886       | 0.07979            | LHEweight_wgt[451] |
| 1.0        | -0.25      | 3.818499       | 0.3505             | 0.914880       | 0.05518            | LHEweight_wgt[452] |
| 1.0        | 0.0        | 2.627360       | 0.2482             | 0.588902       | 0.03881            | LHEweight_wgt[453] |
| 1.0        | 0.25       | 1.719841       | 0.1694             | 0.361621       | 0.02226            | LHEweight_wgt[454] |
| 1.0        | 0.5        | 1.097202       | 0.1133             | 0.233368       | 0.01444            | LHEweight_wgt[455] |
| 1.0        | 0.75       | 0.759024       | 0.08059            | 0.204034       | 0.01222            | LHEweight_wgt[456] |
| 1.0        | 1.0        | 0.705305       | 0.07096            | 0.273617       | 0.01561            | LHEweight_wgt[457] |
| 1.0        | 1.25       | 0.936047       | 0.0839             | 0.442119       | 0.02481            | LHEweight_wgt[458] |
| 1.0        | 1.5        | 1.451249       | 0.1199             | 0.709538       | 0.03935            | LHEweight_wgt[459] |
| 1.0        | 2.0        | 3.335034       | 0.2602             | 1.541132       | 0.08605            | LHEweight_wgt[460] |
| 1.0        | 3.0        | 10.516125      | 0.8210             | 4.391335       | 0.2465             | LHEweight_wgt[461] |
| 1.5        | -3.0       | 45.281492      | 3.845              | 13.426212      | 0.7825             | LHEweight_wgt[462] |
| 1.5        | -2.0       | 27.606715      | 2.371              | 7.809713       | 0.4574             | LHEweight_wgt[463] |
| 1.5        | -1.5       | 20.476088      | 1.784              | 5.594971       | 0.3290             | LHEweight_wgt[464] |
| 1.5        | -1.25      | 17.337465      | 1.518              | 4.635978       | 0.2749             | LHEweight_wgt[465] |
| 1.5        | -1.0       | 14.483302      | 1.287              | 3.775902       | 0.2244             | LHEweight_wgt[466] |
| 1.5        | -0.75      | 11.913599      | 1.067              | 3.014744       | 0.1799             | LHEweight_wgt[467] |
| 1.5        | -0.5       | 9.628357       | 0.874              | 2.352505       | 0.1410             | LHEweight_wgt[468] |
| 1.5        | -0.25      | 7.627574       | 0.702              | 1.789184       | 0.1081             | LHEweight_wgt[469] |
| 1.5        | 0.0        | 5.911882       | 0.5577             | 1.324946       | 0.08056            | LHEweight_wgt[470] |
| 1.5        | 0.25       | 4.479390       | 0.4365             | 0.959295       | 0.05893            | LHEweight_wgt[471] |
| 1.5        | 0.5        | 3.331988       | 0.3343             | 0.692727       | 0.04277            | LHEweight_wgt[472] |
| 1.5        | 0.75       | 2.469046       | 0.2558             | 0.525078       | 0.03263            | LHEweight_wgt[473] |
| 1.5        | 1.0        | 1.890565       | 0.2003             | 0.456347       | 0.02768            | LHEweight_wgt[474] |
| 1.5        | 1.25       | 1.596544       | 0.1689             | 0.486534       | 0.02864            | LHEweight.wgt[475] |
| 1.5        | 1.5        | 1.586983       | 0.1594             | 0.615638       | 0.03509            | LHEweight.wgt[476] |
| 1.5        | 2.0        | 2.421241       | 0.2105             | 1.170602       | 0.06515            | LHEweight.wgt[477] |
| 1.5        | 3.0        | 7.503280       | 0.5889             | 3.467546       | 0.1930             | LHEweight.wgt[478] |
| 0.5        | -3.0       | 27.432685      | 2.260              | 8.929074       | 0.5136             | LHEweight.wgt[479] |
| 0.5        | -2.0       | 13.956013      | 1.160              | 4.419093       | 0.2547             | LHEweight.wgt[480] |
| 0.5        | -1.5       | 8.924438       | 0.7478             | 2.757611       | 0.1591             | LHEweight.wgt[481] |
| 0.5        | -1.25      | 6.835341       | 0.5726             | 2.075247       | 0.1204             | LHEweight.wgt[482] |
| 0.5        | -1.0       | 5.030704       | 0.4273             | 1.491801       | 0.08696            | LHEweight.wgt[483] |
| 0.5        | -0.75      | 3.510528       | 0.2999             | 1.007273       | 0.05885            | LHEweight.wgt[484] |
| 0.5        | -0.5       | 2.274811       | 0.1982             | 0.621663       | 0.03658            | LHEweight.wgt[485] |
| 0.5        | -0.25      | 1.323555       | 0.1189             | 0.334972       | 0.01996            | LHEweight.wgt[486] |
| 0.5        | 0.0        | 0.656969       | 0.06223            | 0.147253       | 0.008986           | LHEweight.wgt[487] |
| 0.5        | 0.25       | 0.274423       | 0.02830            | 0.058342       | 0.003608           | LHEweight.wgt[488] |
| 0.5        | 0.5        | 0.176548       | 0.01778            | 0.068404       | 0.003902           | LHEweight.wgt[489] |
| 0.5        | 0.75       | 0.363132       | 0.03008            | 0.177385       | 0.009854           | LHEweight.wgt[490] |
| 0.5        | 1.0        | 0.834177       | 0.06550            | 0.385283       | 0.02145            | LHEweight.wgt[491] |
| 0.5        | 1.25       | 1.589682       | 0.1241             | 0.692099       | 0.03848            | LHEweight.wgt[492] |
| 0.5        | 1.5        | 2.629647       | 0.2047             | 1.097834       | 0.06136            | LHEweight.wgt[493] |
| 0.5        | 2.0        | 5.562958       | 0.4358             | 2.206057       | 0.1246             | LHEweight.wgt[494] |
| 0.5        | 3.0        | 14.843102      | 1.177              | 5.609519       | 0.3172             | LHEweight.wgt[495] |

Table 2:  $\kappa_V$  and  $\kappa_t$  combinations generated for the two signal samples and their NLO cross sections. The tHq cross section is multiplied by the branching fraction of the enforced leptonic decay of the top quark (0.324). See also Ref. [5].

| Sample   | $\sigma$ [pb] |
|--|---------------|
| TTWJetsToLNu_TuneCUETP8M1_13TeV-amcatnloFXFX-madspin-pythia8           | 0.2043        |
| TTZToLLNuNu_M-10_TuneCUETP8M1_13TeV-amcatnlo-pythia8                   | 0.2529        |
| ttHJetToNonbb_M125_13TeV_amcatnloFXFX_madspin_pythia8_mWCutfix         | 0.2151        |
| /store/cmst3/group/susy/gpetrucc/13TeV/u/TTLL_m1to10_LO_NoMS_for76X/   | 0.0283        |
| WGToLNUG_TuneCUETP8M1_13TeV-madgraphMLM-pythia8                        | 585.8         |
| ZGTo2LG_TuneCUETP8M1_13TeV-amcatnloFXFX-pythia8                        | 131.3         |
| TGJets_TuneCUETP8M1_13TeV_amcatnlo_madspin_pythia8                     | 2.967         |
| TTGJets_TuneCUETP8M1_13TeV-amcatnloFXFX-madspin-pythia8                | 3.697         |
| WpWpJJ_EWK-QCD_TuneCUETP8M1_13TeV-madgraph-pythia8                     | 0.03711       |
| ZZZ_TuneCUETP8M1_13TeV-amcatnlo-pythia8                                | 0.01398       |
| WWZ_TuneCUETP8M1_13TeV-amcatnlo-pythia8                                | 0.1651        |
| WZZ_TuneCUETP8M1_13TeV-amcatnlo-pythia8                                | 0.05565       |
| WW_DoubleScattering_13TeV-pythia8                                      | 1.64          |
| tZq_ll_4f_13TeV-amcatnlo-pythia8_TuneCUETP8M1                          | 0.0758        |
| ST_tWll_5f_LO_13TeV-MadGraph-pythia8                                   | 0.01123       |
| TTTT_TuneCUETP8M1_13TeV-amcatnlo-pythia8                               | 0.009103      |
| WZTo3LNu_TuneCUETP8M1_13TeV-powheg-pythia8                             | 4.4296        |
| ZZTo4L_13TeV_powheg_pythia8  | 1.256         |
| TTJets_SingleLeptFromTbar_TuneCUETP8M1_13TeV-madgraphMLM-pythia8       | 182.1754      |
| TTJets_SingleLeptFromT_TuneCUETP8M1_13TeV-madgraphMLM-pythia8          | 182.1754      |
| TTJets_DiLept_TuneCUETP8M1_13TeV-madgraphMLM-pythia8                   | 87.3          |
| DYJetsToLL_M-10to50_TuneCUETP8M1_13TeV-amcatnloFXFX-pythia8            | 18610         |
| DYJetsToLL_M-50_TuneCUETP8M1_13TeV-madgraphMLM-pythia8                 | 6024          |
| WJetsToLNu_TuneCUETP8M1_13TeV-amcatnloFXFX-pythia8                     | 61526.7       |
| ST_tW_top_5f_inclusiveDecays_13TeV-powheg-pythia8_TuneCUETP8M1         | 35.6          |
| ST_tW_antitop_5f_inclusiveDecays_13TeV-powheg-pythia8_TuneCUETP8M1     | 35.6          |
| ST_t-channel_4f_leptonDecays_13TeV-amcatnlo-pythia8_TuneCUETP8M1       | 70.3144       |
| ST_t-channel_antitop_4f_leptonDecays_13TeV-powheg-pythia8_TuneCUETP8M1 | 26.2278       |
| ST_s-channel_4f_leptonDecays_13TeV-amcatnlo-pythia8_TuneCUETP8M1       | 3.68064       |
| WWTo2L2Nu_13TeV-powheg   | 10.481        |

Table 3: List of background samples used in this analysis (CMSSW 80X). In the first section of the table are listed the samples of the processes for which we use the simulation to extract the final yields and shapes, in the second section the samples of the processes we will estimate from data. The MC simulation is used to design the data driven methods and derive the associated systematics.

| Sample                    | $\sigma$ [pb] |
|---------------------------|---------------|
| ttWJets_13TeV_madgraphMLM | 0.6105        |
| ttZJets_13TeV_madgraphMLM | 0.5297/0.692  |

Table 4: Leading-order  $t\bar{t}W$  and  $t\bar{t}Z$  samples used in the signal BDT training.

---

Same-sign dilepton (==2 muons)

```

HLT_Mu17_TrkIsoVVL_Mu8_TrkIsoVVL_DZ_v*
HLT_Mu17_TrkIsoVVL_TkMu8_TrkIsoVVL_DZ_v*
HLT_IsoMu22_v*
HLT_IsoTkMu22_v*
HLT_IsoMu22_eta2p1_v*
HLT_IsoTkMu22_eta2p1_v*
HLT_IsoMu24_v*
HLT_IsoTkMu24_v*

```

---

## Same-sign dilepton (==2 electrons)

```

HLT_Ele23_Ele12_CaloIdL_TrackIdL_IsoVL_DZ_v*
HLT_Ele27_eta2p1_WP Loose_Gsf_v*
HLT_Ele27_WPTight_Gsf_v*
HLT_Ele25_eta2p1_WPTight_Gsf_v*

```

---

## Same-sign dilepton (==1 muon, ==1 electron)

```

HLT_Mu23_TrkIsoVVL_Ele8_CaloIdL_TrackIdL_IsoVL_v*
HLT_Mu8_TrkIsoVVL_Ele23_CaloIdL_TrackIdL_IsoVL_v*
HLT_Mu23_TrkIsoVVL_Ele8_CaloIdL_TrackIdL_IsoVL_DZ_v*
HLT_Mu8_TrkIsoVVL_Ele23_CaloIdL_TrackIdL_IsoVL_DZ_v*
HLT_IsoMu22_v*
HLT_IsoTkMu22_v*
HLT_IsoMu22_eta2p1_v*
HLT_IsoTkMu22_eta2p1_v*
HLT_IsoMu24_v*
HLT_IsoTkMu24_v*
HLT_Ele27_WPTight_Gsf_v*
HLT_Ele25_eta2p1_WPTight_Gsf_v*
HLT_Ele27_eta2p1_WP Loose_Gsf_v*

```

---

## Three lepton and Four lepton

```

HLT_DiMu9_Ele9_CaloIdL_TrackIdL_v*
HLT_Mu8_DiEle12_CaloIdL_TrackIdL_v*
HLT_TripleMu_12_10_5_v*
HLT_Ele16_Ele12_Ele8_CaloIdL_TrackIdL_v*
HLT_Mu23_TrkIsoVVL_Ele8_CaloIdL_TrackIdL_IsoVL_v*
HLT_Mu23_TrkIsoVVL_Ele8_CaloIdL_TrackIdL_IsoVL_DZ_v*
HLT_Mu8_TrkIsoVVL_Ele23_CaloIdL_TrackIdL_IsoVL_v*
HLT_Mu8_TrkIsoVVL_Ele23_CaloIdL_TrackIdL_IsoVL_DZ_v*
HLT_Ele23_Ele12_CaloIdL_TrackIdL_IsoVL_DZ_v*
HLT_Mu17_TrkIsoVVL_Mu8_TrkIsoVVL_DZ_v*
HLT_Mu17_TrkIsoVVL_TkMu8_TrkIsoVVL_DZ_v*
HLT_IsoMu22_v*
HLT_IsoTkMu22_v*
HLT_IsoMu22_eta2p1_v*
HLT_IsoTkMu22_eta2p1_v*
HLT_IsoMu24_v*
HLT_IsoTkMu24_v*
HLT_Ele27_WPTight_Gsf_v*
HLT_Ele25_eta2p1_WPTight_Gsf_v*
HLT_Ele27_eta2p1_WP Loose_Gsf_v*

```

---

Table 5: Table of high-level triggers that we consider in the analysis.

| Category | Scale Factor    |
|----------|-----------------|
| ee       | $1.01 \pm 0.02$ |
| $e\mu$   | $1.01 \pm 0.01$ |
| $\mu\mu$ | $1.00 \pm 0.01$ |
| 3l       | $1.00 \pm 0.03$ |

Table 6: Trigger efficiency scale factors and associated uncertainties, shown here rounded to the nearest percent.

## 3 Object identification and event selection

### 3.1 Jets and b tagging

The analysis uses anti- $k_T$  (0.4) particle-flow (PF) jets, corrected for charged hadrons not coming from the primary vertex (charged hadron subtraction), and having jet energy corrections (Summer16\_23Sep2016V3) applied as a function of the jet  $E_T$  and  $\eta$ . Jets are only considered if they have a transverse energy above 25 GeV.

In addition, they are required to be separated from any lepton candidates passing the fakeable object selections (see Tables 7 and 8) by  $\Delta R > 0.4$ .

The loose and medium working points of the CSV b-tagging algorithm are used to identify b jets. Data/simulation differences in the b tagging performance are corrected by applying per-jet weights to the simulation, dependent on the jet  $p_T$ , eta, b tagging discriminator, and flavor (from simulation truth) [7]. The per-event weight is taken as the product of the per-jet weights, including those of the jets associated to the leptons.

More details can be found in the corresponding  $t\bar{t}H$  documentation [3, 6].

### 3.2 Lepton selection

The lepton reconstruction and selection is identical to that used in the  $t\bar{t}H$  multilepton analysis, as documented in Refs. [3, 6]. For details on the reconstruction algorithms, isolation, pileup mitigation, and a description of the lepton MVA discriminator and validation plots thereof, we refer to that document.

Three different selections are defined both for the electron and muon object identification: the *Loose*, *Fakeable Object*, and *Tight* selection. As described in more detail later, these are used for event level vetoes, the fake rate estimation application region, and the final signal selection, respectively. The  $p_T$  of fakeable objects is defined as  $0.85 \times p_T(\text{jet})$ , where the jet is the one associated to the lepton object. This mitigates the dependence of the fake rate on the momentum of the fakeable object and thereby improves the precision of the method.

Tables 7 and 8 list the full criteria for the different selections of muons and electrons.

Table 7: Requirements on each of the three muon selections. In the cases where the cut values change between the selections, those values are listed in the table. Otherwise, whether the cut is applied is indicated. For the two  $p_T^{\text{ratio}}$  and CSV rows, the cuts marked with a † are applied to leptons that fail the lepton MVA cut, while the loose cut value is applied to those that pass the lepton MVA cut.

| Cut                            | Loose             | Fakeable object    | Tight              |
|--------------------------------|-------------------|--------------------|--------------------|
| $ \eta  < 2.4$                 | ✓                 | ✓                  | ✓                  |
| $p_T$                          | $> 5 \text{ GeV}$ | $> 15 \text{ GeV}$ | $> 15 \text{ GeV}$ |
| $ d_{xy}  < 0.05 \text{ (cm)}$ | ✓                 | ✓                  | ✓                  |
| $ d_z  < 0.1 \text{ (cm)}$     | ✓                 | ✓                  | ✓                  |
| $\text{SIP}_{3D} < 8$          | ✓                 | ✓                  | ✓                  |
| $I_{\text{mini}} < 0.4$        | ✓                 | ✓                  | ✓                  |
| is Loose Muon                  | ✓                 | ✓                  | ✓                  |
| jet CSV                        | —                 | $< 0.8484$         | $< 0.8484$         |
| is Medium Muon                 | —                 | —                  | ✓                  |
| tight-charge                   | —                 | —                  | ✓                  |
| lepMVA $> 0.90$                | —                 | —                  | ✓                  |

Table 8: Criteria for each of the three electron selections. In cases where the cut values change between selections, those values are listed in the table. Otherwise, whether the cut is applied is indicated. In some cases, the cut values change for different  $\eta$  ranges. These ranges are  $0 < |\eta| < 0.8$ ,  $0.8 < |\eta| < 1.479$ , and  $1.479 < |\eta| < 2.5$  and the respective cut values are given in the form (value<sub>1</sub>, value<sub>2</sub>, value<sub>3</sub>).

| Cut  | Loose             | Fakeable Object            | Tight              |
|--|-------------------|----------------------------|--------------------|
| $ \eta  < 2.5$                                 | ✓                 | ✓                          | ✓                  |
| $p_T$  | $> 7 \text{ GeV}$ | $> 15 \text{ GeV}$         | $> 15 \text{ GeV}$ |
| $ d_{xy}  < 0.05 \text{ (cm)}$                 | ✓                 | ✓                          | ✓                  |
| $ d_z  < 0.1 \text{ (cm)}$                     | ✓                 | ✓                          | ✓                  |
| $\text{SIP}_{3D} < 8$                          | ✓                 | ✓                          | ✓                  |
| $I_{\text{mini}} < 0.4$                        | ✓                 | ✓                          | ✓                  |
| MVA ID $> (0.0, 0.0, 0.7)$                     | ✓                 | ✓                          | ✓                  |
| $\sigma_{i\eta i\eta} < (0.011, 0.011, 0.030)$ | –                 | ✓                          | ✓                  |
| $H/E < (0.10, 0.10, 0.07)$                     | –                 | ✓                          | ✓                  |
| $\Delta\eta_{in} < (0.01, 0.01, 0.008)$        | –                 | ✓                          | ✓                  |
| $\Delta\phi_{in} < (0.04, 0.04, 0.07)$         | –                 | ✓                          | ✓                  |
| $-0.05 < 1/E - 1/p < (0.010, 0.010, 0.005)$    | –                 | ✓                          | ✓                  |
| $p_T^{\text{ratio}}$                           | –                 | $> 0.5 \dagger / -$        | –                  |
| jet CSV  | –                 | $< 0.3 \dagger / < 0.8484$ | $< 0.8484$         |
| tight-charge conversion rejection              | –                 | –                          | ✓                  |
| Number of missing hits                         | $< 2$             | $= 0$                      | $= 0$              |
| lepMVA $> 0.90$                                | –                 | –                          | ✓                  |

### 3.3 Lepton selection efficiency

Efficiencies of reconstruction and selecting loose leptons are measured both for muons and electrons using a tag and probe method on both data and MC, using  $Z \rightarrow \ell^+ \ell^-$ . Corresponding scale factors are derived from the ratio of efficiencies and applied to the selected events. These are produced for the leptonic SUSY analyses using equivalent lepton selections and recycled for the  $t\bar{t}H$  analysis as well as for this analysis.

The efficiencies of applying the tight selection as defined in Tables 7 and 8, on the loose leptons are determined again by using a tag and probe method on a sample of DY-enriched events. They are documented for the  $t\bar{t}H$  analysis in Ref. [6] and are exactly equivalent for this analysis.

### 3.4 Event selection

Events are selected considering the features of the signal process and the decay signatures.

At least two same-sign or three leptons of any sign, passing the tight selection are required. In the dilepton channels, events are vetoed if they contain additional tight leptons.

Events are required to have fired one of the corresponding trigger paths, and are vetoed if any loose lepton pair has an invariant mass below 12 GeV.

In the dilepton channels, the leptons are required to have  $p_T > 25$  GeV for the leading, and  $p_T > 15$  GeV for the sub-leading lepton. In the three lepton channel, they are required to have respectively  $p_T > 25$  GeV,  $> 15$  GeV, and  $> 15$  GeV.

Three lepton events with an opposite-sign, same-flavor lepton combination with invariant mass within 15 GeV of the Z boson mass are discarded to reject events from WZ +jets production. Same-sign di-electron events where the two electrons have invariant mass within 10 GeV of the Z boson mass are equally discarded to reject events from DY+jets production with charge mis-identified electrons.

Leptons in the three lepton channel are not required to pass the triple charge consistency criteria (for electrons), or the  $\Delta p_T / p_T < 0.2$  cut (for muons).

Furthermore we require at least two jets of which at least one passes the medium b tagging working point ( $p_T > 25$  GeV and  $|\eta| < 2.4$ ), and at least one not passing the loose working point ( $p_T > 25$  GeV for  $|\eta| < 2.4$  and  $p_T > 40$  GeV for  $|\eta| > 2.4$ ).

The event selection is summarized in Tab 9.

|   |  |  |
|---|--|--|
| No loose leptons with $m_{\ell\ell} < 12$ GeV<br>One or more jets passing CSV medium ( $ \eta  < 2.4$ )<br>One or more jets failing CSV loose | Exactly two tight same-sign leptons<br>$p_T > 25/15$ GeV<br>No ee events with $ m_{ee} - m_Z  < 10$ GeV<br>Triple charge consistent electrons<br>Muons with $\Delta p_T / p_T < 0.2$ | Exactly three tight leptons<br>$p_T > 25/15/15$ GeV<br>No OSSF pair with $ m_{\ell\ell} - m_Z  < 15$ GeV |
|---|--|--|

Table 9: Summary of event selection.

In the multi-leptonic final states of the signal processes, the largest contribution is from Higgs decays to WW,  $\sim 75\%$  of the time, as shown in Tab 11. This is followed by the  $\tau\tau$  and ZZ decay modes respectively. A minor contribution is also there from Higgs to  $\mu\mu$  and  $\gamma\gamma$  decays.

|                                 | $3\ell$           | $\mu\mu$          | $e\mu$            | $ee$              |
|---------------------------------|-------------------|-------------------|-------------------|-------------------|
| t $\bar{t}$ W                   | $22.50 \pm 0.35$  | $68.03 \pm 0.61$  | $97.00 \pm 0.71$  | $29.63 \pm 0.39$  |
| t $\bar{t}$ Z/ $\gamma^*$       | $32.80 \pm 1.79$  | $25.89 \pm 1.12$  | $64.82 \pm 2.42$  | $28.74 \pm 1.70$  |
| WZ                              | $8.22 \pm 0.86$   | $15.07 \pm 1.19$  | $26.25 \pm 1.57$  | $9.31 \pm 0.93$   |
| ZZ                              | $1.62 \pm 0.33$   | $1.16 \pm 0.29$   | $2.86 \pm 0.45$   | $1.09 \pm 0.27$   |
| $W^\pm W^\pm qq$                | –                 | $3.96 \pm 0.52$   | $6.99 \pm 0.69$   | $2.19 \pm 0.37$   |
| $W^\pm W^\pm(\text{DPS})$       | –                 | $2.48 \pm 0.42$   | $4.17 \pm 0.54$   | $0.81 \pm 0.24$   |
| VVV                             | $0.42 \pm 0.16$   | $2.99 \pm 0.34$   | $4.85 \pm 0.43$   | $1.19 \pm 0.21$   |
| ttt $t$                         | $1.84 \pm 0.44$   | $2.32 \pm 0.45$   | $4.06 \pm 0.57$   | $0.89 \pm 0.31$   |
| tZq                             | $3.92 \pm 1.48$   | $5.77 \pm 2.24$   | $10.73 \pm 3.03$  | $7.56 \pm 1.72$   |
| tZW                             | $1.70 \pm 0.12$   | $2.13 \pm 0.13$   | $3.91 \pm 0.18$   | $1.13 \pm 0.10$   |
| $\gamma$ conversions            | $7.43 \pm 1.94$   | –                 | $23.81 \pm 6.04$  | $9.87 \pm 4.17$   |
| Non-prompt                      | $25.61 \pm 1.26$  | $80.94 \pm 2.02$  | $135.34 \pm 2.83$ | $47.72 \pm 1.79$  |
| Charge mis-ID                   | –                 | –                 | $58.50 \pm 0.31$  | $44.52 \pm 0.31$  |
| All backgrounds                 | $106.05 \pm 3.45$ | $210.74 \pm 3.61$ | $443.30 \pm 8.01$ | $184.65 \pm 5.29$ |
| tHq ( $\kappa_t = -1.0$ )       | $7.48 \pm 0.14$   | $18.48 \pm 0.22$  | $27.41 \pm 0.27$  | $8.47 \pm 0.15$   |
| tHW ( $\kappa_V = -1.0$ )       | $7.38 \pm 0.16$   | $7.72 \pm 0.17$   | $11.23 \pm 0.20$  | $3.66 \pm 0.11$   |
| t $\bar{t}$ H                   | $18.29 \pm 0.41$  | $24.18 \pm 0.48$  | $35.21 \pm 0.58$  | $11.07 \pm 0.32$  |
| Data ( $35.9 \text{ fb}^{-1}$ ) | 149               | 280               | 525               | 208               |

Table 10: Expected and observed yields for  $35.9 \text{ fb}^{-1}$  after the selection in all final states. Uncertainties are statistical only.

|                                      | $3\ell$     | $\mu\mu$ |              |        |
|--------------------------------------|-------------|----------|--------------|--------|
| tHq (Inclusive)                      | <b>6.57</b> | 100.0%   | <b>17.38</b> | 100.0% |
| tHq ( $H \rightarrow WW$ )           | 4.84        | 73.9%    | 13.33        | 76.9%  |
| tHq ( $H \rightarrow \tau\tau$ )     | 1.04        | 15.9%    | 3.62         | 20.6%  |
| tHq ( $H \rightarrow ZZ$ )           | 0.48        | 7.2%     | 0.37         | 2.2%   |
| tHq ( $H \rightarrow \mu\mu$ )       | 0.21        | 3.0%     | 0.04         | 0.2%   |
| tHq ( $H \rightarrow \gamma\gamma$ ) | < 0.01      | 0.1%     | 0.02         | 0.1%   |
| tHq ( $H \rightarrow bb$ )           | < 0.01      | < 0.1%   | 0.01         | < 0.1% |
| tHW (Inclusive)                      | <b>7.32</b> | 100.0%   | <b>7.62</b>  | 100.0% |
| tHW ( $H \rightarrow WW$ )           | 5.50        | 76.9%    | 5.60         | 74.1%  |
| tHW ( $H \rightarrow \tau\tau$ )     | 1.40        | 20.6%    | 1.81         | 23.1%  |
| tHW ( $H \rightarrow ZZ$ )           | 0.31        | 2.2%     | 0.21         | 2.7%   |
| tHW ( $H \rightarrow \mu\mu$ )       | 0.12        | 0.2%     | 0.01         | 0.1%   |
| tHW ( $H \rightarrow \gamma\gamma$ ) | < 0.01      | < 0.1%   | < 0.01       | < 0.1% |
| tHW ( $H \rightarrow bb$ )           | < 0.01      | < 0.1%   | < 0.01       | < 0.1% |

Table 11: Signal yields split by decay channels of the Higgs boson. (Note that these numbers are with a forward jet  $p_T$  cut at 25 GeV.)

## 4 Background predictions

The modeling of reducible and irreducible backgrounds in this analysis uses the exact methods, analysis code, and ROOT trees used for the  $t\bar{t}H$  multilepton analysis which is being finalized concurrently. We give a brief description of the methods and refer to the documentation of that analysis in Refs. [3, 6] for any details.

The backgrounds in three-lepton and same-sign dilepton final states can be split in two broad categories: irreducible backgrounds with genuine prompt leptons (i.e. from on-shell W and Z boson decays); and reducible backgrounds where at least one of the leptons is “non-prompt”, i.e. produced within a hadronic jet, either a genuine lepton from heavy flavor decays, or simply mis-reconstructed jets. A further class of reducible backgrounds consists of leptons with a mis-reconstructed electric charge sign, only truly relevant for electrons.

Irreducible backgrounds can be reliably estimated directly from Monte-Carlo simulated events, using higher-order cross sections or data control regions for the overall normalization. This is done in this analysis for all backgrounds involving prompt leptons:  $t\bar{t}W$ ,  $t\bar{t}Z$ ,  $t\bar{t}H$ ,  $WZ$ ,  $ZZ$ ,  $W^\pm W^\pm qq$ ,  $t\bar{t}t\bar{t}$ ,  $tZq$ ,  $tZW$ ,  $WWW$ ,  $WWZ$ ,  $WZZ$ ,  $ZZZ$ .

Reducible backgrounds, on the other hand, are not well predicted by simulation, and are estimated using data-driven methods. In the case of non-prompt leptons, a fake rate method is used where the contribution to the final selection is estimated by extrapolating from a side-band (or “application region”) with a looser lepton definition (the fakeable object definitions in Tabs. 7 and 8) to the signal selection. The tight-to-loose ratios (or “fake rates”) are measured in several background dominated data events with dedicated triggers, subtracting the residual prompt lepton contribution using MC. Non-prompt leptons in our signal regions are predominantly produced in  $t\bar{t}$  events, with a much smaller contribution, mainly in the three-lepton channel, from Drell–Yan production. The systematic uncertainty on the normalization of the non-prompt background estimation is on the order of 50%, and thereby one of the dominant limitations on the performance of multilepton analyses in general and this analysis in particular. It consists of several individual sources, such as the result of closure tests of the method using simulated events, limited statistics in the data control regions due to necessary prescaling of lepton triggers, and the uncertainty in the subtraction of residual prompt leptons from the control region.

The fake background where the leptons pass the looser selection are weighted according to how many of them fail the tight criteria. Events with a single failing lepton are weighted with the factor  $f/(1-f)$  for the estimate to the tight selection region, where  $f$  is the fake rate. Events with two failing leptons are given the negative weight  $-f_i f_j / (1-f_i)(1-f_j)$ , and for three leptons the weight is positive and equal to the product of  $f/(1-f)$  factor evaluated for each failing lepton.

Finally, backgrounds from electron charge mis-identification (muon charge mis-id. is negligible) are estimated from the yield of opposite-sign event in the signal region using a measured charge mis-identification probability. The mis-id. probability is measured in same-sign and opposite-sign Drell–Yan events, in several bins of  $p_T$  and  $\eta$ . As for non-prompt leptons, the contribution from charge mis-identified electrons in our signal selection is predominantly from  $t\bar{t}$  and Drell–Yan events. The systematic uncertainty of the normalization of the charge mis-id. estimate is evaluated at about 30%, stemming from a slight disagreement of the mis-id. probability between data and simulation. As it only affects the  $e\mu$  channel, however, the impact of this background on the final sensitivity is very limited.

Figures 2, 3 and 4 show the distributions of some relevant kinematic variables, normalized to

the cross section of the respective processes and to the integrated luminosity.

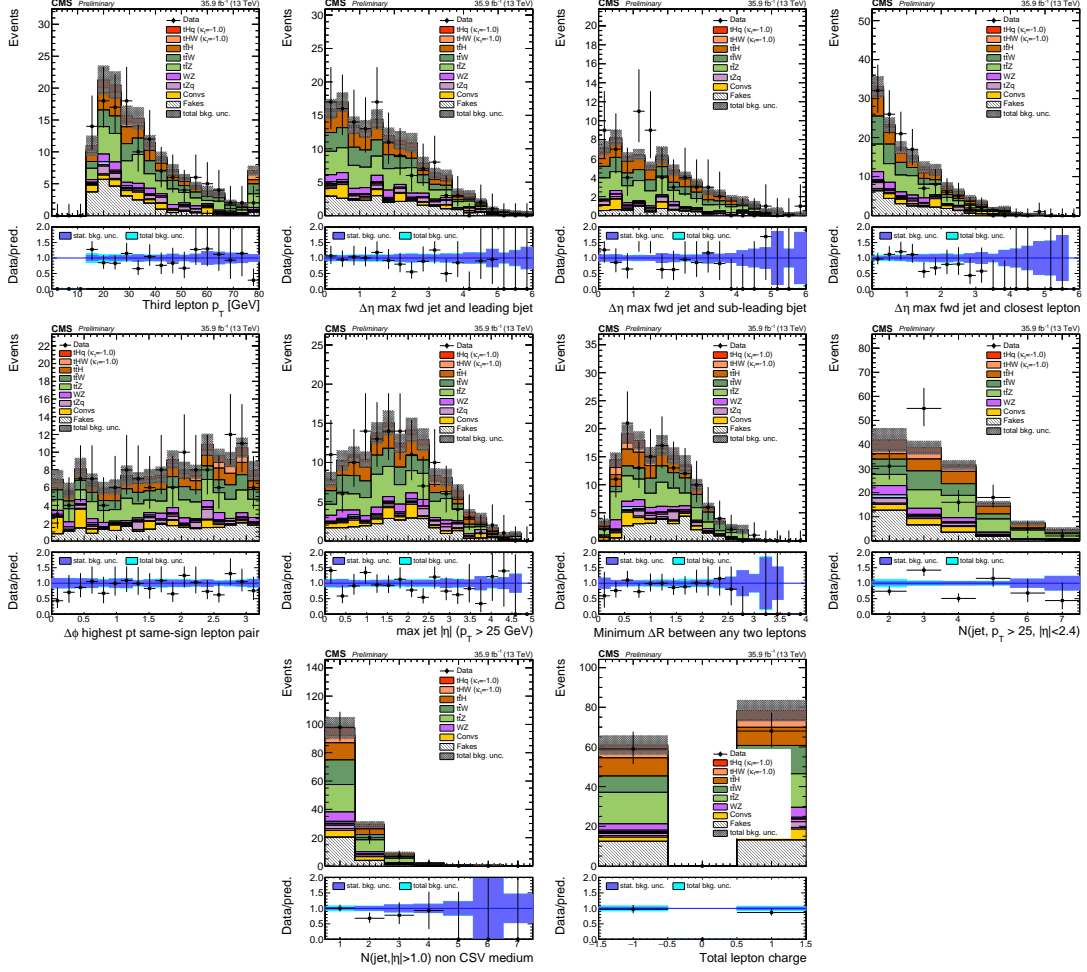


Figure 2: Distributions of input variables to the BDT for signal discrimination, three lepton channel, normalized to their cross section and to  $35.9 \text{ fb}^{-1}$ .

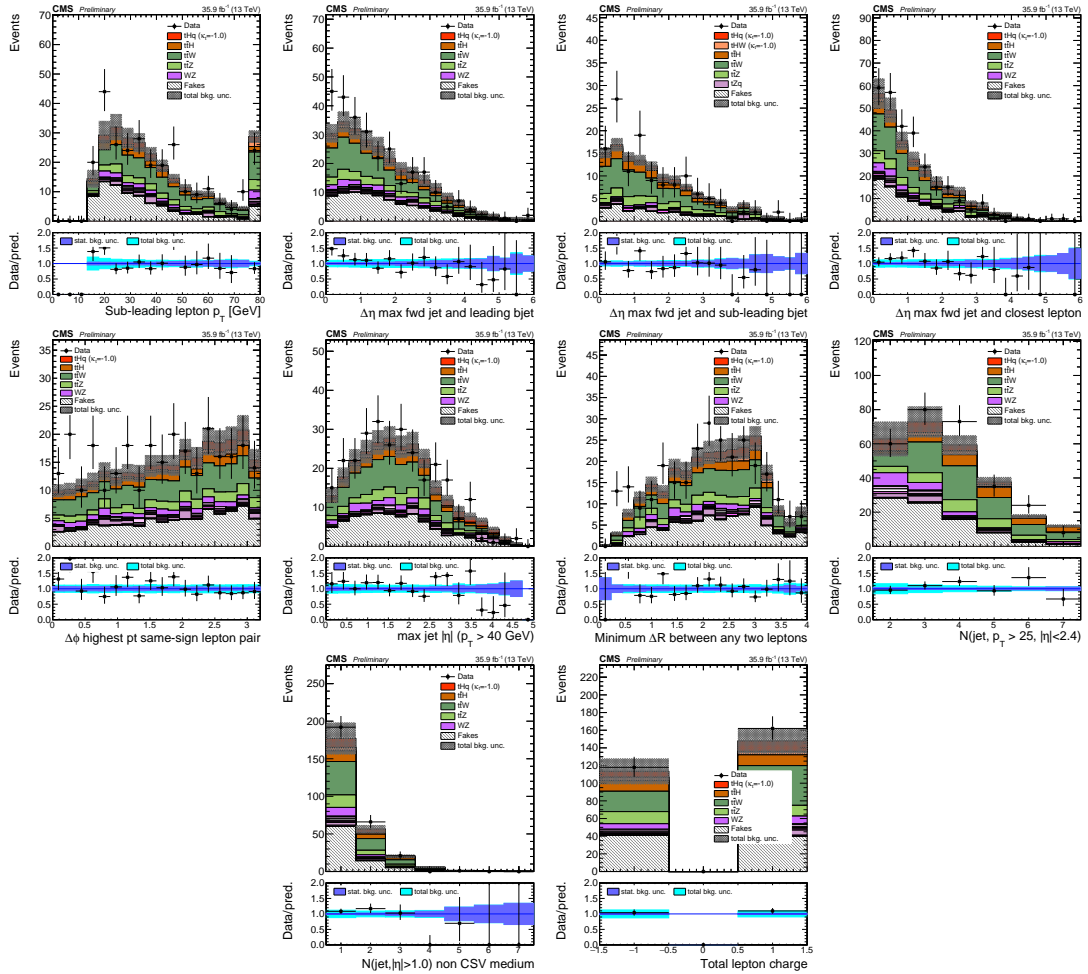


Figure 3: Distributions of input variables to the BDT for signal discrimination, in  $\mu^\pm \mu^\pm$  channel, normalized to their cross section and to  $35.9 \text{ fb}^{-1}$ .

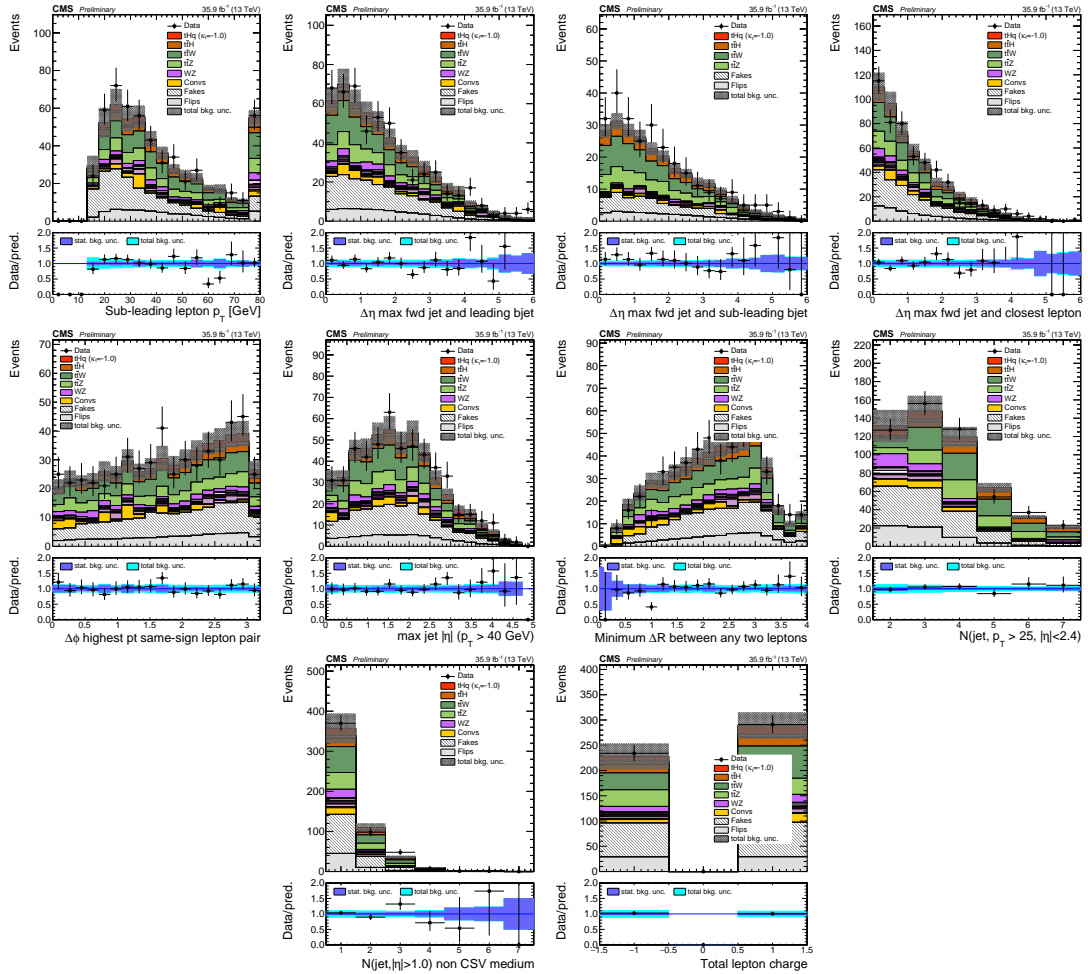


Figure 4: Distributions of input variables to the BDT for signal discrimination, in  $e^\pm \mu^\pm$  channel, normalized to their cross section and to  $35.9 \text{ fb}^{-1}$ .

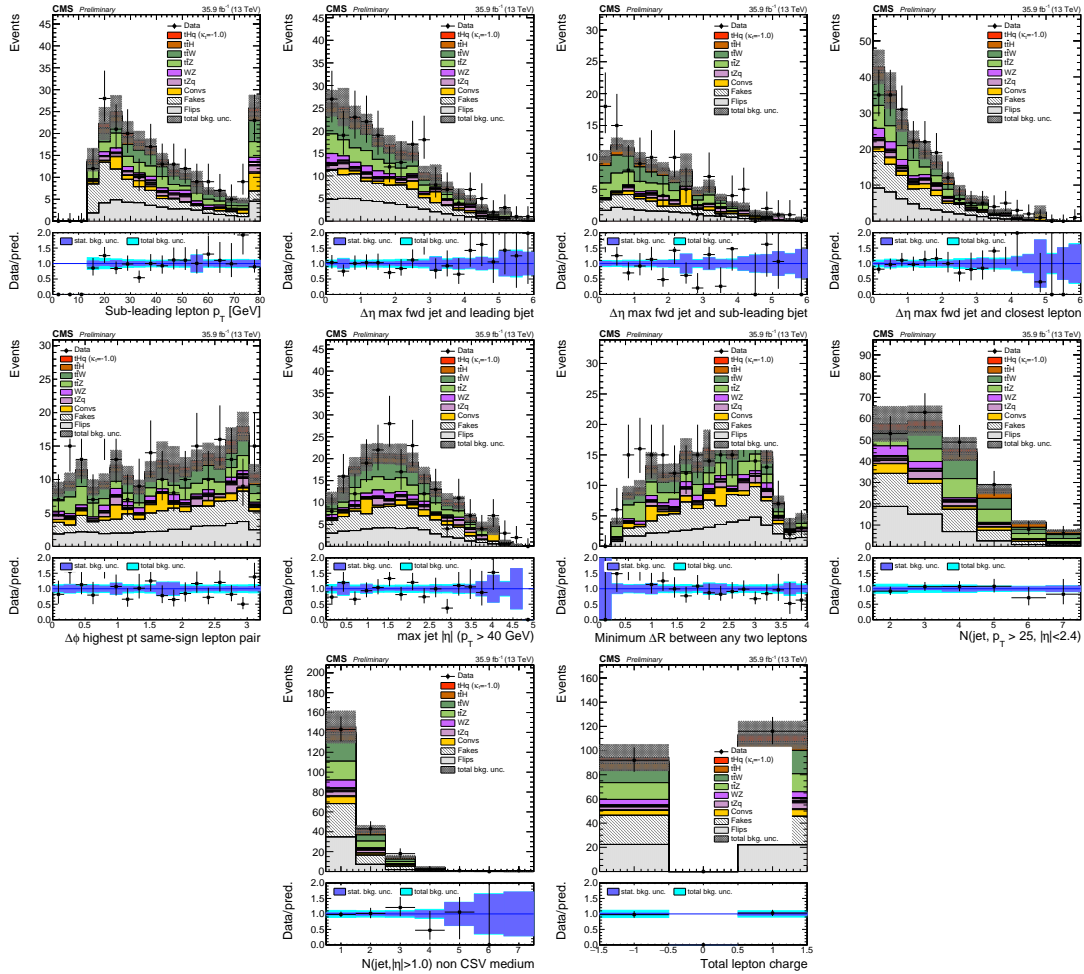


Figure 5: Distributions of input variables to the BDT for signal discrimination, in  $e^\pm e^\pm$  channel, normalized to their cross section and to  $35.9 \text{ fb}^{-1}$ .

## 5 Signal discrimination

The tHq signal is separated from the main backgrounds using a boosted decision tree (BDT) classifier, trained on simulated signal and background events. A set of discriminating variables are given as input to the BDT which produces a output distribution maximizing the discrimination power. Table 12 lists the input variables used while Figures 6 and 7 show their distributions for the relevant signal and background samples, for the three lepton and same-sign dilepton channels, respectively. The same or equivalent input variables are found to be performing well for both three lepton and same-sign dilepton channels.

Two BDT classifiers are trained for the two main backgrounds expected in the analysis: events with prompt leptons from  $t\bar{t}W$  and  $t\bar{t}Z$  (also referred to as  $t\bar{t}V$ ), and events with non-prompt leptons from  $t\bar{t}$ . The datasets used in the training are the tHq signal (see Tab. 1), and LO MADGRAPH samples of  $t\bar{t}W$  and  $t\bar{t}Z$ , in an admixture proportional to their respective cross sections (see Tab. 4).

| Variable name        | Description  |
|----------------------|--|
| nJet25               | Number of jets with $p_T > 25 \text{ GeV}$ , $ \eta  < 2.4$  |
| MaxEtaJet25          | Maximum $ \eta $ of any (non-CSV-loose) jet with $p_T > 25 \text{ GeV}$  |
| totCharge            | Sum of lepton charges  |
| nJetEta1             | Number of jets with $ \eta  > 1.0$ , non-CSV-loose   |
| detaFwdJetBJet       | $\Delta\eta$ between forward light jet and hardest CSV loose jet   |
| detaFwdJet2BJet      | $\Delta\eta$ between forward light jet and second hardest CSV loose jet (defaults to -1 in events with only one CSV loose jet) |
| detaFwdJetClosestLep | $\Delta\eta$ between forward light jet and closest lepton  |
| dphiHighestPtSSPair  | $\Delta\phi$ of highest $p_T$ same-sign lepton pair  |
| minDRll              | minimum $\Delta R$ between any two leptons   |
| Lep3Pt/Lep2Pt        | $p_T$ of the 3 <sup>rd</sup> lepton (2 <sup>nd</sup> for ss2l)   |

Table 12: MVA input discriminating variables

The MVA analysis consist of two stages: first a “training” where the MVA method is trained to discriminate between simulated signal and background events, then a “test” stage where the trained algorithm is used to classify different events from the samples. The sample is obtained from a pre-selection (see Tab. 9 with pre-selection cuts).

Figures 8 and 9 show the input variables distributions as seen by the MVA algorithm. Note that in contrast to the distributions in Fig. 6 only the main backgrounds ( $t\bar{t}$  from simulation,  $t\bar{t}V$ ) are included.

The input variables distributions for 2lss channel for signal against the  $t\bar{t}$  and  $t\bar{t}V$  are shown in Figure 10 and Figure 11 respectively.

Note that splitting the training in two groups reveals that some variables show opposite behavior for the two background sources; potentially screening the discrimination power if they were to be used in a single discriminant. For some other variables the distributions are similar in both background cases.

From table 12, it is clear that the input variables are correlated to some extend. These correlations play an important role for some MVA methods like the Fisher discriminant method in which the first step consist of performing a linear transformation to an phase space where the correlations between variables are removed. In case a boosted decision tree (BDT) method however, correlations do not affect the performance.

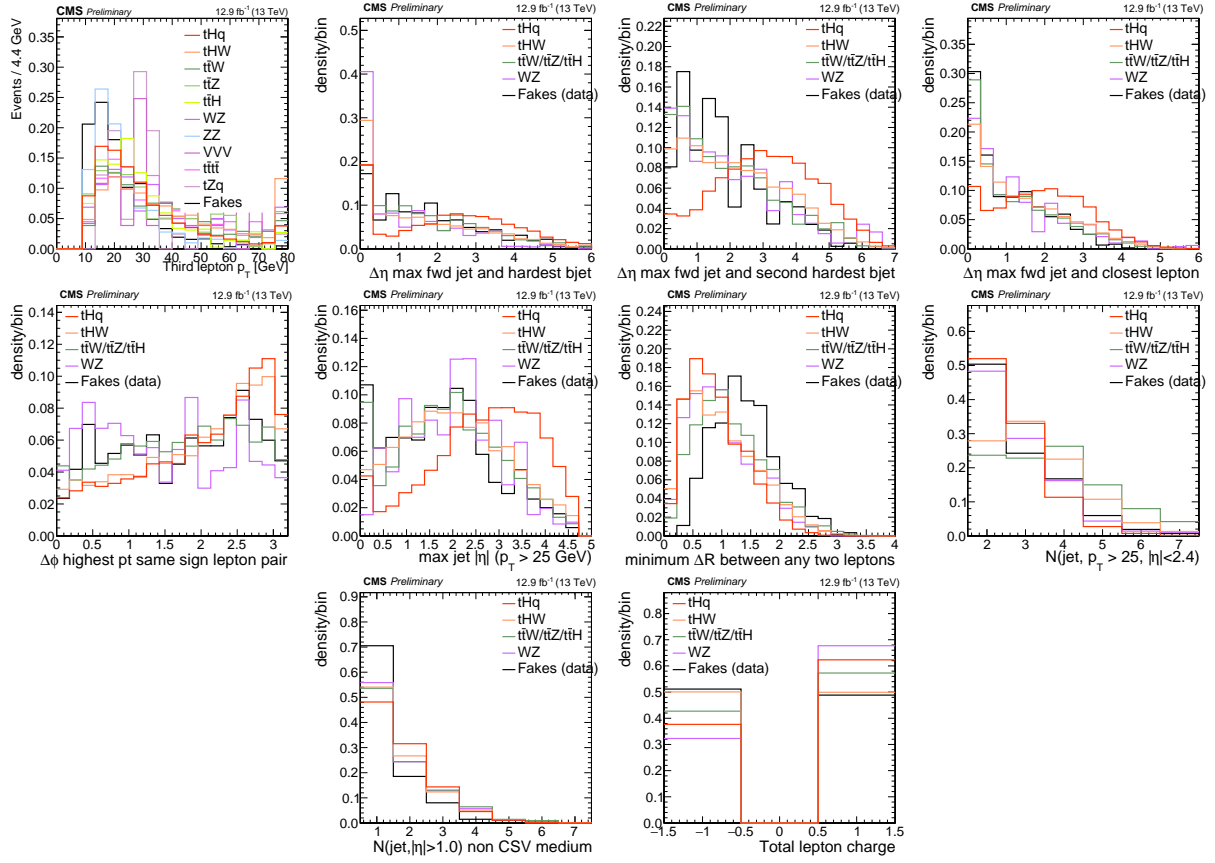


Figure 6: Distributions of input variables to the BDT for signal discrimination, three lepton channel.

Figure 12 show the linear correlation coefficients for signal and background for the two training cases (the signal values are identical by construction). As expected, strong correlations appears for variables related to the forward jet activity. Same trend is seen in case of the same sign dilepton channel in Figure 13.

### 5.1 Classifiers response

Several MVA algorithms were evaluated to determine the most appropriate method for this analysis. The plots in Fig. 14 (top) show the background rejection as a function of the signal efficiency for  $t\bar{t}$  and  $t\bar{t}V$  trainings (ROC curves) for the different algorithms that were evaluated.

In both cases the gradient boosted decision tree (“BDTA\_GRAD”) classifier offers the best results, followed by an adaptive BDT classifier (“BDTA”). The BDTA\_GRAD classifier output distributions for signal and backgrounds are shown on the bottom of Fig. 14. As expected, a good discrimination power is obtained using default discriminator parameter values, with minimal overtraining. TMVA provides a ranking of the input variables by their importance in the classification process, shown in Tab. 14.

The TMVA settings used in the BDT training are shown in Tab. 15.

## 6 Additional discriminating variables

Two additional discriminating variables were tested considering the fact that the forward jet in the background could come from the pileup; since we have a real forward jet in the signal, it

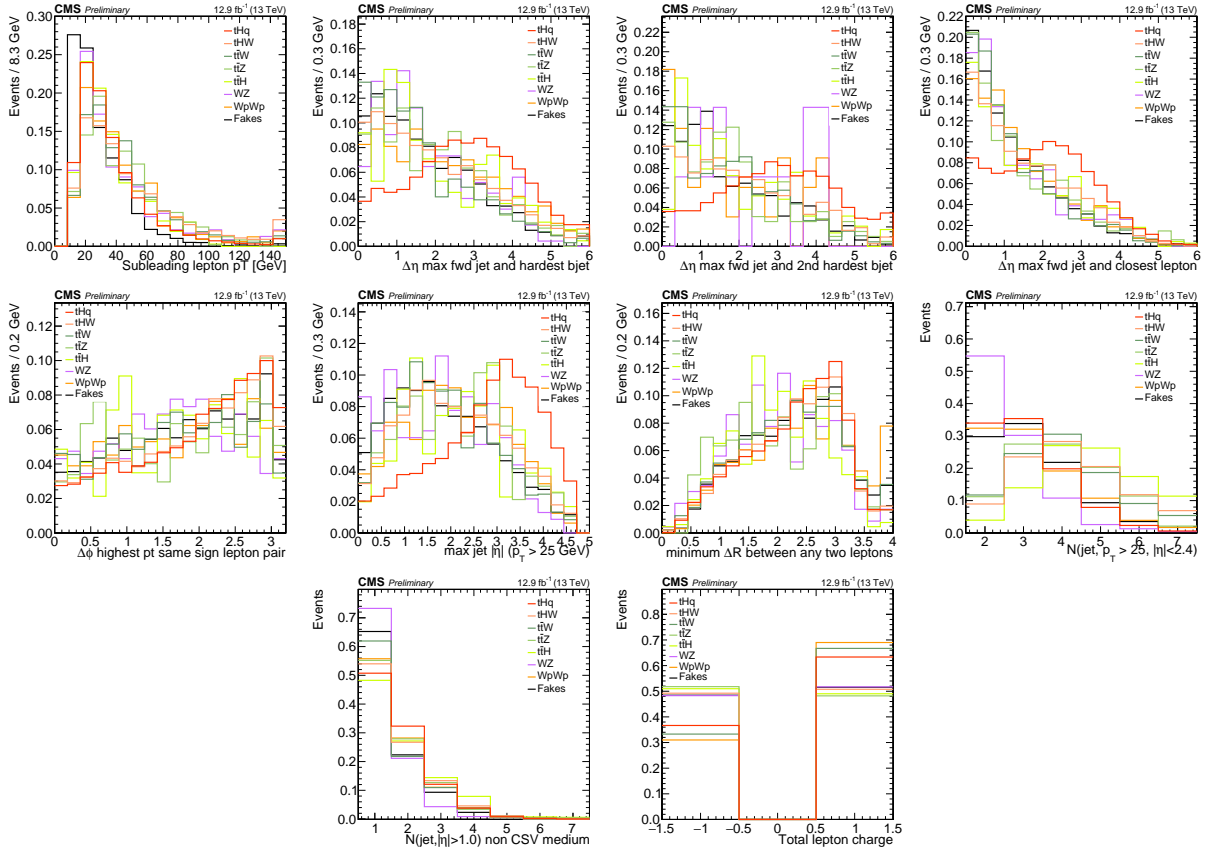


Figure 7: Distributions of input variables to the BDT for signal discrimination, two lepton same sign channel.

| ttbar training |                      |            | ttV training         |            |  |
|----------------|----------------------|------------|----------------------|------------|--|
| Rank           | Variable             | Importance | Variable             | Importance |  |
| 1              | minDRll              | 1.329e-01  | dEtaFwdJetBJet       | 1.264e-01  |  |
| 2              | dEtaFwdJetClosestLep | 1.294e-01  | Lep3Pt               | 1.224e-01  |  |
| 3              | dEtaFwdJetBJet       | 1.209e-01  | maxEtaJet25          | 1.221e-01  |  |
| 4              | dPhiHighestPtSSPair  | 1.192e-01  | dEtaFwdJet2BJet      | 1.204e-01  |  |
| 5              | Lep3Pt               | 1.158e-01  | dEtaFwdJetClosestLep | 1.177e-01  |  |
| 6              | maxEtaJet25          | 1.121e-01  | minDRll              | 1.143e-01  |  |
| 7              | dEtaFwdJet2BJet      | 9.363e-02  | dPhiHighestPtSSPair  | 9.777e-02  |  |
| 8              | nJetEta1             | 6.730e-02  | nJet25_Recl          | 9.034e-02  |  |
| 9              | nJet25_Recl          | 6.178e-02  | nJetEta1             | 4.749e-02  |  |
| 10             | lepCharge            | 4.701e-02  | lepCharge            | 4.116e-02  |  |

Table 13: TMVA input variables ranking for BDTA\_GRAD method for the trainings in the three lepton channel. For both trainings the rankings show almost the same 5 variables in the first places.

could give some improvement in the discriminating power. The additional variables describe the forward jet momentum (fwdJetPt25) and the forward jet identification(fwdJetPUID). Distributions for these variables in the three lepton channel are shown in the figure 16. The forward jet identification distribution show that for both, signal and background, jets are mostly real jets.

The testing was made including in the MVA input one variable at a time, so we can evaluate the discrimination power of each variable, and then both simultaneously. fwdJetPUID was ranked in the last place in importance (11) in both training (ttV and tt) while fwdJetPt25 was ranked 3

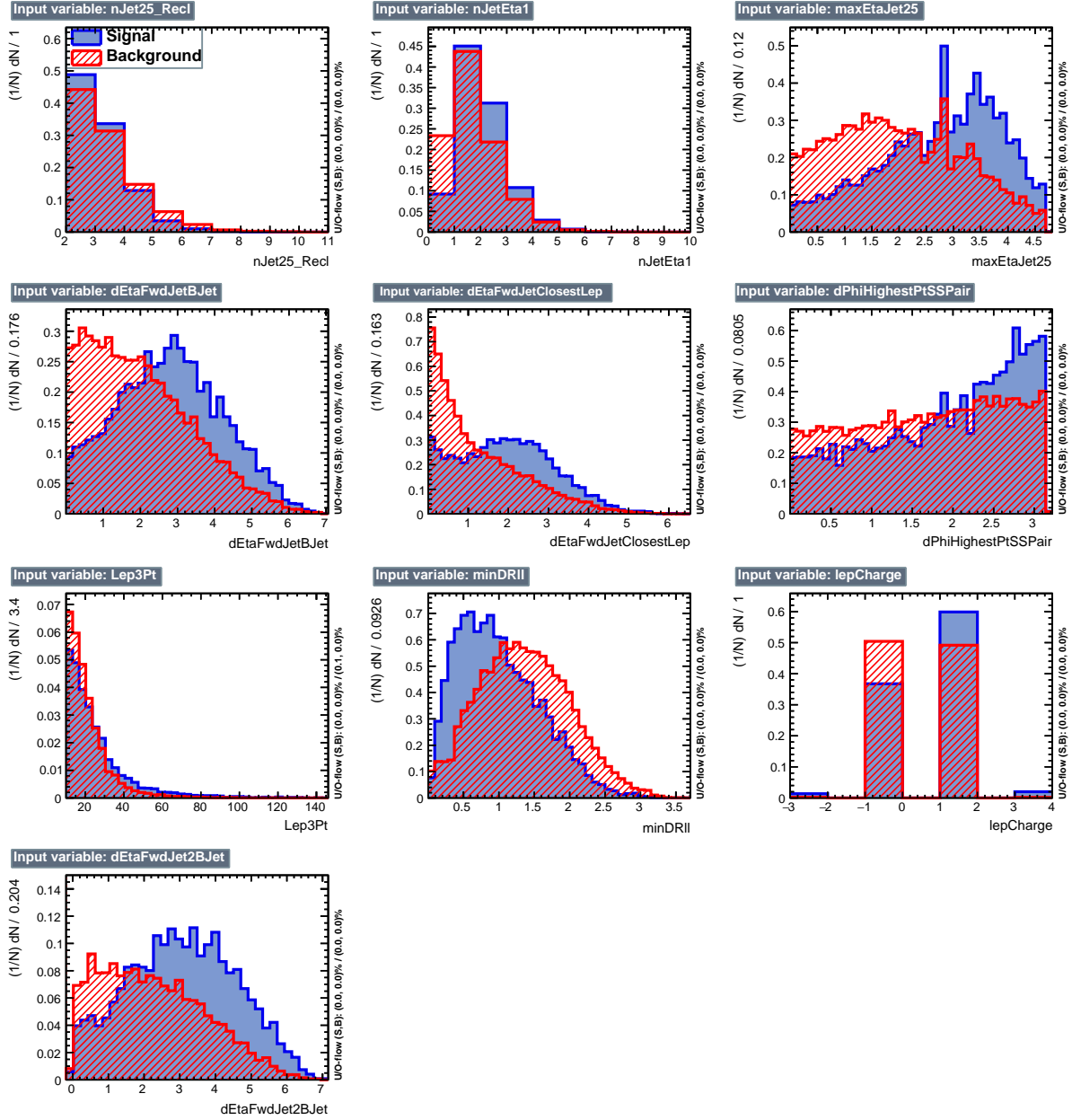


Figure 8: BDT inputs as seen by TMVA (signal, in blue, is  $t\bar{t}q$ , background, in red, is  $t\bar{t}$ ) for the three lepton channel, discriminated against  $t\bar{t}$  (fakes) background.

in the  $t\bar{t}V$  training and 7 in the  $t\bar{t}$  training. When training using 12 variables, `fwdJetPt25` was ranked 5 and 7 in the  $t\bar{t}V$  and  $t\bar{t}$  trainings respectively, while `fwdJetPUID` was ranked 12 in both cases.

The improvement in the discrimination performance provided by the additional variables is about 1%, so we decided not to include them in the current procedure. Table 16 show the ROC-integral for all the testing cases we made.

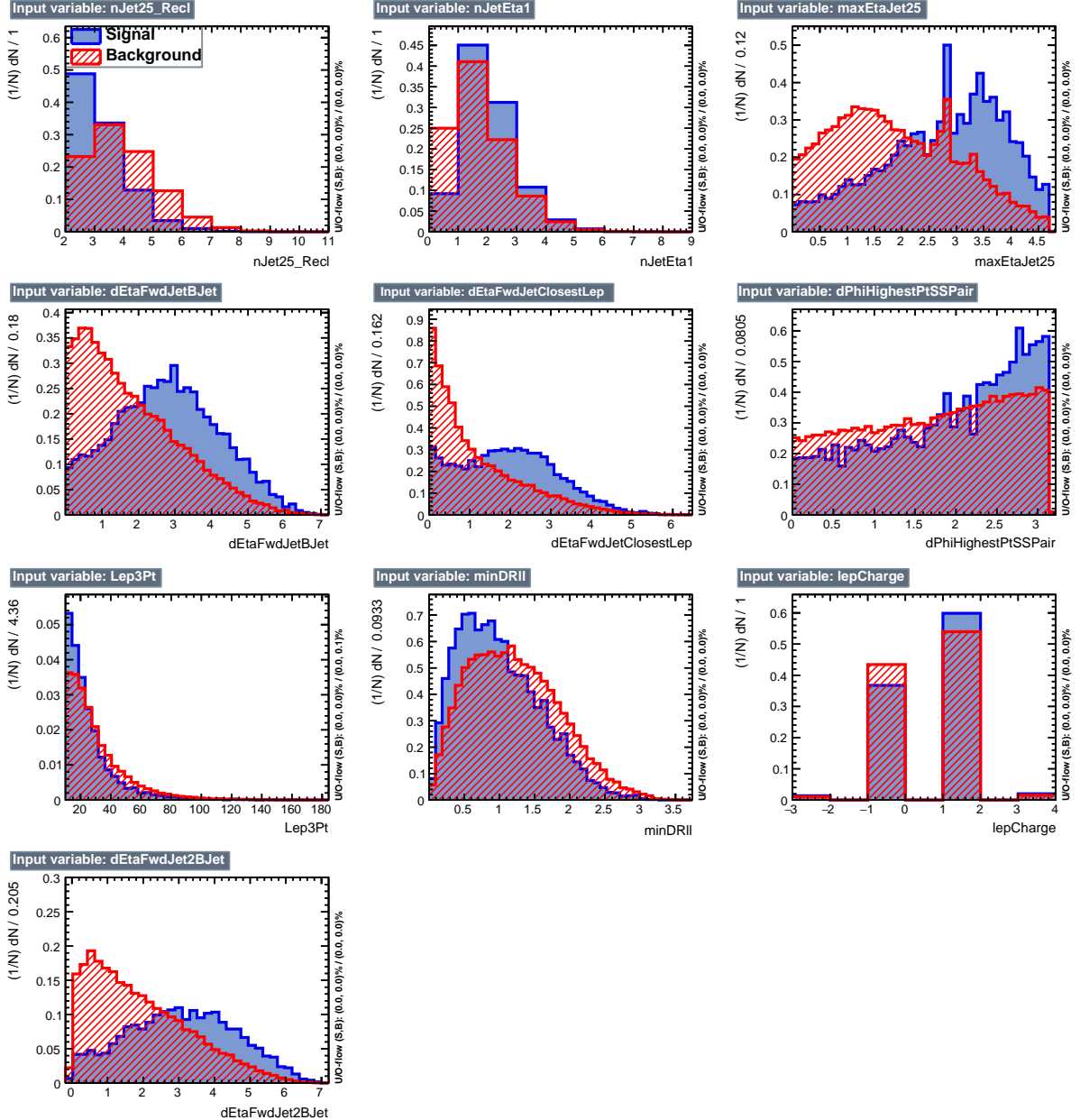


Figure 9: BDT inputs as seen by TMVA (signal, in blue, is  $t\bar{t}q$ , background, in red, is  $t\bar{t}W+t\bar{t}Z$ ) for the three lepton channel, discriminated against  $t\bar{t}V$  background.

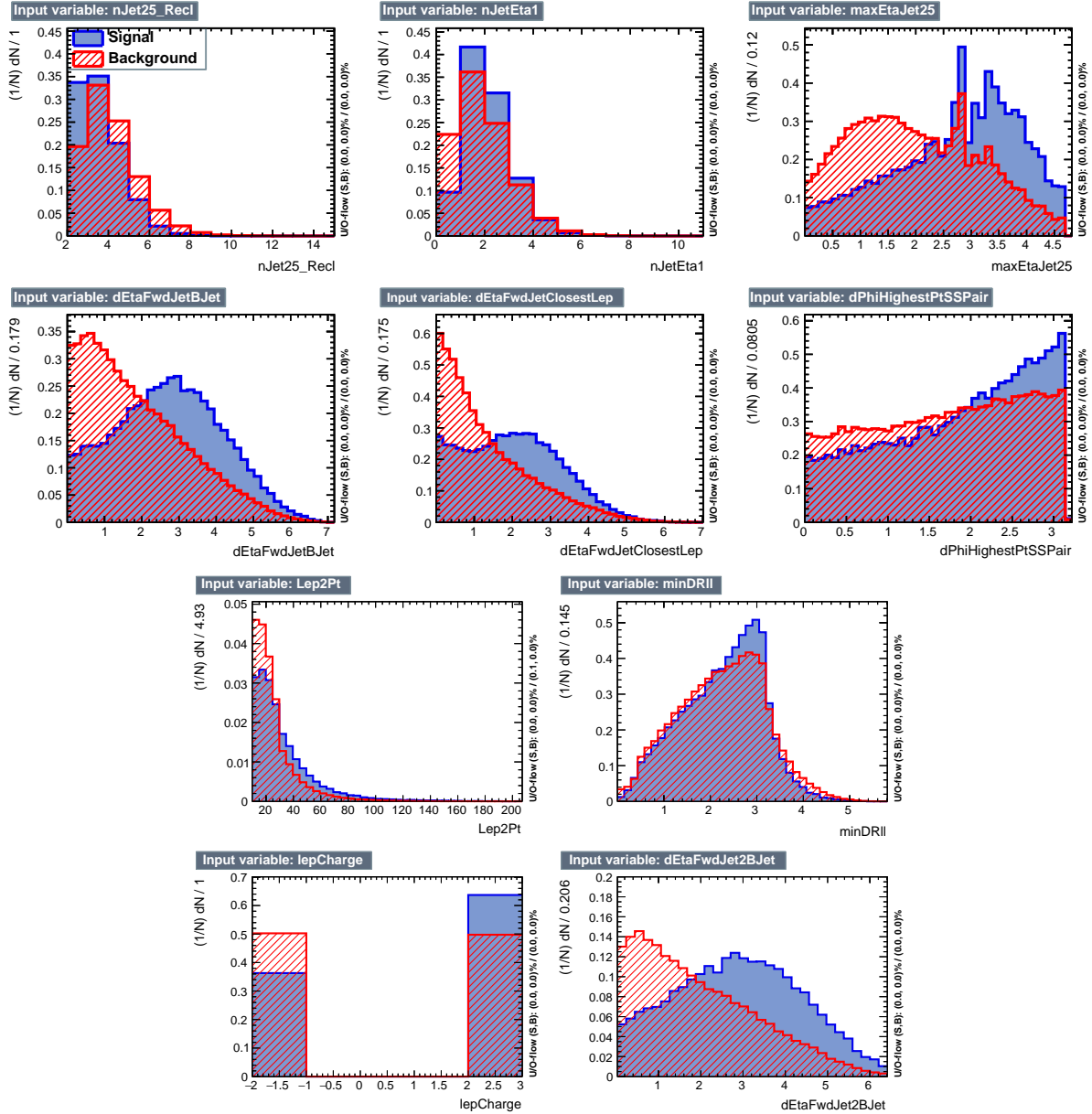


Figure 10: BDT inputs as seen by TMVA (signal, in blue, is  $t\bar{t}q$ , background, in red, is  $t\bar{t}$ ) for the same sign dilepton channel, discriminated against  $t\bar{t}$  background.

| ttbar training |                      |            | ttV training         |            |  |
|----------------|----------------------|------------|----------------------|------------|--|
| Rank           | Variable             | Importance | Variable             | Importance |  |
| 1              | dEtaFwdJetClosestLep | 1.394e-01  | maxEtaJet25          | 1.357e-01  |  |
| 2              | minDRll              | 1.359e-01  | dEtaFwdJet2BJet      | 1.267e-01  |  |
| 3              | maxEtaJet25          | 1.308e-01  | dEtaFwdJetBJet       | 1.200e-01  |  |
| 4              | dPhiHighestPtSSPair  | 1.116e-01  | Lep2Pt               | 1.196e-01  |  |
| 5              | Lep2Pt               | 1.111e-01  | dEtaFwdJetClosestLep | 1.145e-01  |  |
| 6              | dEtaFwdJetBJet       | 1.067e-01  | minDRll              | 1.077e-01  |  |
| 7              | dEtaFwdJet2BJet      | 8.906e-02  | nJet25_Recl          | 1.020e-01  |  |
| 8              | nJetEta1             | 6.445e-02  | dPhiHighestPtSSPair  | 8.232e-02  |  |
| 9              | nJet25_Recl          | 6.254e-02  | nJetEta1             | 5.948e-02  |  |
| 10             | lepCharge            | 4.848e-02  | lepCharge            | 3.198e-02  |  |

Table 14: TMVA input variables ranking for BDTA\_GRAD method in same-sign dilepton channel.

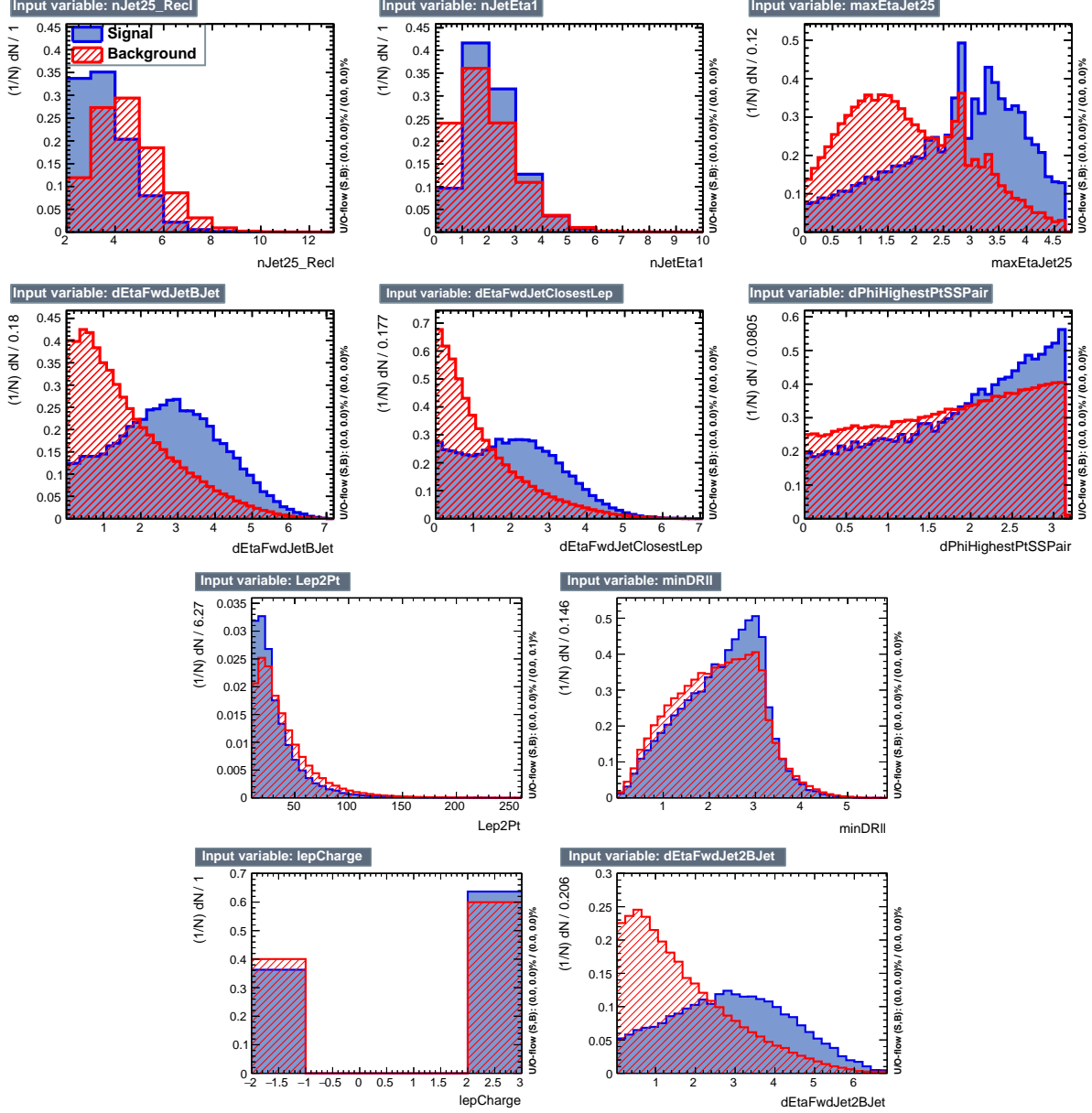


Figure 11: BDT inputs as seen by TMVA (signal, in blue, is  $t\bar{t}q$ , background, in red, is  $t\bar{t}W+t\bar{t}Z$ ) for the same sign dilepton channel, discriminated against  $t\bar{t}V$  background.

---

```

TMVA.Types.kBDT
NTrees=800
BoostType=Grad
Shrinkage=0.10
!UseBaggedGrad
nCuts=50
MaxDepth=3
NegWeightTreatment=PairNegWeightsGlobal
CreateMVAPdfs

```

---

Table 15: TMVA configuration used in the BDT training.

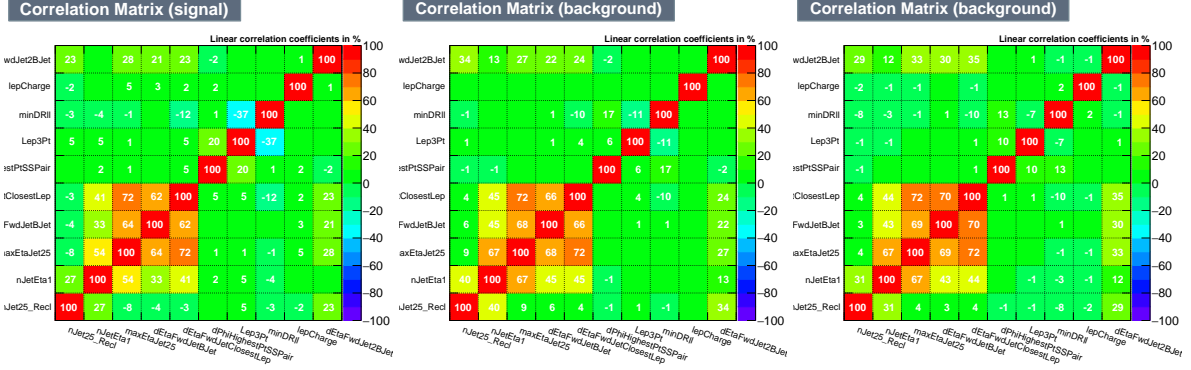


Figure 12: Signal (left),  $t\bar{t}$  background (middle), and  $t\bar{t}V$  background (right.) correlation matrices for the input variables in the TMVA analysis for the three lepton channel.

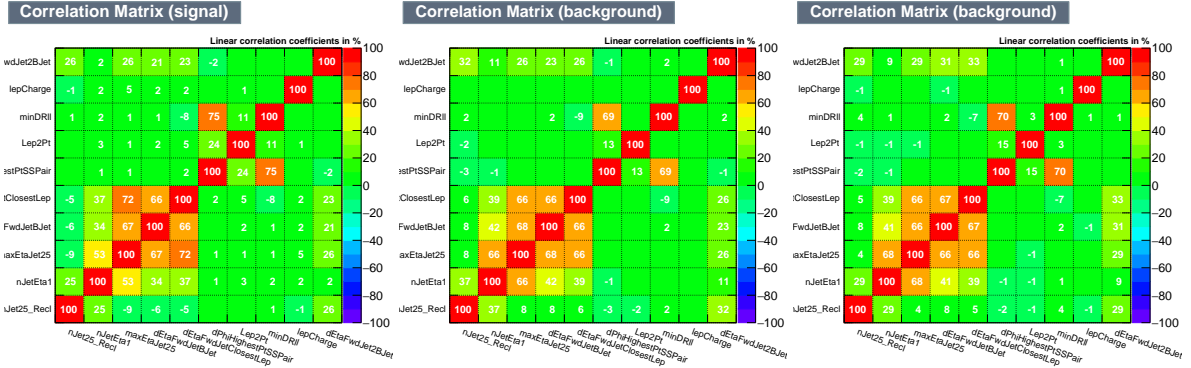


Figure 13: Signal and Background correlation matrices for the input variables in the TMVA analysis for the same sign dilepton channel, for the signal (left),  $t\bar{t}$  background (middle), and  $t\bar{t}V$  background (right.)

| ROC-integral     |       |
|------------------|-------|
| base 10 var ttv  | 0.848 |
| + fwdJetPUID ttv | 0.849 |
| + fwdJetPt25 ttv | 0.856 |
| 12 var ttv       | 0.856 |
| base 10 var tt   | 0.777 |
| + fwdJetPUID tt  | 0.777 |
| + fwdJetPt25 tt  | 0.787 |
| 12 var           | 0.787 |

Table 16: ROC-integral for all the testing cases we made in the evaluation of the additional variables discriminating power. The improvement in the discrimination performance provided by the additional variables is about 1%

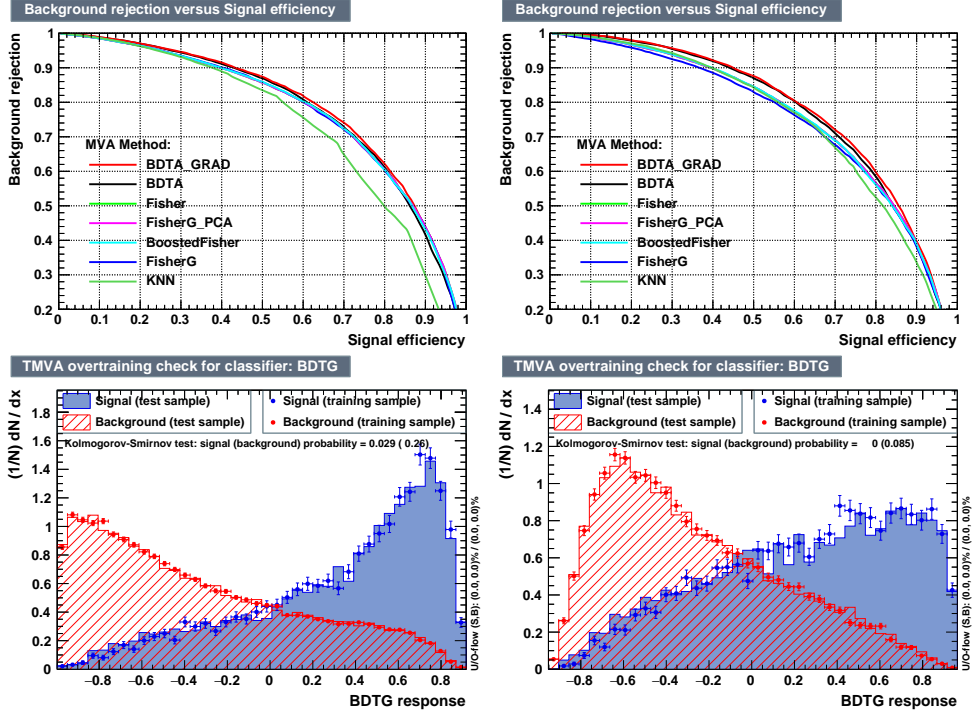


Figure 14: Top: background rejection vs signal efficiency (ROC curves) for various MVA classifiers (top) in the three lepton channel against  $t\bar{t}V$  (left) and  $t\bar{t}$  (right). Bottom: classifier output distributions for the gradient boosted decision trees, for training against  $t\bar{t}V$  (left) and against  $t\bar{t}$  (right).

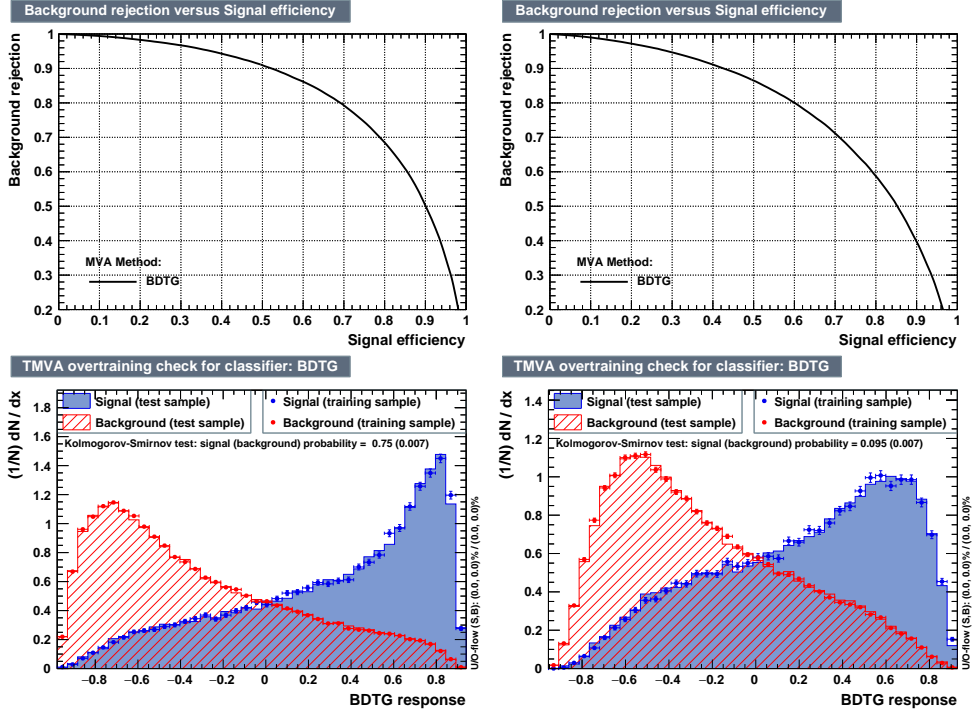


Figure 15: Top: background rejection vs signal efficiency (ROC curve) in the same sign dilepton channel for a single discriminator: BDTG, against  $t\bar{t}V$  (left) and  $t\bar{t}$  (right). Bottom: classifier output distribution, for training against  $t\bar{t}V$  (left) and against  $t\bar{t}$  (right).

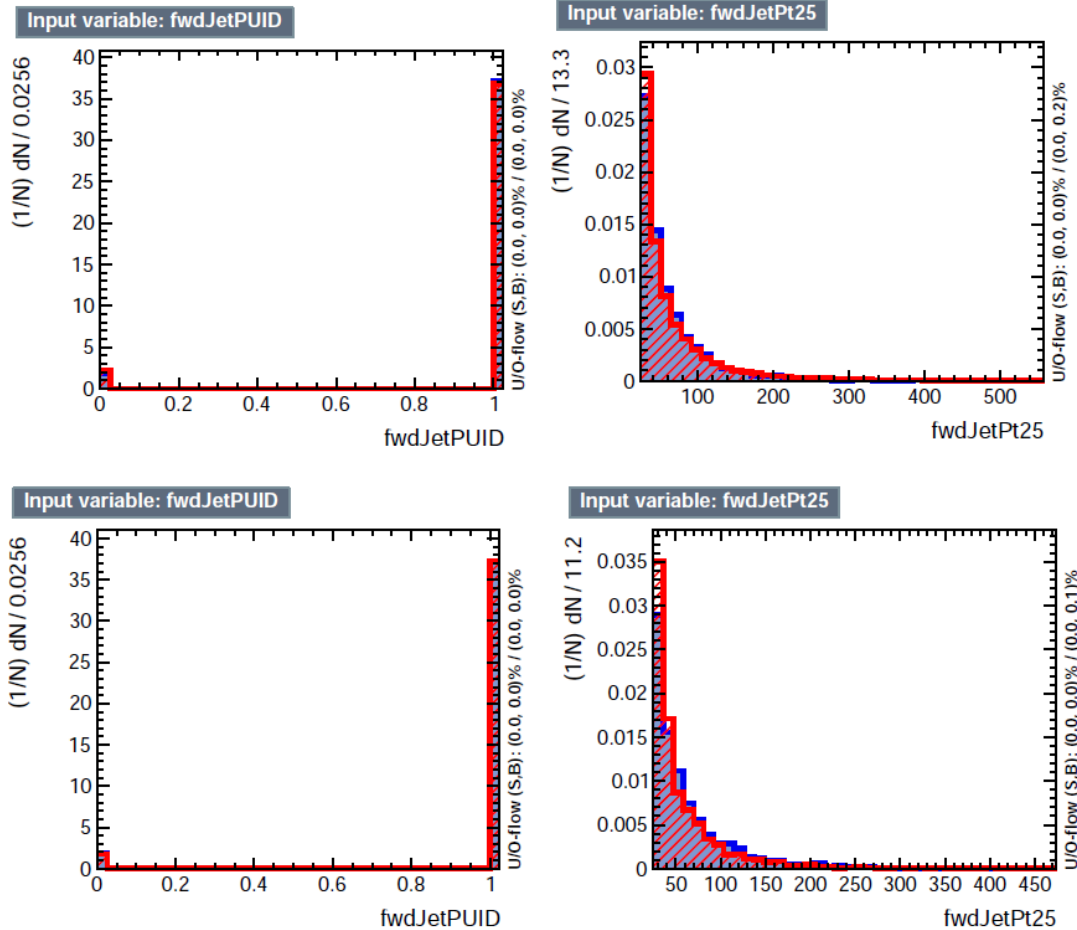


Figure 16: Additional discriminating variables distributions for ttv training (Top row) and tt training (bottom row) in the three lepton channel. The origin of the jets in the forward jet identification distribution is tagged as 0 for “pileup jets” while “real jets” are tagged as 1.

## 7 Signal extraction

### 7.1 Signal extraction procedure

The two BDT classifiers introduced in the previous section, trained against the dominant  $t\bar{t}$  and  $t\bar{t}V$  backgrounds in each channel, are used to evaluate the limits in a fit to the classifier shape. Figure 17 shows the expected output distributions in a 2D plane of one training vs. the other. Each event is now classified into one of ten 2D-bins according to its position in the plane, see Fig. 18. The number of bins is chosen such that no bins are entirely empty for any process. The bin boundary positions have been studied and optimized with respect to the expected limit, see Sec. 7.3.

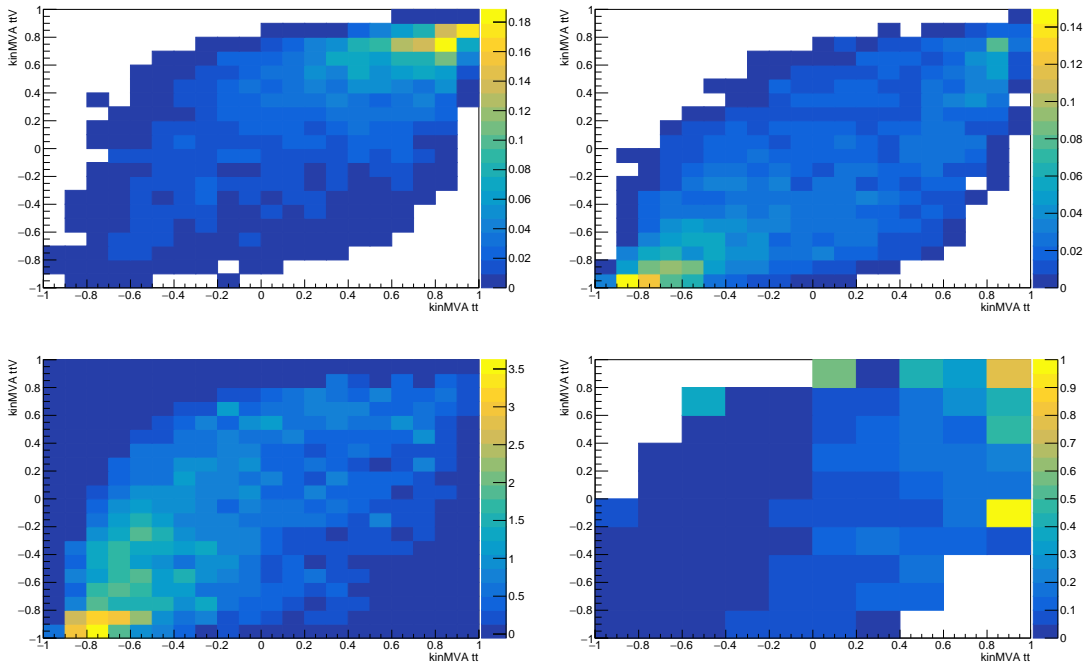


Figure 17: BDT classifier output planes (training vs  $t\bar{t}$  on x-axis and vs  $t\bar{t}V$  on y-axis) for the  $tHq$  and  $tHW$  signals (top row), and for the combined backgrounds (bottom left). Backgrounds are evaluated as in the final background prediction, i.e. these are not the samples used in the MVA training and this includes data-driven backgrounds. Bottom right shows the S/B ratio (combining  $tHq$  and  $tHW$ ) in the same plane. Three lepton channel only.

From this event categorization, a 1D histogram of expected distribution is produced for each signal and background process, and fit to the observed data (or the Asimov dataset for expected limits).

### 7.2 Signal model

The goal of this analysis is to test the compatibility of points in the parameter space of Higgs-to-vector boson and Higgs-to-top quark couplings. The simulated  $tHq$ ,  $tHW$ , and  $t\bar{t}H$  signal events are used with event-by-event weights to reflect the impact of the couplings on kinematic distributions, and together with different predictions of the respective production cross sections and branching ratios, we can produce limits for different values of  $\kappa_V$  and  $\kappa_t$ . (See Tab. 2 for the set of  $\kappa_t$  and  $\kappa_V$  values generated.) The slight shape-dependence of the BDT outputs as a function of the couplings is documented in App. B.

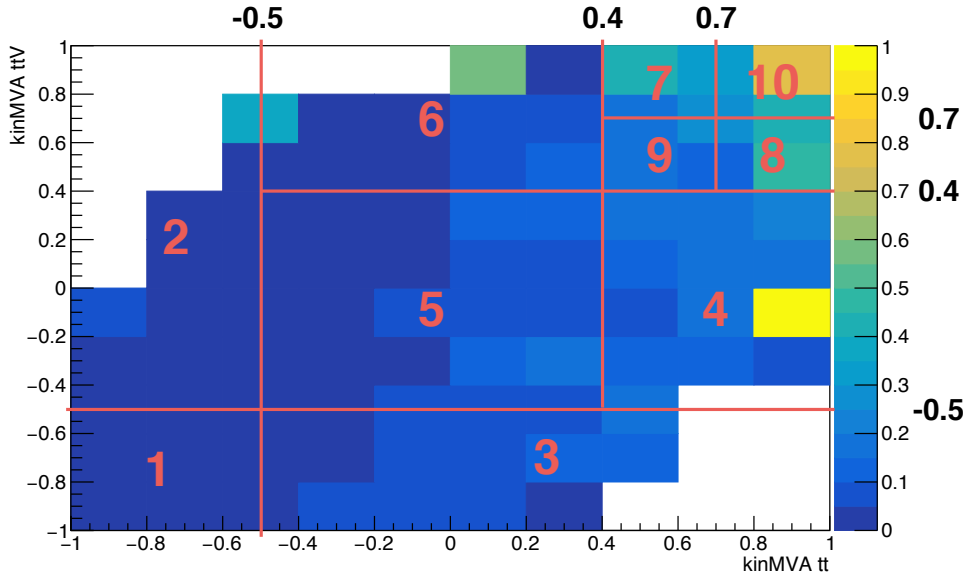


Figure 18: Binning overlaid on the S/B ratio map on the plane of classifier outputs.

Apart from the  $\kappa_t/\kappa_V$  interference of the tHq and tHW production cross sections, the cross section of t $\bar{t}H$  scales as  $\kappa_t^2$ . Furthermore, the Higgs branching fractions to vector bosons depend on  $\kappa_V$ , and the overall Higgs decay width depend both on  $\kappa_t$  and  $\kappa_V$  when considering resolved top-quark loops in the  $H \rightarrow \gamma\gamma$ ,  $H \rightarrow Z\gamma$ , and  $H \rightarrow gg$  decays. The relative contributions from  $H \rightarrow WW$ ,  $H \rightarrow ZZ$ , and  $H \rightarrow \tau\tau$  changes with changing  $\kappa_V$ .

We hence set an upper limit on the combined cross section times branching ratio of tHq, tHW, and t $\bar{t}H$ .

If we assume a modifier for the Higgs-to-tau coupling ( $\kappa_\tau$ ) to be equal to  $\kappa_t$ , the relative fractions of WW, ZZ, and  $\tau\tau$  in our selection will only depend on the ratio of  $\kappa_t/\kappa_V$ . Any limit set at any given value of  $\kappa_t/\kappa_V$  is thus valid for all values of  $\kappa_t$  and  $\kappa_V$  with that ratio, and could then be compared with theoretical predictions of cross sections at different values of either modifier. Rather than as a function of the  $\kappa_t/\kappa_V$  ratio, limits could (equivalently) be reported as a function of the relative strength of Higgs-top and Higgs-vector-boson couplings, multiplied by the relative sign. Such a parameter, further referred to as  $f_t$ , as defined in Eq. 1, spans the entire possible parameter space between  $-1.0$  and  $1.0$ , with the SM expectation at  $0.5$ . Absolute values of  $1.0$  or  $0.0$  would then correspond to purely Higgs-top and purely Higgs-V couplings, respectively.

$$f_t = \text{sign}(\kappa_t/\kappa_V) \times \frac{\kappa_t^2}{\kappa_t^2 + \kappa_V^2}. \quad (1)$$

Table 17 shows the points in the  $\kappa_t/\kappa_V$  and  $f_t$  parameter space that are mapped by the 51 individual  $\kappa_t$  and  $\kappa_V$  points.

The overall higgs decay width (modified by both  $\kappa_t$  and  $\kappa_V$ ) becomes irrelevant if limits are quoted as absolute cross sections rather than multiples of the expected cross section (which depends on the overall Higgs decay width).

The 1D histograms of events as categorized in regions of the 2D BDT plane is then used in a maximum likelihood fit of signal and background shapes, where the tHq, tHW, and t $\bar{t}H$  signals are floating with a common signal strength modifier  $r$ , producing a 95% C.L. upper limit the observed cross section of tHq + tHW + t $\bar{t}H$ .

| $f_t$  | $\kappa_t/\kappa_V$ | $\kappa_V = 0.5$ | $\kappa_V = 1.0$ | $\kappa_V = 1.5$ |
|--------|---------------------|------------------|------------------|------------------|
| -0.973 | -6.000              | -3.00            |                  |                  |
| -0.941 | -4.000              | -2.00            |                  |                  |
| -0.900 | -3.000              | -1.50            | -3.00            |                  |
| -0.862 | -2.500              | -1.25            |                  |                  |
| -0.800 | -2.000              | -1.00            | -2.00            | -3.00            |
| -0.692 | -1.500              | -0.75            | -1.50            |                  |
| -0.640 | -1.333              |                  |                  | -2.00            |
| -0.610 | -1.250              |                  | -1.25            |                  |
| -0.500 | -1.000              | -0.50            | -1.00            | -1.50            |
| -0.410 | -0.833              |                  |                  | -1.25            |
| -0.360 | -0.750              |                  | -0.75            |                  |
| -0.308 | -0.667              |                  |                  | -1.00            |
| -0.200 | -0.500              | -0.25            | -0.50            | -0.75            |
| -0.100 | -0.333              |                  |                  | -0.50            |
| -0.059 | -0.250              |                  | -0.25            |                  |
| -0.027 | -0.167              |                  |                  | -0.25            |
| 0.000  | 0.000               | 0.00             | 0.00             | 0.00             |
| 0.027  | 0.167               |                  |                  | 0.25             |
| 0.059  | 0.250               |                  | 0.25             |                  |
| 0.100  | 0.333               |                  |                  | 0.50             |
| 0.200  | 0.500               | 0.25             | 0.50             | 0.75             |
| 0.308  | 0.667               |                  |                  | 1.00             |
| 0.360  | 0.750               |                  | 0.75             |                  |
| 0.410  | 0.833               |                  |                  | 1.25             |
| 0.500  | 1.000               | 0.50             | 1.00             | 1.50             |
| 0.610  | 1.250               |                  | 1.25             |                  |
| 0.640  | 1.333               |                  |                  | 2.00             |
| 0.692  | 1.500               | 0.75             | 1.50             |                  |
| 0.800  | 2.000               | 1.00             | 2.00             | 3.00             |
| 0.862  | 2.500               | 1.25             |                  |                  |
| 0.900  | 3.000               | 1.50             | 3.00             |                  |
| 0.941  | 4.000               | 2.00             |                  |                  |
| 0.973  | 6.000               | 3.00             |                  |                  |

Table 17: The 33 distinct values of  $\kappa_t/\kappa_V$  and  $f_t$  as mapped by the 51  $\kappa_t$  and  $\kappa_V$  points.

This is done separately for each point of  $\kappa_t$  and  $\kappa_V$ , where the cross sections and branching fractions are scaled accordingly in each point. Limits at fixed values of  $\kappa_t/\kappa_V$  are by construction identical. Tables 28–30 and 31–33 in Appendix D show the scalings of cross section times branching fraction, as well as branching fractions alone for each of the Higgs decay modes and each of the signal components.

### 7.3 Binning and selection optimization

*Note that the numbers in this subsection are upper limits on the tHq+tHW cross sections only (without t̄tH), and are always evaluated at  $\kappa_t = -1.0$ ,  $\kappa_V = 1.0$ .*

The effect on the cross section limit of the choice of pre-selection cuts is evaluated by varying the most important cuts and re-calculating the limit (in the three lepton channel) in each case. Table 18 shows the several variations made, compared to a baseline corresponding to the selection reported in Tab. 9, but with only a loose CSV jet and a Z veto of  $\pm 10$  GeV. The optimal

limit is found when requiring a slightly tighter selection with respect to the baseline. This is the selection reported in Tab. 9.

| Selection                            | Variation                                       | Expected limit |
|--------------------------------------|---|----------------|
| Baseline                             | see Tab. 9                                      | < 2.93         |
| Loose CSV tags                       | $\geq 1 \rightarrow \geq 2$                     | < 3.81         |
| Medium CSV tags                      | $\geq 0 \rightarrow \geq 1$                     | < 2.76         |
| Light forward jet $\eta$             | $\geq 0 \rightarrow \geq 1$                     | < 2.94         |
| Light forward jet $\eta$             | $\geq 0 \rightarrow \geq 1.5$                   | < 3.00         |
| $E_T^{\text{miss}} > 30 \text{ GeV}$ |   | < 2.91         |
| Z veto ( $ m_{\ell\ell} - m_Z $ )    | $> 10 \text{ GeV} \rightarrow > 15 \text{ GeV}$ | < 2.79         |
| One medium CSV + 15 GeV Z veto       | combined  | < 2.62         |

Table 18: Limit variation as a function of tighter cuts. The baseline selection corresponds to a looser selection as the one reported in Tab. 9 (which is the optimal selection determined here (last line)), where only a CSV-loose b-tagged jet is required, and the Z veto is loosened to  $\pm 10 \text{ GeV}$ .

The obtained cross section limit also depends on the chosen binning in the 2D plane as the S/B ratio varies across the plane, hence several sizes and binning combination were tested in order to optimize the limit. Figure 19 show some of the binning combinations tested; in the default combination all the bins have the same size, while the best limit was found for a set of 10 bins.

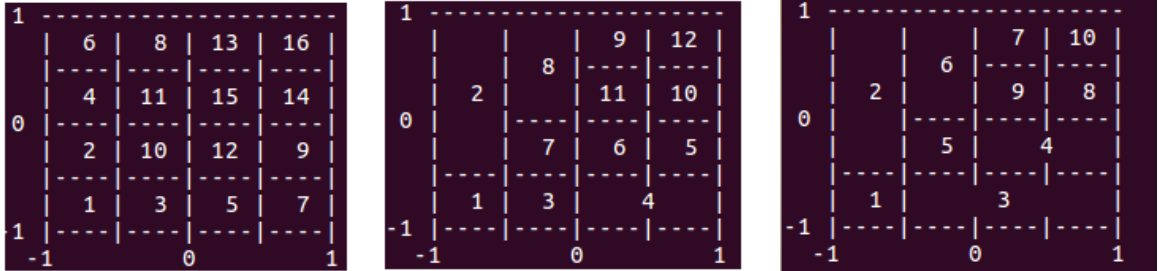


Figure 19: Binning combination scheme.

The bins borders and the resulting cross section limits are shown in Tab. 19:

| Number of bins | Bin borders |            |            |             |            |            | Expected limit   |
|----------------|-------------|------------|------------|-------------|------------|------------|------------------|
|                | $x_1$       | $x_2$      | $x_3$      | $y_1$       | $y_2$      | $y_3$      |                  |
| 16 (default)   | -0.5        | 0.0        | 0.5        | -0.5        | 0.0        | 0.5        | < 2.91           |
| 16             | -0.5        | 0.3        | 0.7        | -0.5        | 0.3        | 0.7        | < 2.83           |
| 10             | -0.5        | 0.0        | 0.5        | -0.5        | 0.0        | 0.5        | < 2.93           |
| 10             | -0.5        | 0.0        | 0.7        | -0.5        | 0.0        | 0.7        | < 2.86           |
| 10             | -0.5        | 0.0        | 0.7        | -0.5        | 0.0        | 0.5        | < 2.84           |
| 10             | -0.5        | 0.0        | 0.5        | -0.5        | 0.0        | 0.7        | < 2.87           |
| <b>10</b>      | <b>-0.5</b> | <b>0.4</b> | <b>0.7</b> | <b>-0.5</b> | <b>0.4</b> | <b>0.7</b> | <b>&lt; 2.81</b> |

Table 19: Limit variation as a function of bin size in the three lepton channel. (In bold: the final bin borders used in the analysis.)

Combining the optimization of binning and using the tighter pre-selection cuts, the expected limit in the three lepton channel alone reaches  $r < 2.59$ .

For same-sign dilepton channel, other binning combinations were also tested. First the three lepton binning was used to estimate the expected limit then bin borders were varied to obtain

the best possible expected limit. The bin borders and the resulting cross section limits for the same-sign dimuon channel are shown in Tab. 20:

| Number of bins | Bin borders |            |            |             |            |            | Expected limit   |
|----------------|-------------|------------|------------|-------------|------------|------------|------------------|
|                | $x_1$       | $x_2$      | $x_3$      | $y_1$       | $y_2$      | $y_3$      |                  |
| 16             | -0.5        | 0.4        | 0.7        | -0.5        | 0.4        | 0.7        | < 1.72           |
| 12             | -0.5        | 0.4        | 0.7        | -0.5        | 0.4        | 0.7        | < 1.72           |
| 12             | -0.3        | 0.4        | 0.7        | -0.5        | 0.4        | 0.7        | < 1.71           |
| 12             | -0.3        | 0.3        | 0.7        | -0.5        | 0.4        | 0.7        | < 1.71           |
| 12             | -0.3        | 0.3        | 0.7        | -0.4        | 0.4        | 0.7        | < 1.70           |
| 12             | -0.3        | 0.3        | 0.7        | -0.3        | 0.4        | 0.7        | < 1.70           |
| 12             | -0.3        | 0.3        | 0.7        | -0.3        | 0.2        | 0.7        | < 1.68           |
| 12             | -0.3        | 0.3        | 0.7        | -0.3        | 0.1        | 0.7        | < 1.70           |
| 12             | -0.3        | 0.3        | 0.7        | -0.3        | 0.2        | 0.6        | < 1.70           |
| 10             | -0.5        | 0.4        | 0.7        | -0.5        | 0.4        | 0.7        | < 1.75           |
| <b>10</b>      | <b>-0.3</b> | <b>0.3</b> | <b>0.7</b> | <b>-0.3</b> | <b>0.2</b> | <b>0.6</b> | <b>&lt; 1.69</b> |

Table 20: Limit variation as a function of bin size in the same-sign dimuon channel. (In bold: the final bin borders used in the analysis.)

The expected limit was found to be  $r < 1.69$  for optimized bin borders in 10 bins.

## 7.4 Other binning strategies

Two further strategies of clustering regions in the 2D plane of  $BDT_{tt}$  vs  $BDT_{t\bar{t}V}$  into bins were attempted, following studies done in the  $t\bar{t}H$  multilepton analysis (and documented in greater detail in [6]).

**Clustering by S/B ratio** The 2D plane is clustered into a given number of bins corresponding to regions where S/B is within a certain range. The bin borders are determined such that the number of background events in each bin is approximately equal. (See Sec. 5.3 in v4 of Ref. [6] for more details.) The resulting regions for same-sign dilepton and three lepton events are shown in Fig. 20, with the expected distribution of signal and main backgrounds in Fig. 21.

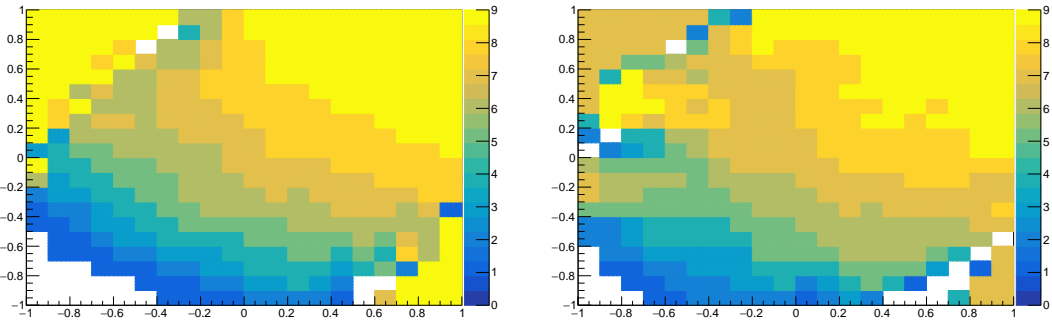


Figure 20: Binning by S/B regions for same-sign dilepton (left) and three leptons (right).

Using this technique, the resulting limits (for the  $\kappa_t = -1, \kappa_V = 1$  scenario) are about 20% worse than with the binnings described above:  $\mu^\pm \mu^\pm$  changed from 1.82 to 2.15,  $\ell\ell\ell$  from 1.52 to 1.75.

**k-Means geometric clustering** A second clustering strategy employs a recursive application of the k-means algorithm (see Appendix D in v4 of Ref. [6]) to separate the 2D plane into geometric

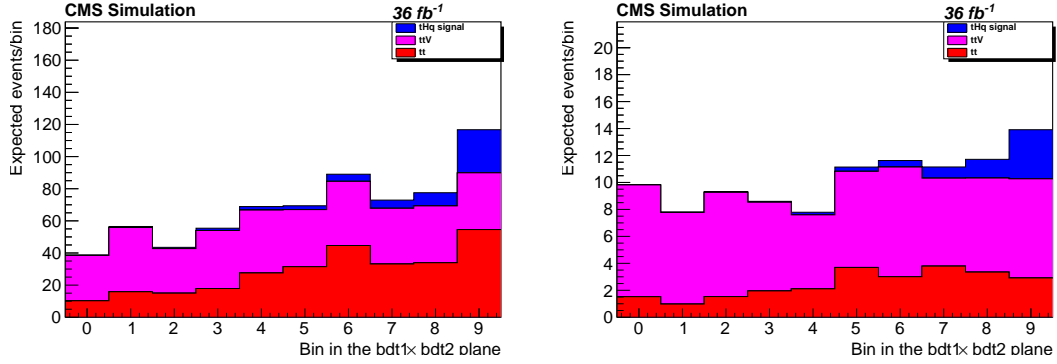


Figure 21: Final bins (corresponding to S/B regions in the 2D plane) for same-sign dilepton (left) and three leptons (right).

regions. The resulting clustering (using the  $t\bar{t}H$  multilepton code on  $tHq$  signal and  $t\bar{t}$  and  $t\bar{t}V$  background events) are shown in Fig. 22. The expected distribution of events for the signal and main background in these bins is shown in Fig. 23.

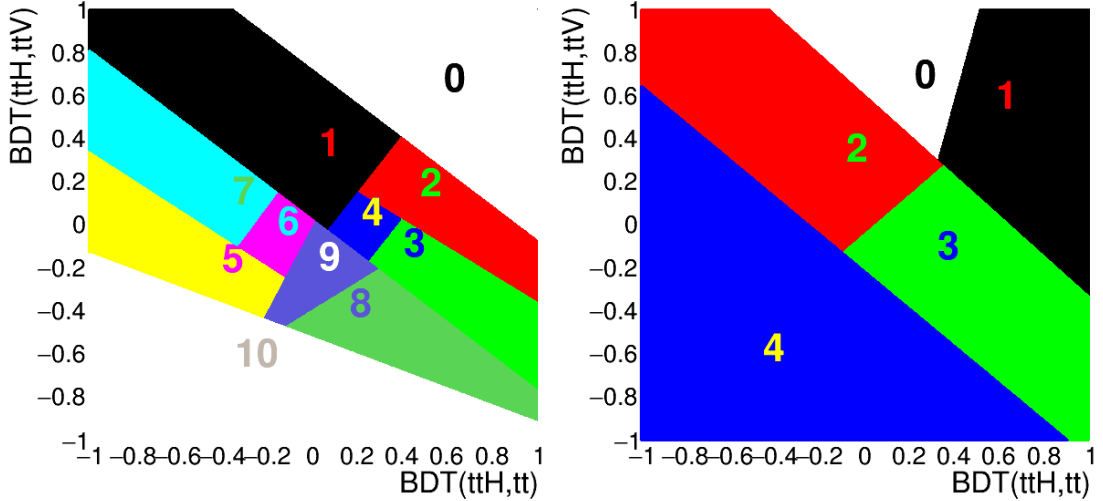


Figure 22: Binning into geometric regions using a  $k$ -means algorithm for same-sign dilepton (left) and three leptons (right).

Similarly to the S/B ratio binning, the limits using the  $k$ -means clustering are significantly worse than those of the bins described before. In the  $\mu^\pm\mu^\pm$  channel, the limit deteriorates from 1.82 to 2.05, whereas in  $\ell\ell\ell$  it changes from 1.58 to 1.78.

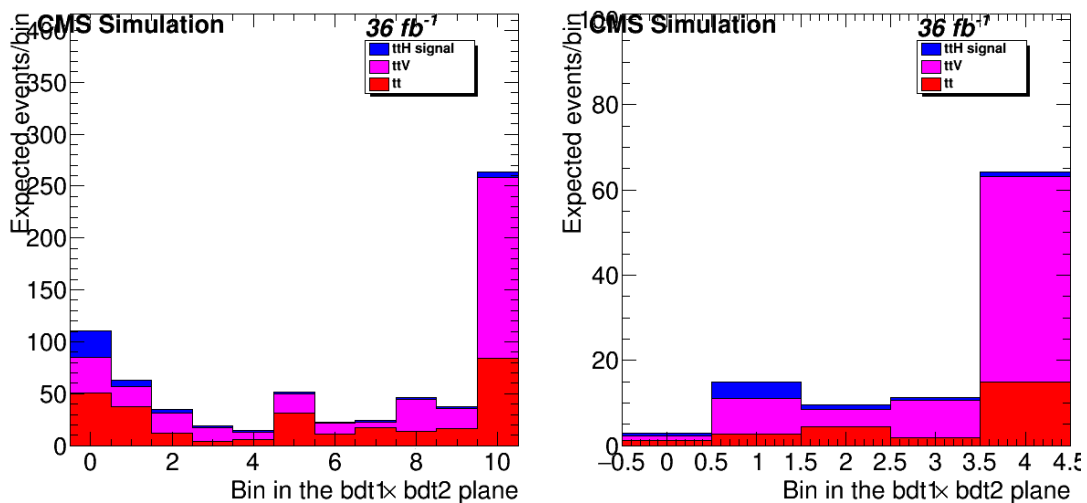


Figure 23: Final bins using a  $k$ -means algorithm for same-sign dilepton (left) and three leptons (right). Note that the bin numbering here is such that signal-like bins are lower.

## 8 Systematics

Table 21 shows all sources of systematic uncertainty currently considered in the analysis.

**Experimental uncertainties** A normalization uncertainty is derived from the measurement of data/MC scale factors for lepton and trigger efficiencies. Jet energy scale uncertainties and b tagging efficiency are evaluated using dedicated shape templates derived from a variation of the jet energy scale within its uncertainty and from varying the b tagging data/MC scale factors within their uncertainty.

The forward jet  $\eta$  distribution is poorly modeled in simulation, see Appendix A.3. To estimate the effect of a mismodeled forward jet distribution, we reweight the events in simulation (i.e. for signal and the irreducible backgrounds) based on the normalized data/MC ratio in the control region and thereby derive an alternative shape of the BDT output distributions that reflects a hypothetical perfect data/MC agreement.

**Theory uncertainties**  $Q^2$  scale and parton distribution function (pdf) uncertainties are applied as an overall normalization uncertainty using numbers from the NLO theory calculation.

**Backgrounds** In addition to the theory uncertainties on the main irreducible backgrounds of  $t\bar{t}W$ ,  $t\bar{t}Z$ , and  $t\bar{t}H$ , the smaller irreducible backgrounds and the charge mis-identification estimate are covered with flat normalization uncertainties. The WZ contribution is normalized in a data control region and an uncertainty on the scale factor is derived in the process. Finally, the dominant uncertainty relates to the estimate of the reducible non-prompt lepton contribution using a fake rate method. The main normalization uncertainty on the used fake rates derives from limited statistics in the data control region, and the subtraction of residual prompt lepton contribution, see Ref. [6]. Furthermore, shape variations resembling data/MC differences and deviations in closure test are evaluated as shape uncertainties.

**Fake rate closure uncertainties** The BDT output shapes are compared between a pure MC estimation of fake leptons (in  $t\bar{t}$ ), and an application of fake-rates as measured in QCD MC, applied in  $t\bar{t}$  MC events. The difference in the resulting normalization and output shapes, both the training vs.  $t\bar{t}$  and vs.  $t\bar{t}V$ , are estimated and propagated to the fit as normalization and shape variations. See Figs 24 to 29 for the results of these closure tests and Tab. 21 for the resulting pre-fit uncertainties.

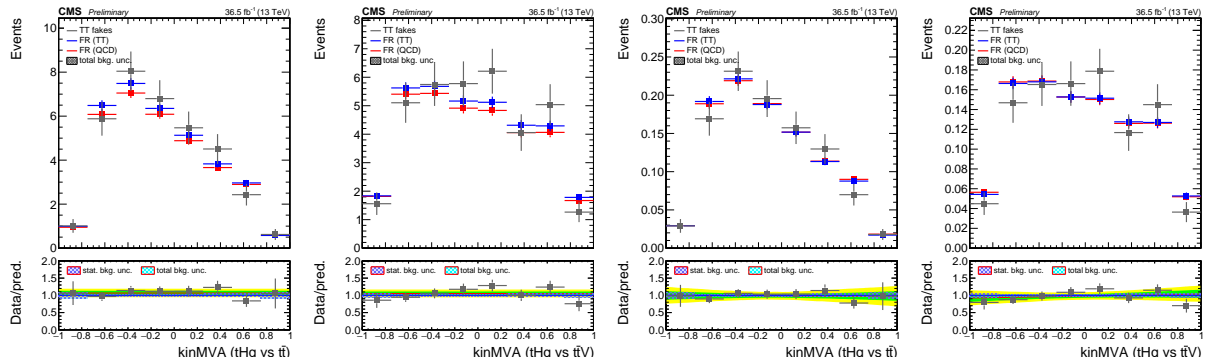


Figure 24: BDT outputs comparing  $t\bar{t}$  MC to a fake-rate prediction using fake rates measured in QCD MC. Agreement in normalization is estimated from the left two plots, shape disagreement is estimated from the right two (normalized) plots. Same-sign  $e^\pm e^\pm$  selection.

| Source                            | Channel   | Size  |
|-----------------------------------|---|---|
| <b>Experimental uncertainties</b> |   |   |
| Luminosity                        | all   | 1.026   |
| Loose lepton efficiency           |   | 1.02 per lepton   |
| Tight lepton efficiency           |   | 1.03 per lepton   |
| Trigger efficiency                | $\mu^\pm\mu^\pm$<br>$e^\pm\mu^\pm$<br>$e^\pm e^\pm$<br>$\ell\ell\ell$ | 1.01<br>1.01<br>1.02<br>1.03  |
| Jet energy scale                  | all   | templates   |
| Forward jet modeling              | all   | templates, see Tab. 26  |
| b tagging efficiency              | all   | templates   |
| <b>Theory uncertainties</b>       |   |   |
| $Q^2$ scale ( $tHq$ )             | all   | 0.92–1.06 (depending on $\kappa_t, \kappa_V$ )  |
| $Q^2$ scale ( $tHW$ )             | all   | 0.93–1.05 (depending on $\kappa_t, \kappa_V$ )  |
| $Q^2$ scale ( $t\bar{t}H$ )       | all   | 0.915/1.058   |
| $Q^2$ scale ( $t\bar{t}W$ )       | all   | 1.12  |
| $Q^2$ scale ( $t\bar{t}Z$ )       | all   | 1.11  |
| pdf ( $t\bar{t}H$ )               | all   | 1.036   |
| pdf gg ( $t\bar{t}Z$ )            | all   | 0.966   |
| pdf $q\bar{q}$ ( $t\bar{t}W$ )    | all   | 1.04  |
| pdf qg ( $tHq$ )                  | all   | 1.037   |
| pdf qg ( $tHW$ )                  | all   | 1.040   |
| <b>Higgs branching fractions</b>  |   |   |
| param_alphaS                      | all   | 1.012   |
| param_mB                          | all   | 0.981   |
| HiggsDecayWidthTHU_hqq            | all   | 0.988   |
| HiggsDecayWidthTHU_hvv            | all   | 1.004   |
| HiggsDecayWidthTHU_hll            | all   | 1.019   |
| <b>Backgrounds</b>                |   |   |
| WZ control region statistics      | $\ell\ell\ell$  | 1.10  |
| WZ control region backgrounds     | $\ell\ell\ell$  | 1.20  |
| WZ modeling                       | $\ell\ell\ell$  | 1.07  |
| WZ + 2jet background              | $\mu^\pm\mu^\pm, e^\pm\mu^\pm$  | 1.50  |
| Rare SM processes                 | all   | 1.50  |
| Charge flips                      | $e^\pm\mu^\pm$  | 1.30  |
| <b>Fake rate estimate</b>         |   |   |
| Electron FR measurement           |   | templates   |
| Muon FR measurement               |   | templates   |
| Electron closure                  | $e^\pm e^\pm$<br>$e^\pm\mu^\pm$<br>$\ell\ell\ell$                     | 1.05 norm., $(0.99(t\bar{t})/1.06(t\bar{t}V))$ shape var.<br>0.94 norm., $(0.98(t\bar{t})/1.07(t\bar{t}V))$ shape var.<br>1.40 norm., $(1.09(t\bar{t})/1.05(t\bar{t}V))$ shape var. |
| Muon closure                      | $\mu^\pm\mu^\pm$<br>$e^\pm\mu^\pm$<br>$\ell\ell\ell$                  | 1.07 norm., $(0.97(t\bar{t})/0.91(t\bar{t}V))$ shape var.<br>1.09 norm., $(1.06(t\bar{t})/1.03(t\bar{t}V))$ shape var.<br>1.09 norm., $(0.95(t\bar{t})/0.83(t\bar{t}V))$ shape var. |

Table 21: Pre-fit size of systematic uncertainties.

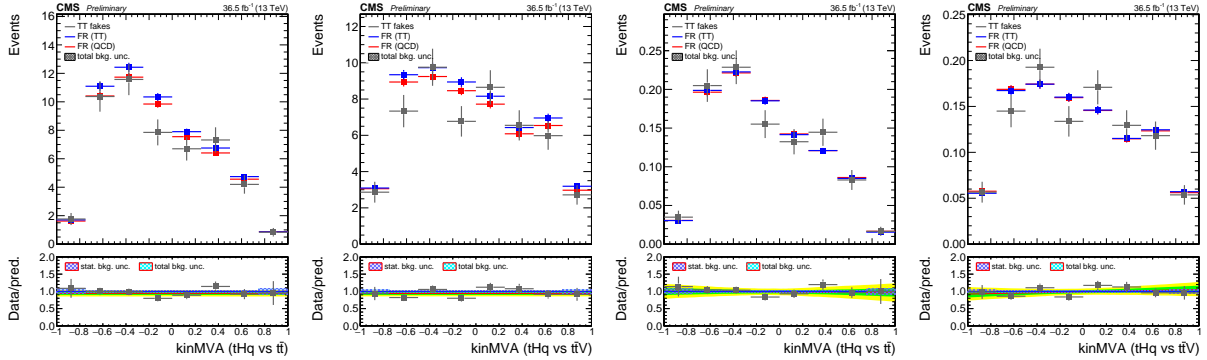


Figure 25: BDT outputs comparing  $t\bar{t}$  MC to a fake-rate prediction using fake rates measured in QCD MC. Agreement in normalization is estimated from the left two plots, shape disagreement is estimated from the right two (normalized) plots. Same-sign  $e^\pm \mu^\pm$  selection with electron fakes.

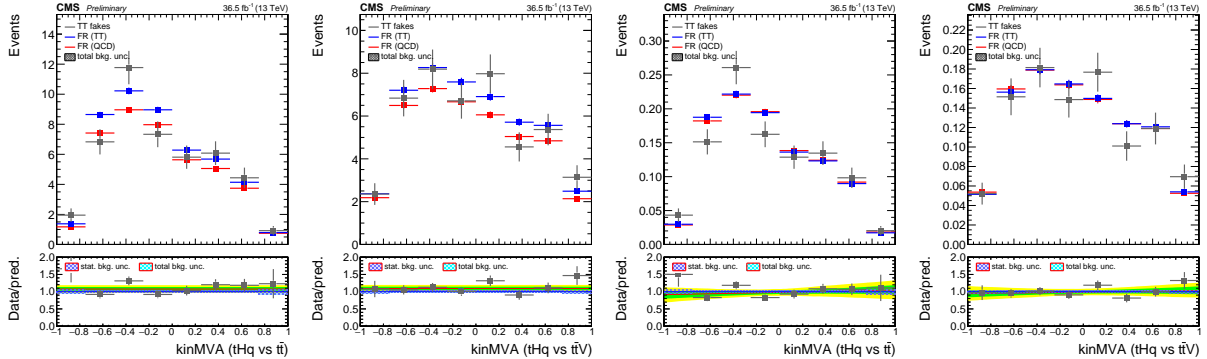


Figure 26: BDT outputs comparing  $t\bar{t}$  MC to a fake-rate prediction using fake rates measured in QCD MC. Agreement in normalization is estimated from the left two plots, shape disagreement is estimated from the right two (normalized) plots. Same-sign  $e^\pm \mu^\pm$  selection with muon fakes.

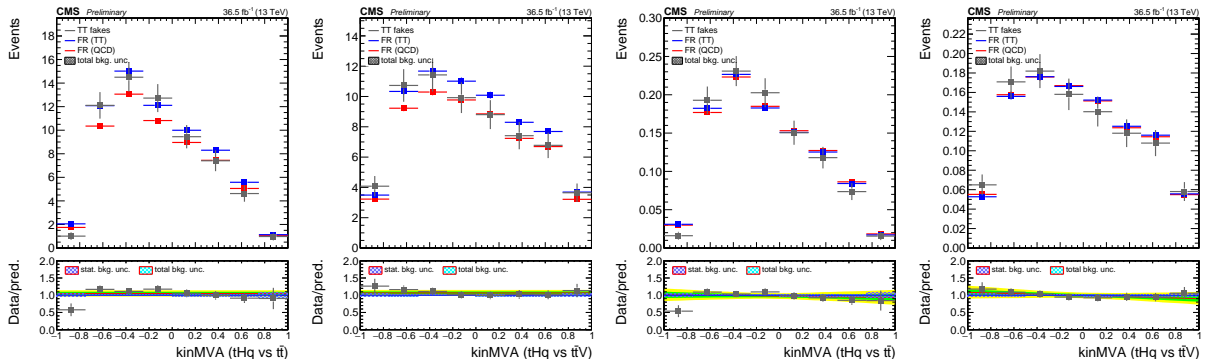


Figure 27: BDT outputs comparing  $t\bar{t}$  MC to a fake-rate prediction using fake rates measured in QCD MC. Agreement in normalization is estimated from the left two plots, shape disagreement is estimated from the right two (normalized) plots. Same-sign  $\mu^\pm \mu^\pm$  selection.

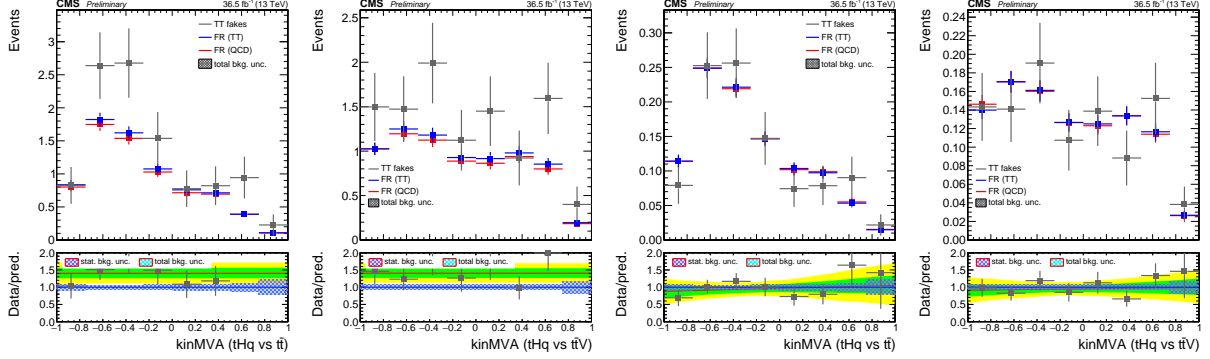


Figure 28: BDT outputs comparing  $t\bar{t}$  MC to a fake-rate prediction using fake rates measured in QCD MC. Agreement in normalization is estimated from the left two plots, shape disagreement is estimated from the right two (normalized) plots. Three lepton selection with electron fakes.

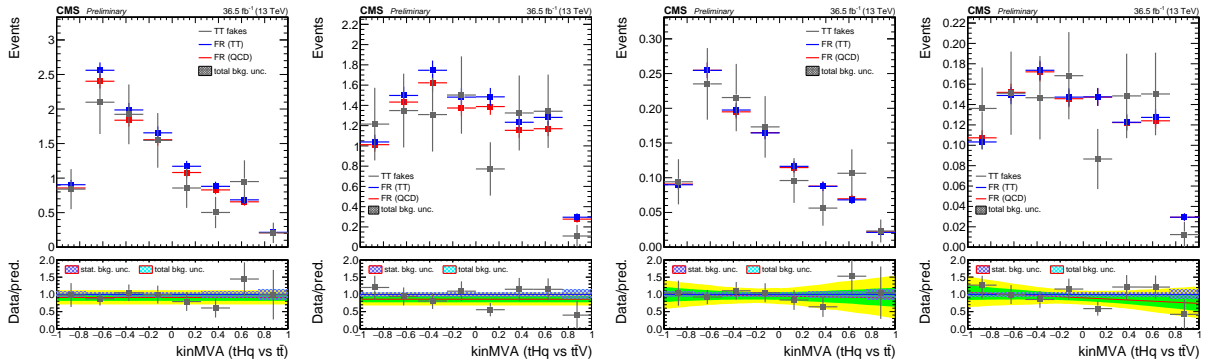


Figure 29: BDT outputs comparing  $t\bar{t}$  MC to a fake-rate prediction using fake rates measured in QCD MC. Agreement in normalization is estimated from the left two plots, shape disagreement is estimated from the right two (normalized) plots. Three lepton selection with muon fakes.

## 9 Results

The unblinded distributions of BDT outputs are shown in Fig. 30. The pre-fit distributions in the final binning used in the signal extraction are shown in Fig. 31, with the post-fit distributions shown in Fig. 32.

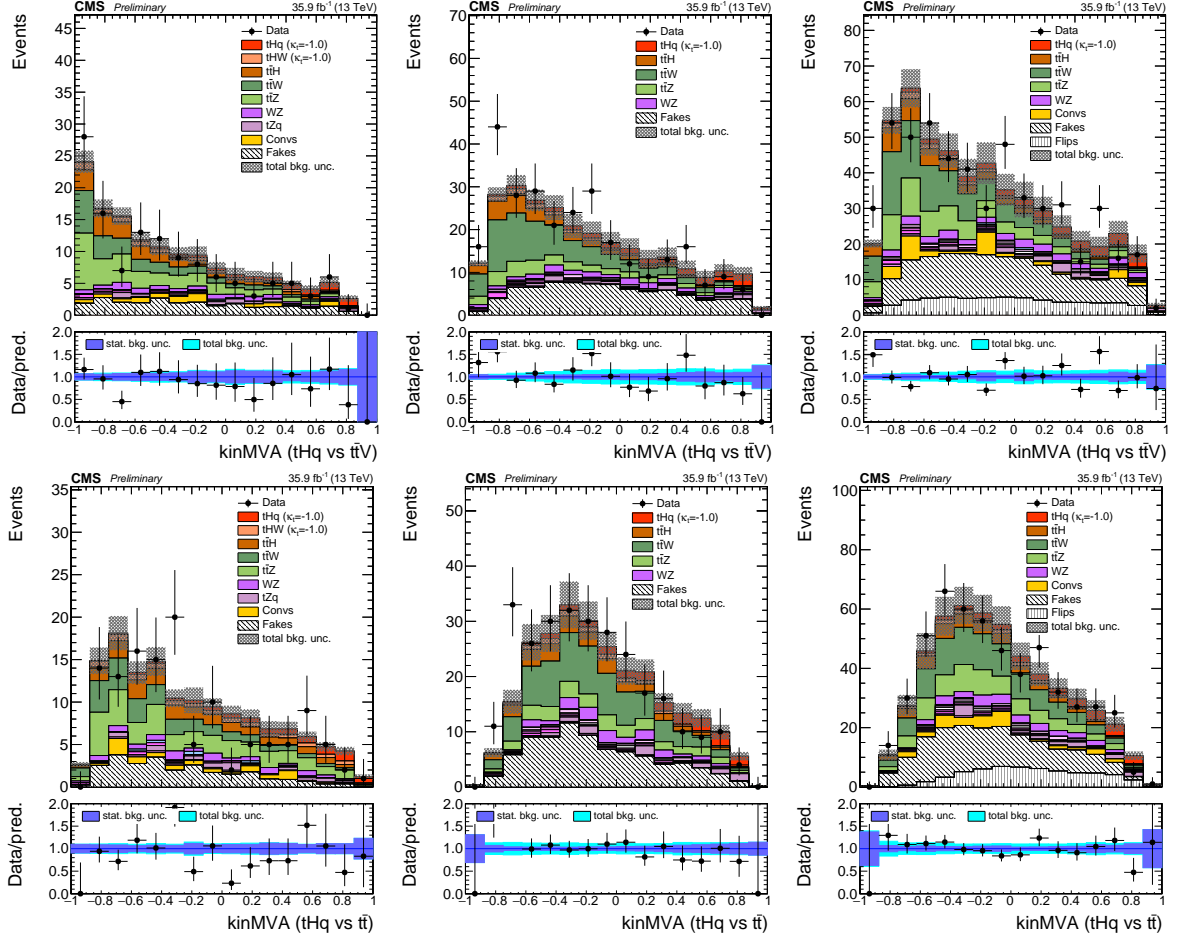


Figure 30: Distribution of individual BDT outputs for (from left to right) the three lepton channel, the  $\mu^\pm\mu^\pm$  channel, and the  $e^\pm\mu^\pm$  channel, for training against  $t\bar{t}V$  (top row) and against  $t\bar{t}$  (bottom row).

We calculate asymptotic upper  $CL_S$  limits at 95% C.L. on the combined production cross section of  $tHq$ ,  $tHW$ , and  $t\bar{t}H$  (reported as an upper limit on the cross section times modified branching ratio), for each of the 51 coupling configurations, see Tab. 22. The limits and best-fit values of the signal cross section (and corresponding signal strength at  $\kappa_V = 1.0$ ) for each point are given in Tab. 24, and in Tab. 23 for the two main hypotheses, split by channel. In the SM point a signal strength of  $1.82^{+0.34}_{-0.33}(\text{stat.})^{+0.55}_{-0.59}(\text{syst.})$  (compared to the SM cross section at  $\kappa_V = 1.0$ ) is obtained, corresponding to a cross section of  $0.33 \pm 0.12 \text{ pb}$ . The observed significance of the signal, in a background-only hypothesis, is  $2.7\sigma$ , with an a-priori expected significance of  $1.5\sigma$ . Without considering systematic uncertainties, the significance increases to  $6.2\sigma$ . A scan of the observed and expected significances for each coupling configuration is shown in Fig. 38.

The pulls and impacts of the most important nuisance parameters are shown in Fig. 39.

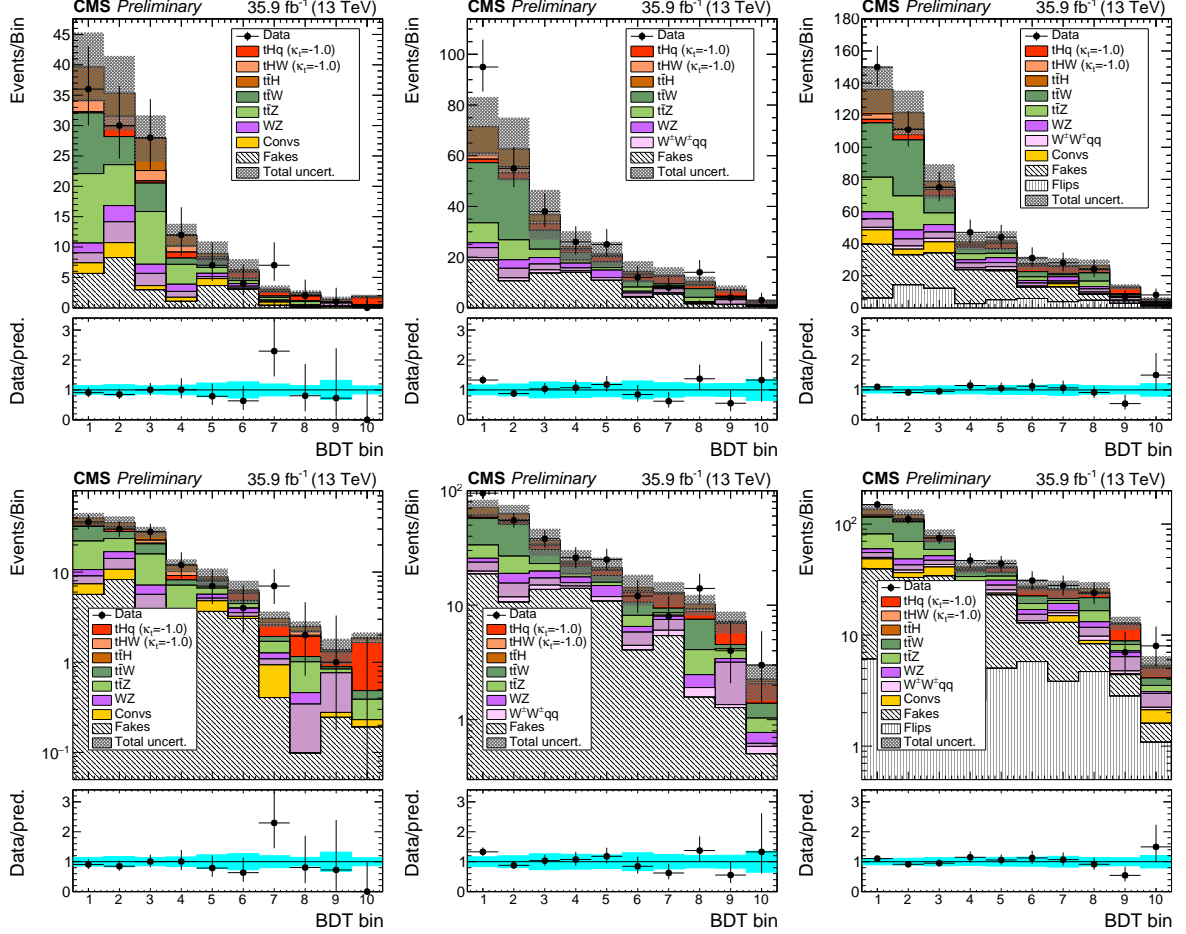


Figure 31: Expected (pre-fit) distributions in the final binning used for the signal extraction, for (from left to right) the three lepton channel, the  $\mu^\pm\mu^\pm$  channel, and the  $e^\pm\mu^\pm$  channel. Linear scale (top row), and logarithmic scale (bottom row).

| Scenario          | Channel                            | Obs. Limit | Exp. Limit |            |             |            |            |
|-------------------|------------------------------------|------------|------------|------------|-------------|------------|------------|
|                   |                                    |            | $-2\sigma$ | $-1\sigma$ | Median      | $+1\sigma$ | $+2\sigma$ |
| $\kappa_V = 1.0$  | $\mu^\pm\mu^\pm$                   | 2.3        | 0.71       | 0.94       | 1.32        | 1.88       | 2.60       |
| $\kappa_t = -1.0$ | $e^\pm\mu^\pm$                     | 1.9        | 0.65       | 0.87       | 1.21        | 1.71       | 2.32       |
|                   | $\ell\ell\ell$                     | 1.6        | 0.43       | 0.59       | 0.86        | 1.26       | 1.78       |
|                   | Combined ( $\mu\mu, 3\ell$ )       | <b>1.6</b> | 0.40       | 0.54       | <b>0.78</b> | 1.12       | 1.57       |
|                   | Combined ( $\mu\mu, e\mu, 3\ell$ ) | <b>1.4</b> | 0.37       | 0.50       | <b>0.71</b> | 1.03       | 1.43       |
| (SM)              | $\mu^\pm\mu^\pm$                   | 4.9        | 1.20       | 1.61       | 2.27        | 3.24       | 4.54       |
| $\kappa_V = 1.0$  | $e^\pm\mu^\pm$                     | 3.3        | 1.10       | 1.48       | 2.07        | 2.95       | 4.06       |
| $\kappa_t = 1.0$  | $\ell\ell\ell$                     | 3.0        | 0.91       | 1.22       | 1.73        | 2.49       | 3.47       |
|                   | Combined ( $\mu\mu, 3\ell$ )       | <b>3.4</b> | 0.79       | 1.07       | <b>1.51</b> | 2.17       | 3.01       |
|                   | Combined ( $\mu\mu, e\mu, 3\ell$ ) | <b>3.1</b> | 0.71       | 0.96       | <b>1.36</b> | 1.94       | 2.70       |

Table 22: Expected and observed CL<sub>S</sub> limits (at 95% C.L.) on the signal strength of combined tH + t̄H production in each channel, and for different combinations thereof, for a scenario with inverted couplings ( $\kappa_V = 1.0, \kappa_t = -1.0$ , top section), and for the standard model ( $\kappa_V = \kappa_t = 1.0$ , bottom section). Numbers are for  $35.9 \text{ fb}^{-1}$ .

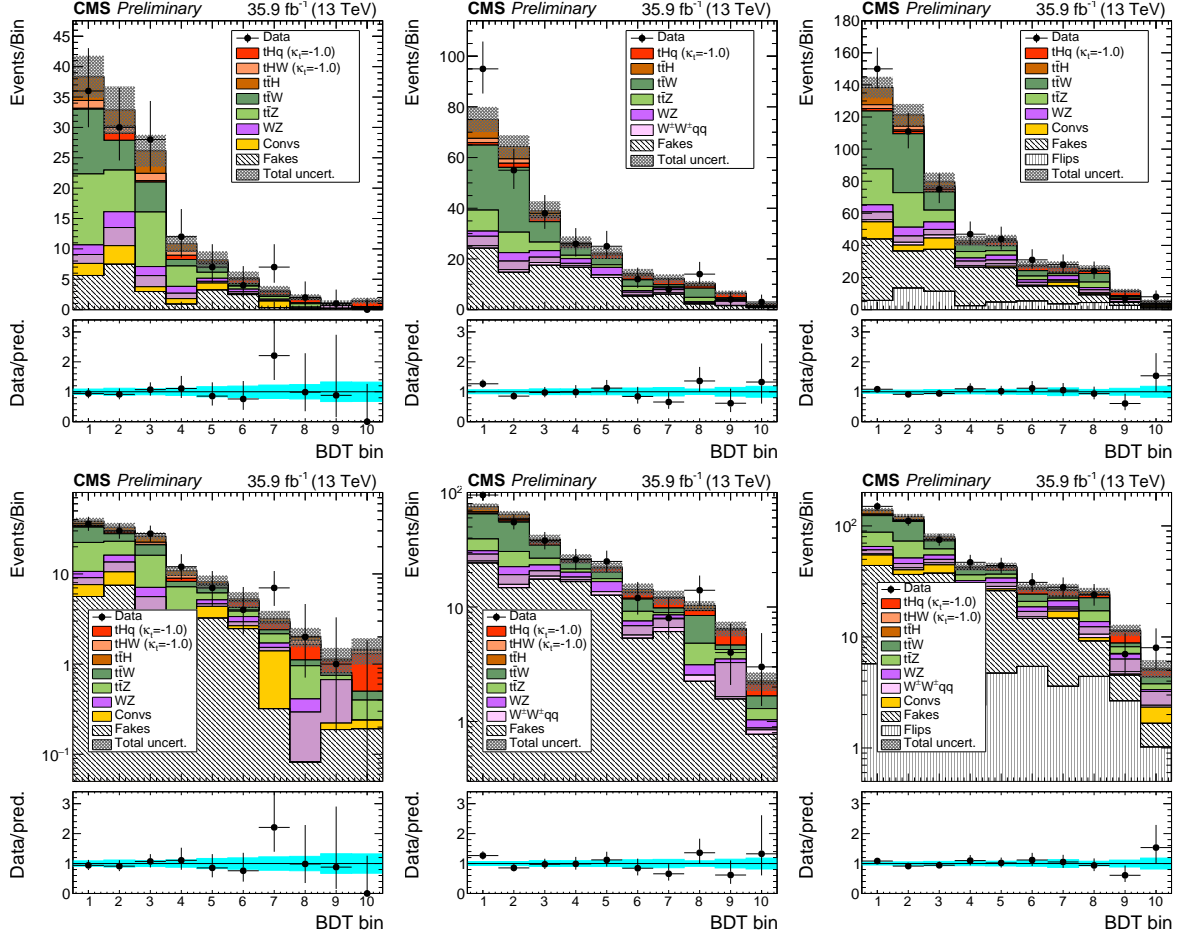


Figure 32: Post-fit distributions in the final binning used for the signal extraction, for (from left to right) the three lepton channel, the  $\mu^\pm\mu^\pm$  channel, and the  $e^\pm\mu^\pm$  channel. Linear scale (top row), and logarithmic scale (bottom row).

| Scenario                             | Channel          | Obs. Limit<br>(pb) | Exp. Limit (pb) |               |               |
|--------------------------------------|------------------|--------------------|-----------------|---------------|---------------|
|                                      |                  |                    | Median          | $\pm 1\sigma$ | $\pm 2\sigma$ |
| $\kappa_t/\kappa_V = -1$             | $\mu^\pm\mu^\pm$ | 1.00               | 0.58            | [0.42, 0.83]  | [0.31, 1.15]  |
|                                      | $e^\pm\mu^\pm$   | 0.84               | 0.54            | [0.39, 0.76]  | [0.29, 1.03]  |
|                                      | $\ell\ell\ell$   | 0.70               | 0.38            | [0.26, 0.56]  | [0.19, 0.79]  |
|                                      | Combined         | <b>0.64</b>        | <b>0.32</b>     | [0.22, 0.46]  | [0.16, 0.64]  |
| $\kappa_t/\kappa_V = 1$<br>(SM-like) | $\mu^\pm\mu^\pm$ | 0.87               | 0.41            | [0.29, 0.58]  | [0.22, 0.82]  |
|                                      | $e^\pm\mu^\pm$   | 0.59               | 0.37            | [0.26, 0.53]  | [0.20, 0.73]  |
|                                      | $\ell\ell\ell$   | 0.54               | 0.31            | [0.22, 0.43]  | [0.16, 0.62]  |
|                                      | Combined         | <b>0.56</b>        | <b>0.24</b>     | [0.17, 0.35]  | [0.13, 0.49]  |

Table 23: Expected and observed 95% C.L. upper limits on the  $tH + \bar{t}\bar{H}$  production cross section times  $H \rightarrow^* \tau\tau + ZZ^*$  branching ratio for a scenario of inverted couplings ( $\kappa_t/\kappa_V = -1.0$ , top rows) and for a standard-model-like signal ( $\kappa_t/\kappa_V = 1.0$ , bottom rows), in pb. The expected limit is calculated on a background-only Asimov dataset and quoted with  $\pm 1\sigma$  and  $\pm 2\sigma$  probability ranges.

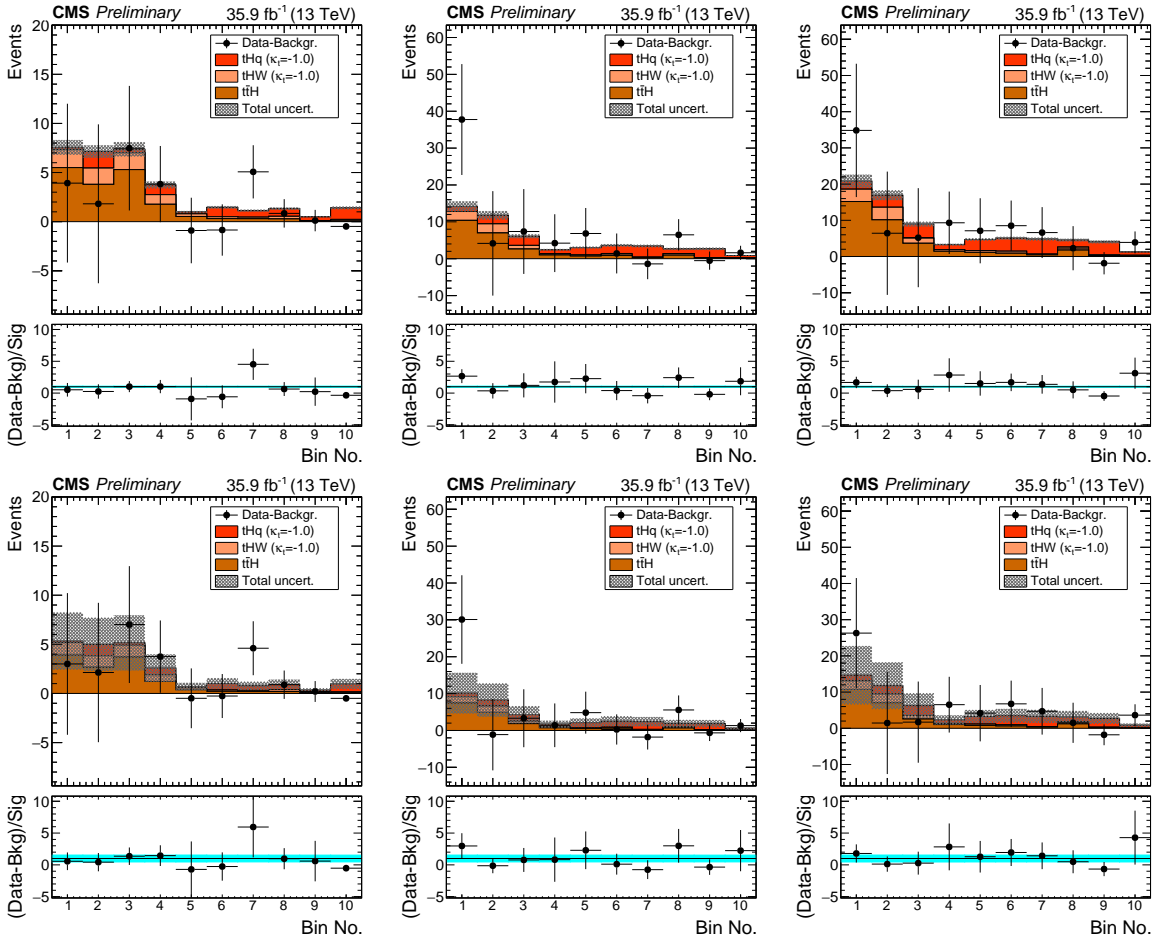


Figure 33: Background-subtracted pre- (top) and post-fit (bottom) distributions in the final binning used for the signal extraction, for (from left to right) the three lepton channel, the  $\mu^{\pm}\mu^{\pm}$  channel, and the  $e^{\pm}\mu^{\pm}$  channel. For a fit in the inverted couplings scenario, as Figs. 31 and 32.

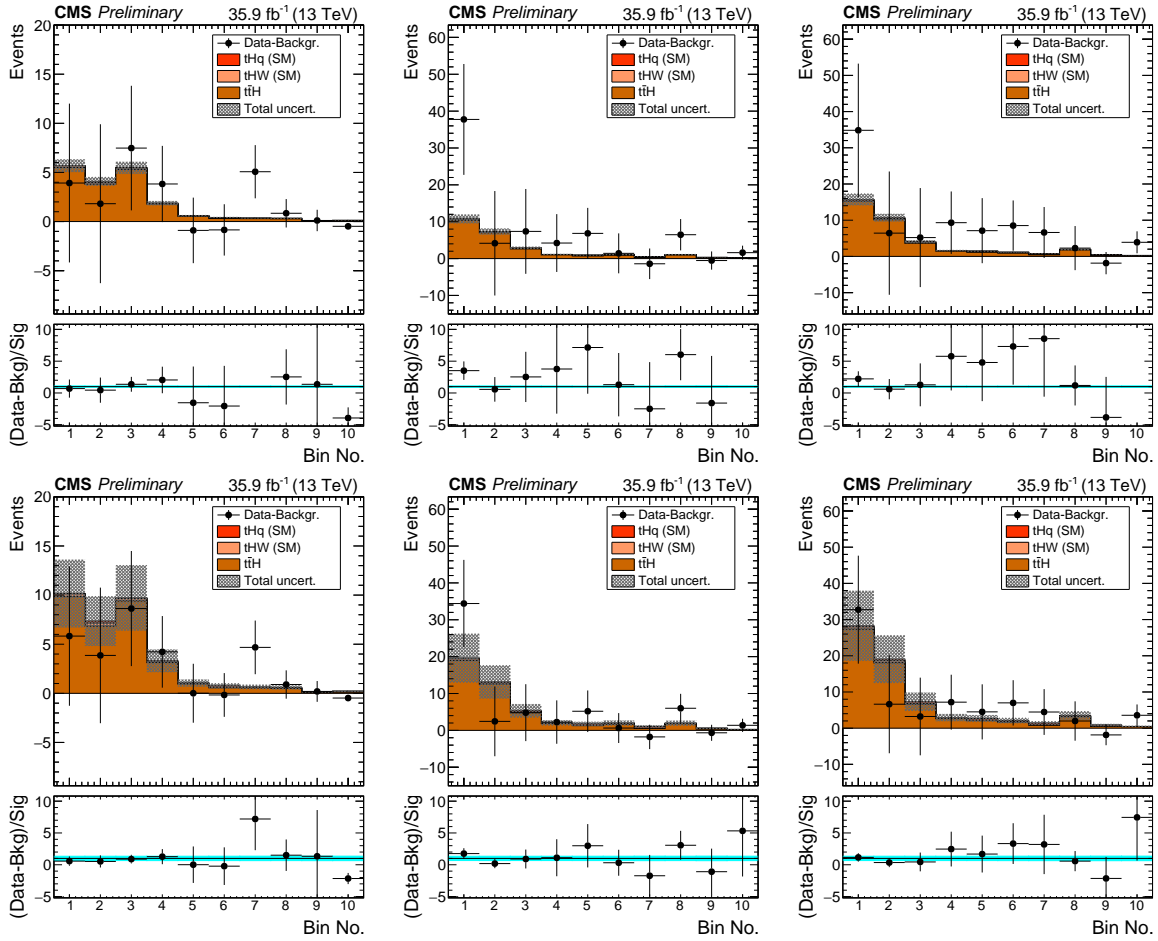


Figure 34: Background-subtracted pre- (top) and post-fit (bottom) distributions in the final binning used for the signal extraction, for (from left to right) the three lepton channel, the  $\mu^\pm\mu^\pm$  channel, and the  $e^\pm\mu^\pm$  channel. For a fit in the SM-like scenario ( $\kappa_t = \kappa_V = 1$ ).

| $f_t$  | $\kappa_t/\kappa_V$ | Exp. lim.                  | SM exp.                    | Obs. lim. | Best fit $\sigma$ [pb]     | Best fit $r$               |
|--------|---------------------|----------------------------|----------------------------|-----------|----------------------------|----------------------------|
| -0.973 | -6.000              | 0.328 $^{+0.136}_{-0.090}$ | 0.507 $^{+0.206}_{-0.158}$ | 0.603     | 0.305 $^{+0.155}_{-0.169}$ | 0.013 $^{+0.007}_{-0.007}$ |
| -0.941 | -4.000              | 0.335 $^{+0.137}_{-0.098}$ | 0.509 $^{+0.215}_{-0.166}$ | 0.627     | 0.322 $^{+0.157}_{-0.174}$ | 0.036 $^{+0.018}_{-0.020}$ |
| -0.900 | -3.000              | 0.335 $^{+0.138}_{-0.096}$ | 0.510 $^{+0.215}_{-0.172}$ | 0.639     | 0.334 $^{+0.160}_{-0.173}$ | 0.075 $^{+0.036}_{-0.039}$ |
| -0.862 | -2.500              | 0.334 $^{+0.139}_{-0.097}$ | 0.505 $^{+0.217}_{-0.173}$ | 0.649     | 0.341 $^{+0.160}_{-0.174}$ | 0.119 $^{+0.056}_{-0.061}$ |
| -0.800 | -2.000              | 0.330 $^{+0.141}_{-0.095}$ | 0.500 $^{+0.212}_{-0.176}$ | 0.656     | 0.345 $^{+0.165}_{-0.176}$ | 0.202 $^{+0.097}_{-0.103}$ |
| -0.692 | -1.500              | 0.325 $^{+0.139}_{-0.095}$ | 0.485 $^{+0.209}_{-0.172}$ | 0.660     | 0.340 $^{+0.164}_{-0.176}$ | 0.369 $^{+0.178}_{-0.191}$ |
| -0.640 | -1.333              | 0.325 $^{+0.139}_{-0.097}$ | 0.482 $^{+0.210}_{-0.173}$ | 0.659     | 0.334 $^{+0.169}_{-0.174}$ | 0.456 $^{+0.231}_{-0.238}$ |
| -0.610 | -1.250              | 0.321 $^{+0.140}_{-0.095}$ | 0.474 $^{+0.210}_{-0.169}$ | 0.653     | 0.328 $^{+0.164}_{-0.177}$ | 0.505 $^{+0.252}_{-0.272}$ |
| -0.500 | -1.000              | 0.315 $^{+0.142}_{-0.093}$ | 0.450 $^{+0.213}_{-0.160}$ | 0.638     | 0.304 $^{+0.175}_{-0.176}$ | 0.685 $^{+0.395}_{-0.396}$ |
| -0.410 | -0.833              | 0.312 $^{+0.138}_{-0.095}$ | 0.424 $^{+0.210}_{-0.147}$ | 0.615     | 0.276 $^{+0.168}_{-0.177}$ | 0.819 $^{+0.498}_{-0.526}$ |
| -0.360 | -0.750              | 0.307 $^{+0.138}_{-0.093}$ | 0.409 $^{+0.200}_{-0.136}$ | 0.593     | 0.256 $^{+0.170}_{-0.176}$ | 0.874 $^{+0.581}_{-0.601}$ |
| -0.308 | -0.667              | 0.301 $^{+0.138}_{-0.092}$ | 0.384 $^{+0.198}_{-0.124}$ | 0.566     | 0.231 $^{+0.165}_{-0.174}$ | 0.915 $^{+0.655}_{-0.689}$ |
| -0.200 | -0.500              | 0.292 $^{+0.136}_{-0.090}$ | 0.345 $^{+0.181}_{-0.109}$ | 0.497     | 0.166 $^{+0.163}_{-0.162}$ | 0.895 $^{+0.879}_{-0.871}$ |
| -0.100 | -0.333              | 0.278 $^{+0.132}_{-0.086}$ | 0.303 $^{+0.156}_{-0.092}$ | 0.409     | 0.092 $^{+0.157}_{-0.162}$ | 0.679 $^{+1.159}_{-0.679}$ |
| -0.059 | -0.250              | 0.268 $^{+0.129}_{-0.083}$ | 0.283 $^{+0.152}_{-0.085}$ | 0.365     | 0.059 $^{+0.148}_{-0.059}$ | 0.515 $^{+1.285}_{-0.515}$ |
| -0.027 | -0.167              | 0.260 $^{+0.125}_{-0.081}$ | 0.266 $^{+0.135}_{-0.077}$ | 0.328     | 0.029 $^{+0.142}_{-0.029}$ | 0.297 $^{+1.434}_{-0.297}$ |
| 0.000  | 0.000               | 0.254 $^{+0.123}_{-0.079}$ | 0.252 $^{+0.123}_{-0.073}$ | 0.294     | 0.000 $^{+0.132}_{-0.000}$ | 0.002 $^{+1.776}_{-0.002}$ |
| 0.027  | 0.167               | 0.275 $^{+0.132}_{-0.086}$ | 0.284 $^{+0.148}_{-0.084}$ | 0.357     | 0.040 $^{+0.154}_{-0.040}$ | 0.650 $^{+2.514}_{-0.650}$ |
| 0.059  | 0.250               | 0.297 $^{+0.141}_{-0.093}$ | 0.329 $^{+0.171}_{-0.099}$ | 0.458     | 0.119 $^{+0.183}_{-0.119}$ | 2.015 $^{+3.098}_{-2.015}$ |
| 0.100  | 0.333               | 0.322 $^{+0.148}_{-0.099}$ | 0.405 $^{+0.220}_{-0.135}$ | 0.611     | 0.246 $^{+0.166}_{-0.184}$ | 4.147 $^{+2.802}_{-3.103}$ |
| 0.200  | 0.500               | 0.324 $^{+0.141}_{-0.096}$ | 0.505 $^{+0.212}_{-0.181}$ | 0.730     | 0.413 $^{+0.150}_{-0.177}$ | 5.982 $^{+2.174}_{-2.559}$ |
| 0.308  | 0.667               | 0.281 $^{+0.122}_{-0.082}$ | 0.462 $^{+0.172}_{-0.159}$ | 0.651     | 0.382 $^{+0.136}_{-0.144}$ | 4.186 $^{+1.492}_{-1.574}$ |
| 0.360  | 0.750               | 0.268 $^{+0.116}_{-0.079}$ | 0.442 $^{+0.160}_{-0.154}$ | 0.620     | 0.364 $^{+0.130}_{-0.135}$ | 3.392 $^{+1.214}_{-1.253}$ |
| 0.410  | 0.833               | 0.258 $^{+0.112}_{-0.075}$ | 0.427 $^{+0.162}_{-0.147}$ | 0.599     | 0.351 $^{+0.127}_{-0.130}$ | 2.754 $^{+0.999}_{-1.022}$ |
| 0.500  | 1.000               | 0.244 $^{+0.105}_{-0.072}$ | 0.401 $^{+0.154}_{-0.137}$ | 0.562     | 0.328 $^{+0.118}_{-0.121}$ | 1.821 $^{+0.657}_{-0.671}$ |
| 0.610  | 1.250               | 0.240 $^{+0.104}_{-0.070}$ | 0.394 $^{+0.154}_{-0.133}$ | 0.545     | 0.315 $^{+0.118}_{-0.119}$ | 1.072 $^{+0.399}_{-0.403}$ |
| 0.640  | 1.333               | 0.242 $^{+0.105}_{-0.071}$ | 0.398 $^{+0.156}_{-0.136}$ | 0.547     | 0.316 $^{+0.122}_{-0.121}$ | 0.921 $^{+0.354}_{-0.352}$ |
| 0.692  | 1.500               | 0.244 $^{+0.106}_{-0.071}$ | 0.401 $^{+0.159}_{-0.136}$ | 0.543     | 0.312 $^{+0.120}_{-0.120}$ | 0.678 $^{+0.262}_{-0.261}$ |
| 0.800  | 2.000               | 0.256 $^{+0.109}_{-0.075}$ | 0.416 $^{+0.169}_{-0.138}$ | 0.552     | 0.311 $^{+0.121}_{-0.127}$ | 0.317 $^{+0.123}_{-0.129}$ |
| 0.862  | 2.500               | 0.268 $^{+0.114}_{-0.078}$ | 0.433 $^{+0.169}_{-0.142}$ | 0.558     | 0.310 $^{+0.127}_{-0.130}$ | 0.170 $^{+0.070}_{-0.072}$ |
| 0.900  | 3.000               | 0.276 $^{+0.118}_{-0.080}$ | 0.442 $^{+0.177}_{-0.144}$ | 0.563     | 0.308 $^{+0.128}_{-0.134}$ | 0.102 $^{+0.042}_{-0.044}$ |
| 0.941  | 4.000               | 0.290 $^{+0.122}_{-0.084}$ | 0.459 $^{+0.184}_{-0.149}$ | 0.566     | 0.304 $^{+0.134}_{-0.140}$ | 0.046 $^{+0.020}_{-0.021}$ |
| 0.973  | 6.000               | 0.306 $^{+0.122}_{-0.081}$ | 0.474 $^{+0.192}_{-0.150}$ | 0.571     | 0.300 $^{+0.131}_{-0.150}$ | 0.016 $^{+0.007}_{-0.008}$ |

Table 24: Expected (for background only, and for a SM-like Higgs signal) and observed 95% C.L. upper limits (in pb), and best fit signal strength  $r$  and corresponding best fit cross section for the combined  $tH + t\bar{t}H$  cross section times modified branching ratio for the combination of all three channels, for different values of  $\kappa_t/\kappa_V$  or the equivalent  $f_t$  numbers.

|                   |                            |
|-------------------|----------------------------|
| $\ell\ell\ell$    | $r = 1.44_{-0.84}^{+0.91}$ |
| $e^\pm \mu^\pm$   | $r = 1.42_{-1.03}^{+1.06}$ |
| $\mu^\pm \mu^\pm$ | $r = 2.75_{-1.11}^{+1.22}$ |
| Combined          | $r = 1.82_{-0.69}^{+0.76}$ |
| Expected          | $r = 1.00_{-0.65}^{+0.70}$ |

Table 25: Best-fit signal strengths for a SM-like Higgs signal for the individual channels.

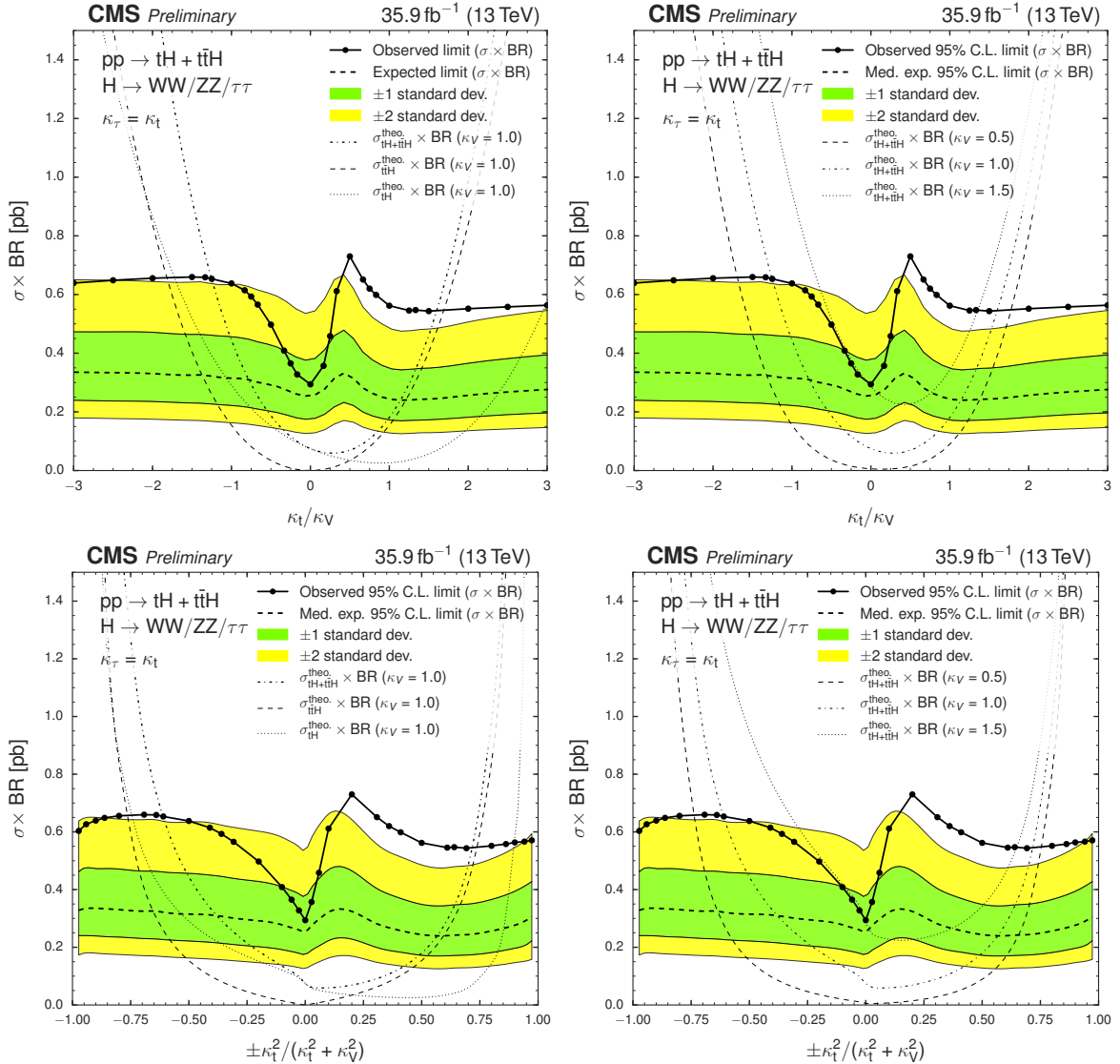


Figure 35: Expected (from background-only) and observed asymptotic limits on the combined  $tH + t\bar{t}H$  cross section times modified BR as a function of  $\kappa_t/\kappa_V$  (top) and  $\text{sign}(\kappa_t/\kappa_V) \times \frac{\kappa_t^2}{(\kappa_t^2 + \kappa_V^2)}$  (bottom) for the combination of three lepton channel,  $\mu^\pm \mu^\pm$ , and  $e^\pm \mu^\pm$  channel.

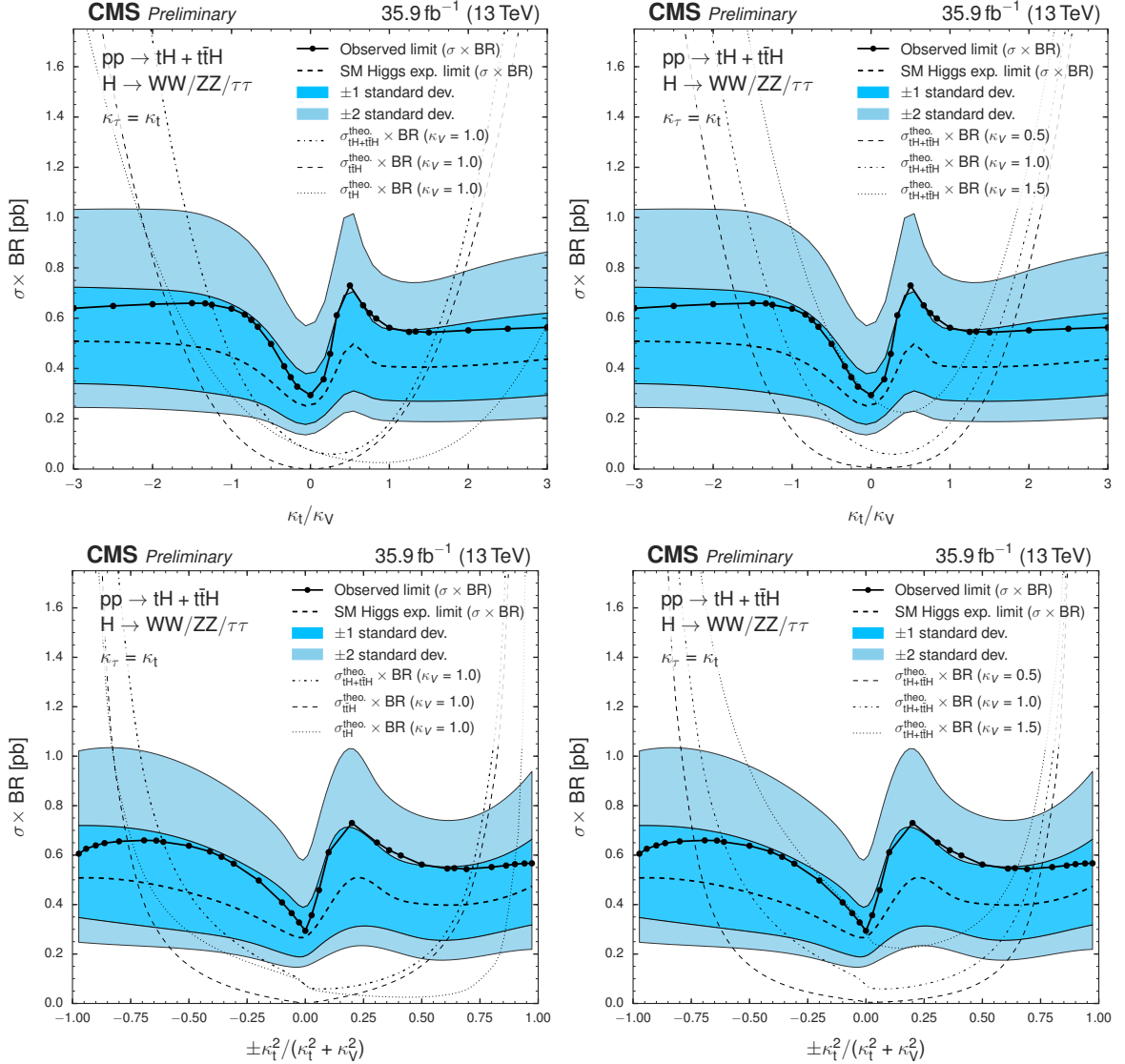


Figure 36: As Fig. 35 but calculating the expected limit on an Asimov dataset that includes SM-like  $t\bar{t}H$  and  $tH$  signals.

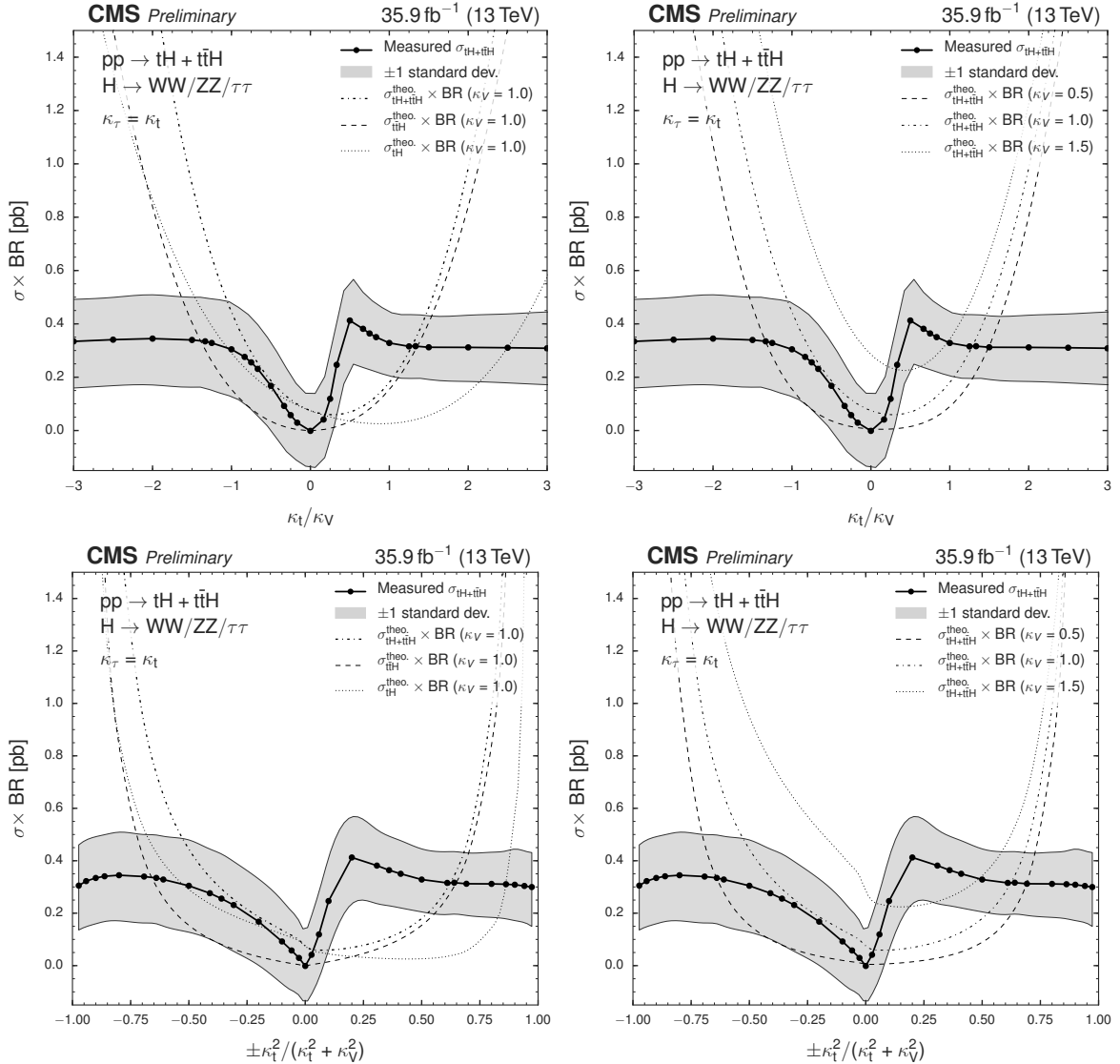


Figure 37: Best fit values of the combined  $tH + t\bar{t}H$  cross section times modified BR as a function of  $\kappa_t/\kappa_V$  (top) and  $\text{sign}(\kappa_t/\kappa_V) \times \frac{\kappa_t^2}{(\kappa_t^2 + \kappa_V^2)}$  (bottom) for the combination of three lepton channel,  $\mu^\pm\mu^\pm$ , and  $e^\pm\mu^\pm$  channel.

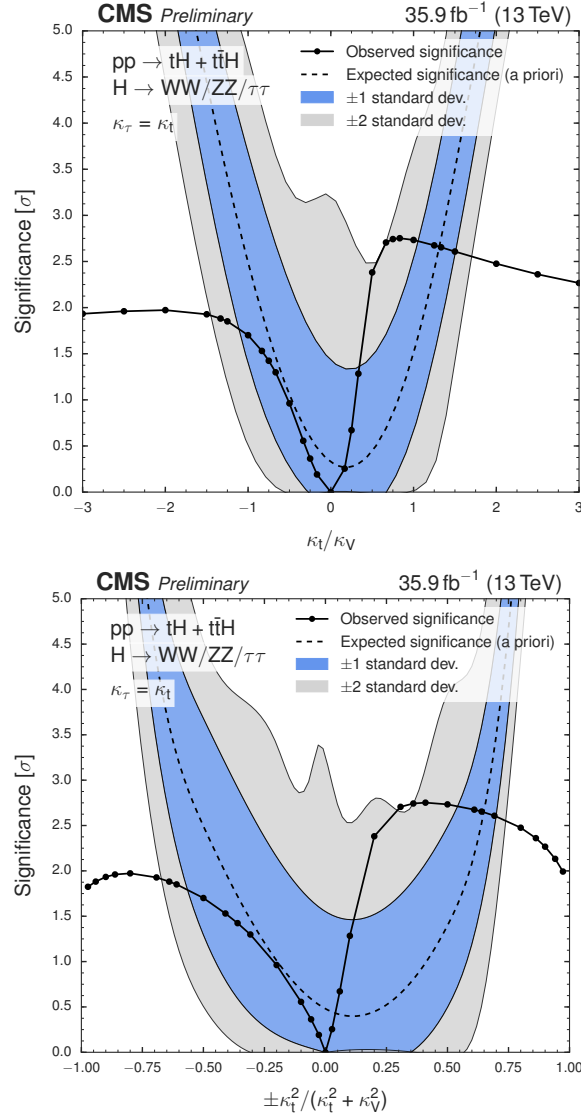


Figure 38: Observed and a priori expected significance of the fit result (in a background-only hypothesis) as a function of  $\kappa_t/\kappa_V$  (top) and  $f_t$  (bottom) for the combination of three lepton channel,  $\mu^\pm\mu^\pm$ , and  $e^\pm\mu^\pm$  channel.

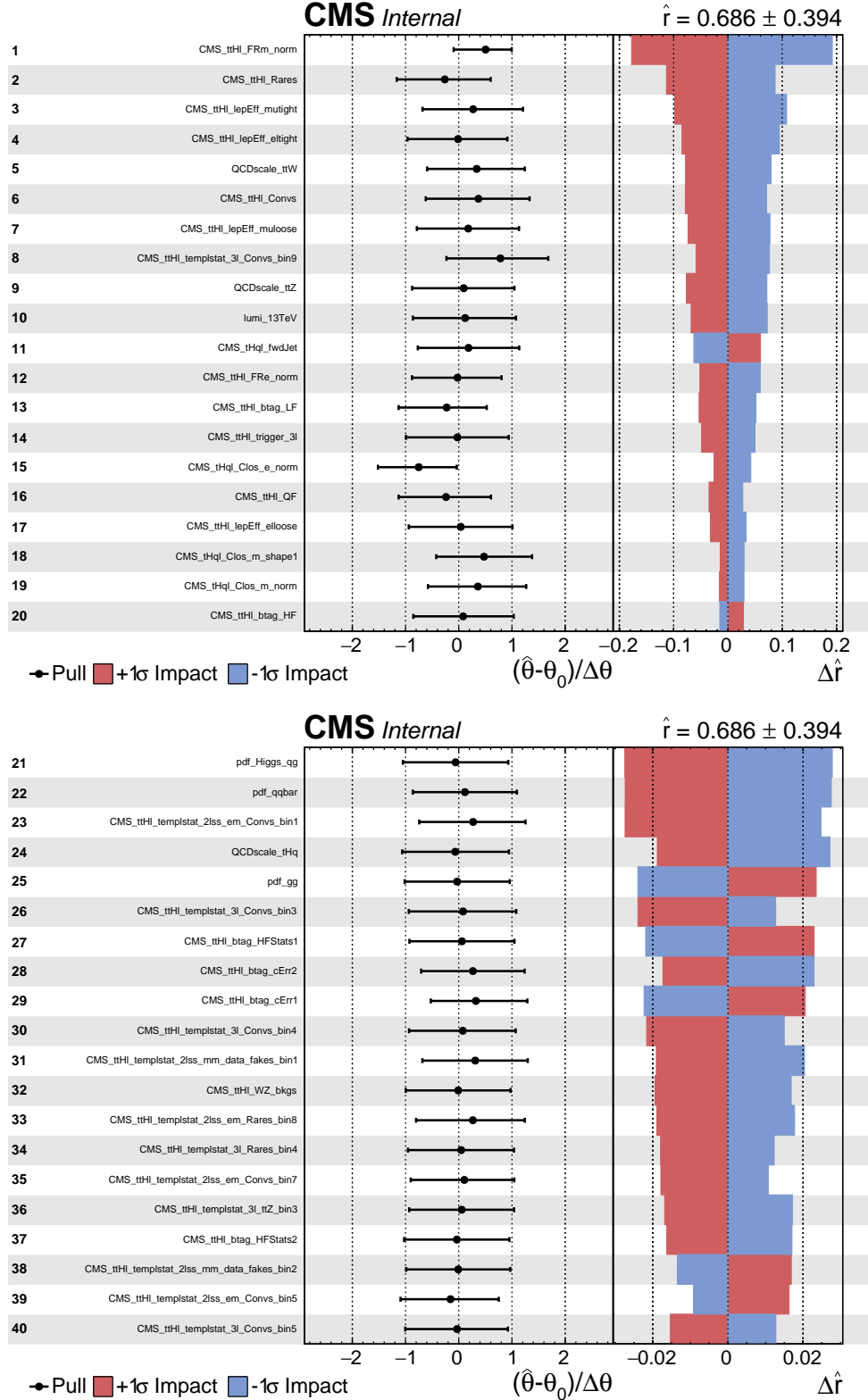


Figure 39: Post-fit pulls and impacts of the 40 nuisance parameters with largest impacts for the fit on the observed data, for the  $\kappa_t/\kappa_V = -1.0$  hypothesis.

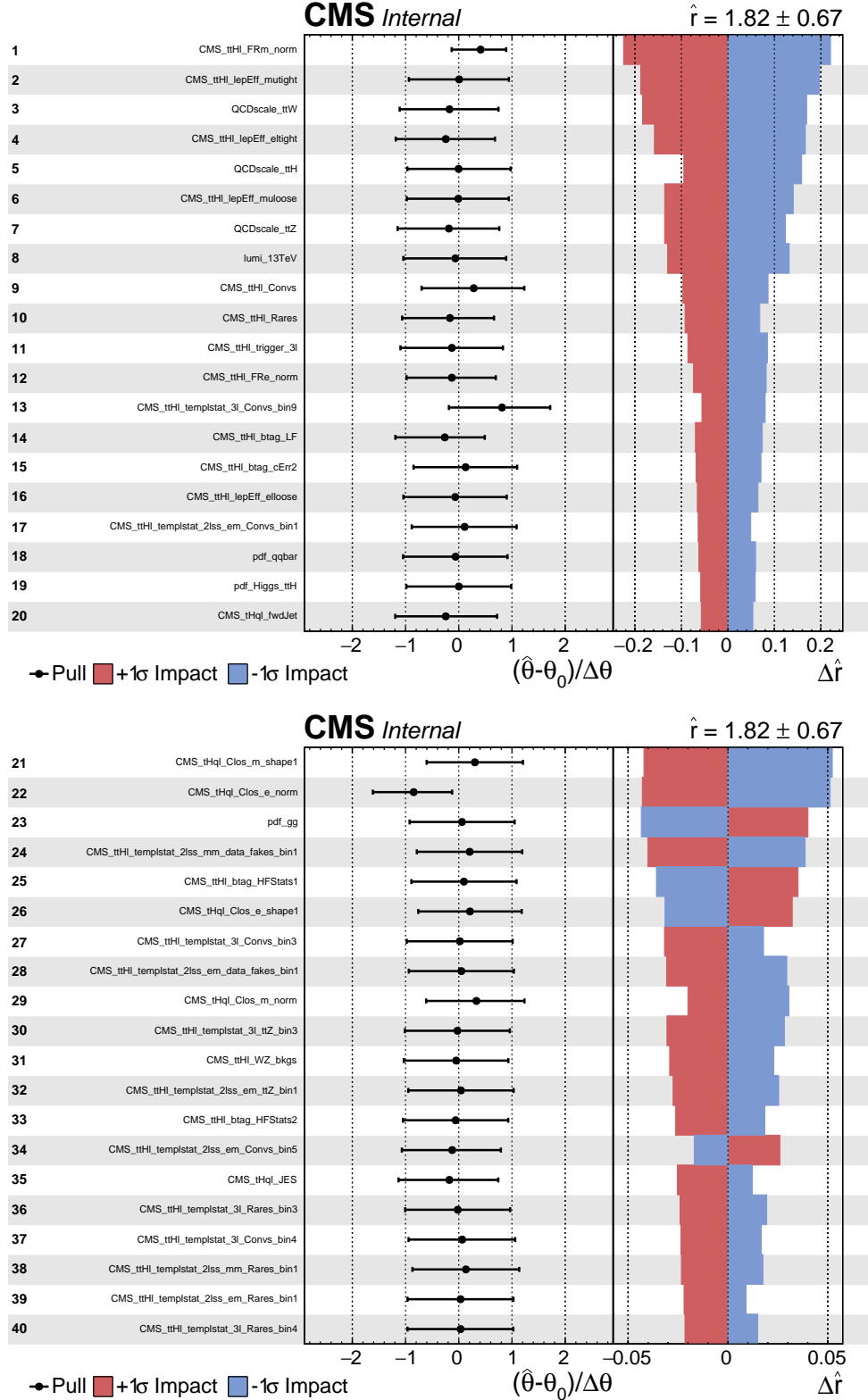


Figure 40: Post-fit pulls and impacts of the 40 nuisance parameters with largest impacts for the fit on the observed data, for the standard model ( $\kappa_t/\kappa_V = 1.0$ ) hypothesis.

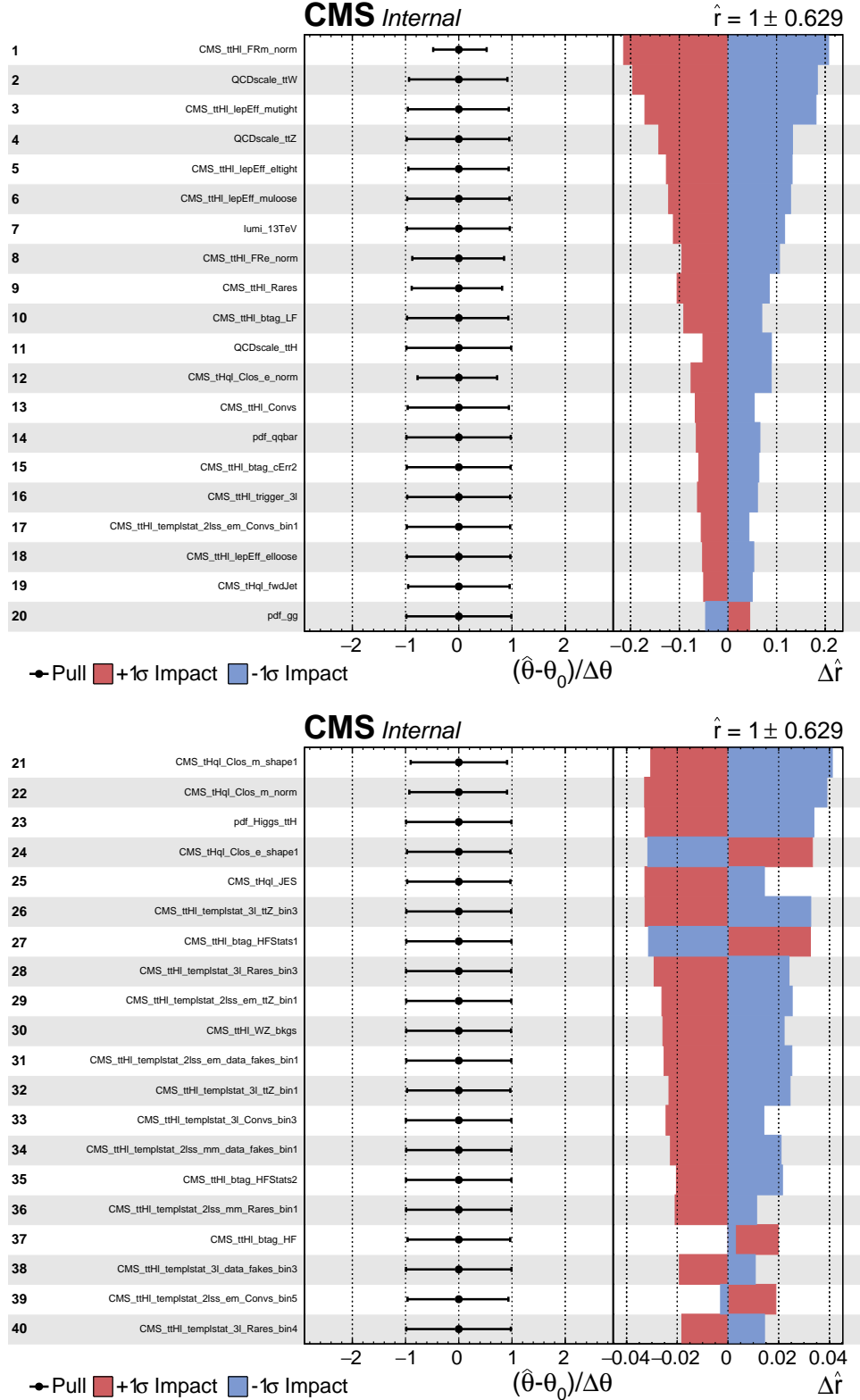


Figure 41: Post-fit pulls and impacts of the 40 nuisance parameters with largest impacts for a fit to the Asimov dataset with fixed signal strength, for the  $\kappa_t/\kappa_V = -1.0$  hypothesis.

## A Control region plots

### A.1 Same-sign dilepton control plots

Control regions are defined by selections similar to the signal region but with some reversed requirement to obtain background rich events. In case of same sign dilepton, the main background contribution from  $t\bar{t}$  is enhanced by requiring no untagged jet with  $|\eta| > 2$ . Furthermore, events with four or more jets are rejected to blind the signal region of the  $t\bar{t}H$  multilepton analysis. Some kinematic distributions in this control region for the same sign di-muon final state are shown in Fig. 42. Fig. 43 shows the distributions in case of  $e^\pm \mu^\pm$  channel.

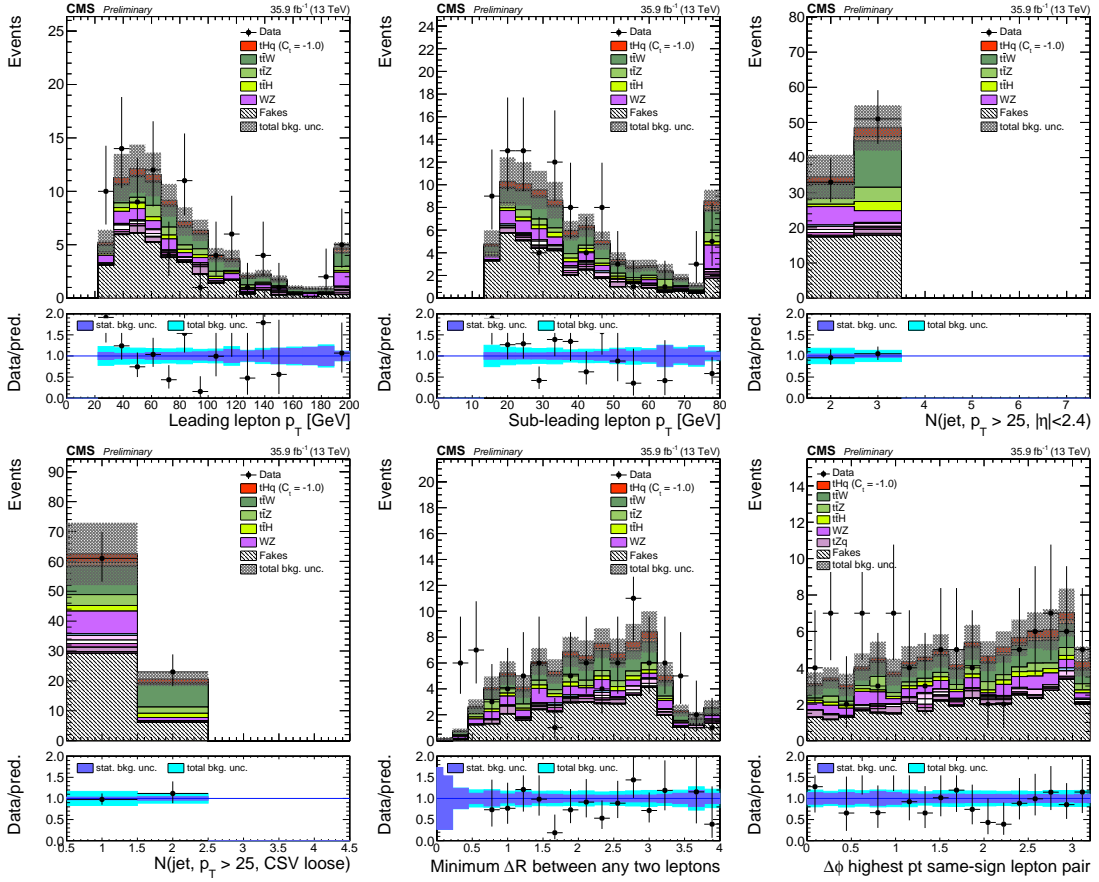


Figure 42: Contributions from signal and background in  $t\bar{t}$  control region for  $\mu^\pm \mu^\pm$  channel.

### A.2 Three lepton control plots

**A.2.0.1 Z-enriched sideband** We first enrich the signal region in  $WZ$  and  $t\bar{t}Z$  events by inverting the  $Z$  veto of Tab. 9, i.e. by requiring an opposite-sign dilepton pair with  $|m_{\ell\ell} - m_Z| < 15 \text{ GeV}$ . To increase the available statistics, only a loose CSV jet is required (rather than a medium tagged one, as in Tab. 9). A few relevant kinematic distributions shown in Fig. 44 show a good overall agreement, albeit with a deficit of data at low momenta of the third lepton.

### A.3 Opposite-sign e $\mu$ control region

We select a sample of dileptonic  $t\bar{t}$  events by requiring two opposite-sign tight leptons in the  $e\mu$  channel, with at least two jets and at least one medium CSV tagged jet. (Otherwise the

## A Control region plots

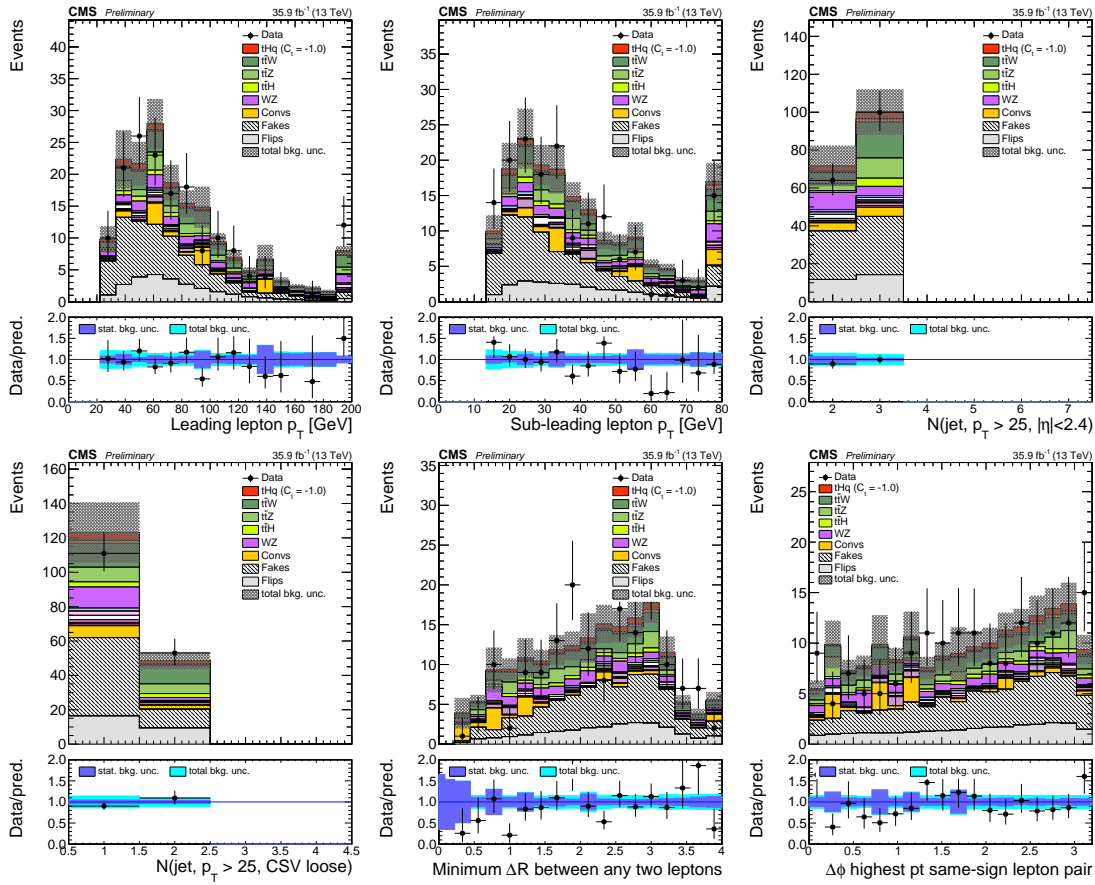


Figure 43: Contributions from signal and background in  $t\bar{t}$  control region for  $e^\pm \mu^\pm$  channel.

selection is identical to the same-sign  $e^\pm \mu^\pm$  channel selection.) We study some distribution related to the forward jet modeling and compare the observed data with the predictions from  $t\bar{t}$  MC, see Fig. 45. The agreement of the  $\eta$  distribution of forward jets for a  $p_T$  cut of 25 GeV is poor, especially at higher values of  $|\eta|$ . The (central) jet multiplicity is poorly modeled by the MadgraphMLM sample used here; consistent with other observations of the same sample. Note that the  $t\bar{t}$  background in this analysis is modeled with a data-driven method and these disagreements do not directly affect the  $t\bar{t}$  contribution in the analysis. They do however reflect the expected agreement in these distributions for the irreducible backgrounds and the signal.

The data/MC agreement in the forward jet  $\eta$  distribution improves significantly at higher jet  $p_{TS}$ .

The effect of higher  $p_T$  cuts on the forward jet has been studied for three values: 25, 30 and 40 GeV. In order to take into account the data/MC disagreement in the high  $\eta$  regions, the events are weighted accordingly to the data/MC ratio of the unity normalized control plots shown in Fig. 46.

Table 26 shows the scale factors obtained for the three  $p_T$  values.

With higher cuts in  $p_T$ , the expected limit on cross section in the three lepton channel improves from 1.54 at 25 GeV to 1.51 at 30 GeV and 1.50 at 40 GeV. Adjusting the data/MC ratios by hand to half the obtained value in case of forward jet  $\eta$  cut at 25 GeV, improves the limit from 1.54 to 1.51 in the three lepton channel. The impact of the data/MC disagreement for forward jet  $\eta$  is observed to reduce with higher  $p_T$  cuts. Fig. 47, Fig. 48 and Fig. 49 show this reduction in the impact of the forward jet  $\eta$  nuisance in the fit.

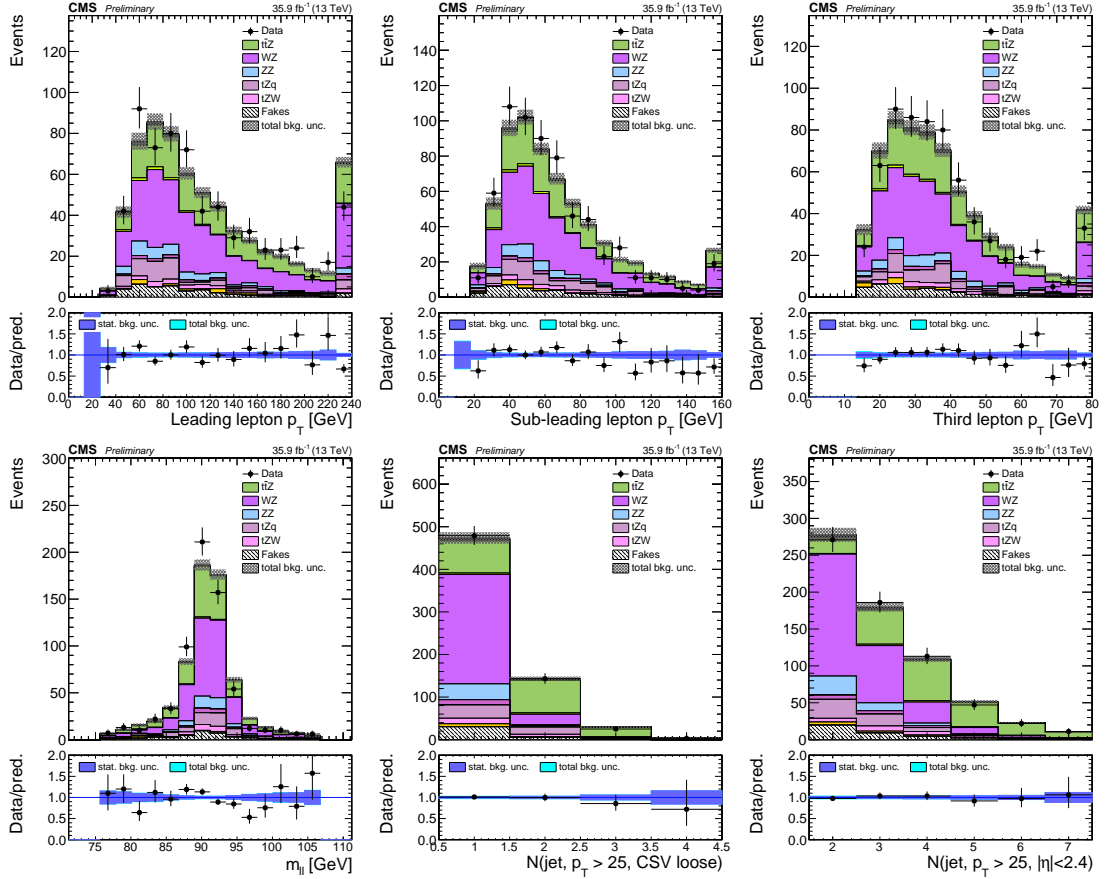


Figure 44: Kinematic distributions in the Z-enriched sideband to the three-lepton signal region.

| $\eta$ range                  | $p_T > 25$ GeV | $p_T > 30$ GeV | $p_T > 40$ GeV |
|-------------------------------|----------------|----------------|----------------|
| 0 – 0.278                     | 1.0925         | 1.0566         | 1.0326         |
| 0.278 – 0.556                 | 1.0920         | 1.0617         | 1.0407         |
| 0.556 – 0.833                 | 1.0675         | 1.0459         | 1.0244         |
| 0.833 – 1.111                 | 1.0888         | 1.0593         | 1.0340         |
| 1.111 – 1.389                 | 1.0759         | 1.0508         | 1.0322         |
| 1.389 – 1.667                 | 1.0109         | 0.9847         | 0.9661         |
| 1.667 – 1.944                 | 1.0727         | 1.0448         | 1.0239         |
| 1.944 – 2.222                 | 1.0715         | 1.0457         | 1.0169         |
| 2.222 – 2.500                 | 1.0112         | 0.9871         | 0.9746         |
| 2.500 – 2.778                 | 1.0387         | 0.9942         | 0.9816         |
| 2.778 – 3.056                 | 0.9687         | 0.9427         | 0.9200         |
| 3.056 – 3.333                 | 0.8137         | 0.8695         | 0.9092         |
| 3.333 – 3.611                 | 0.9010         | 0.9387         | 0.9807         |
| 3.611 – 3.889                 | 0.8685         | 0.8887         | 0.9213         |
| 3.889 – 4.167                 | 0.9277         | 0.9466         | 1.0135         |
| 4.167 – 4.444                 | 0.8111         | 0.8278         | 0.8637         |
| 4.444 – 4.722                 | 0.6497         | 0.6485         | 0.6367         |
| 4.722 – 5.000                 | 1.0000         | 1.0000         | 1.0000         |
| Exp. limit ( $\ell\ell\ell$ ) | $r < 1.54$     | $r < 1.51$     | $r < 1.50$     |

Table 26: Data/MC scale factors for  $\eta$  distribution of most forward, non-tagged jet with three different  $p_T$  cuts, see Fig. 46.

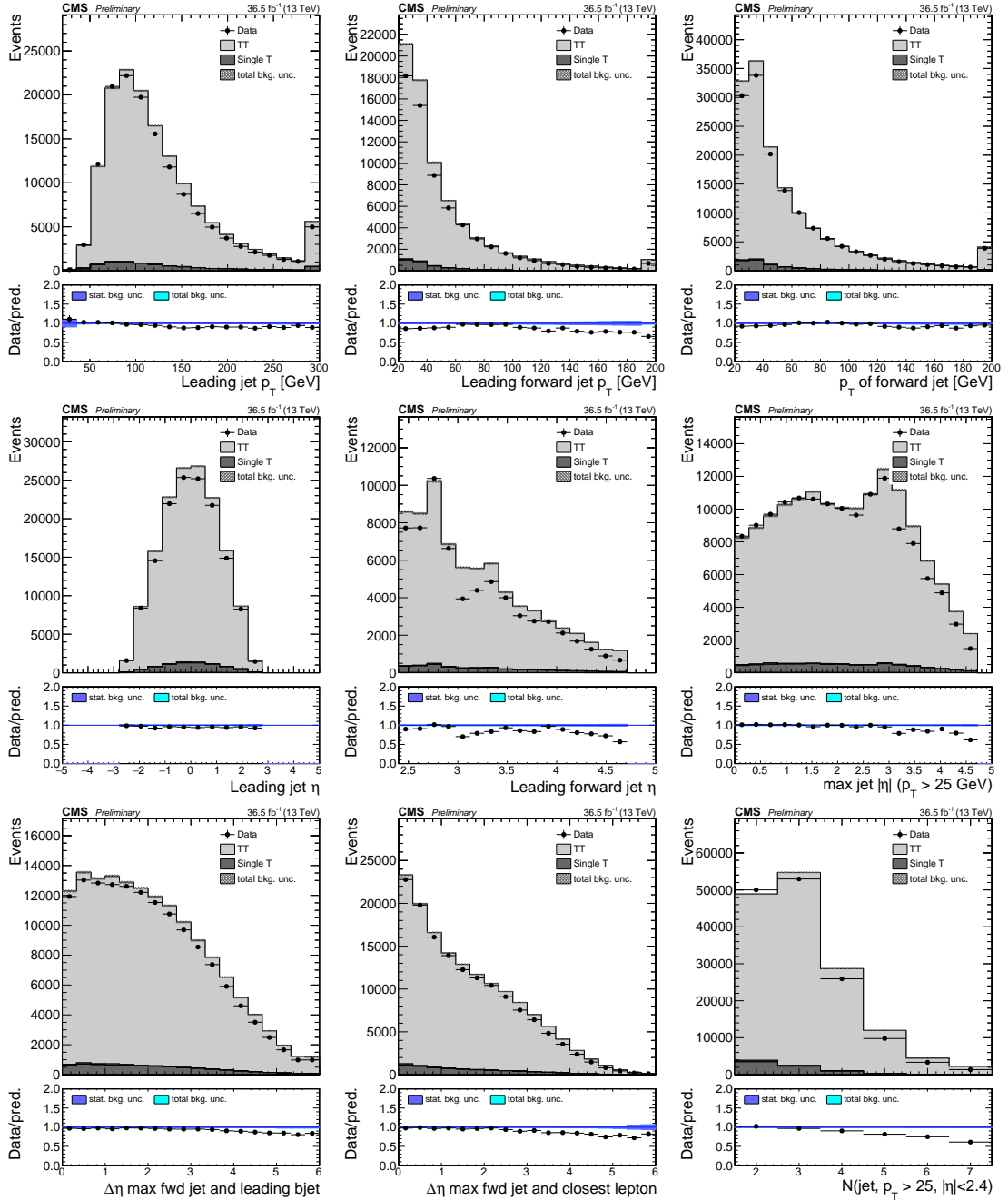


Figure 45: Kinematic distributions in the  $t\bar{t}$ -enriched opposite-sign  $e\mu$  selection. Top row, left to right: leading central ( $\eta < 2.4$ ) jet  $p_T$ , leading forward ( $\eta > 2.4$ ) jet  $p_T$ ,  $p_T$  of non-CSV-loose jet with highest  $\eta$  (“light forward jet”). Middle row:  $\eta$  distribution of those same jets. Bottom row:  $\Delta\eta$  between light forward jet and leading CSV-loose tagged jet;  $\Delta\eta$  between light forward jet and closest lepton; number of central jets.

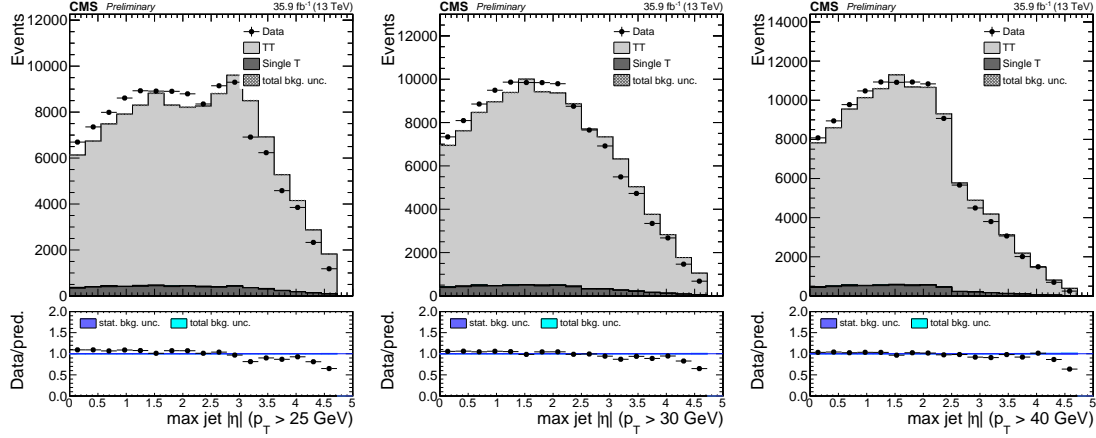


Figure 46: Pseudorapidity distributions of the most forward, non-CSV-loose tagged jet in the  $t\bar{t}$ -enriched opposite-sign  $e\mu$  selection for the three  $p_T$  cut values.

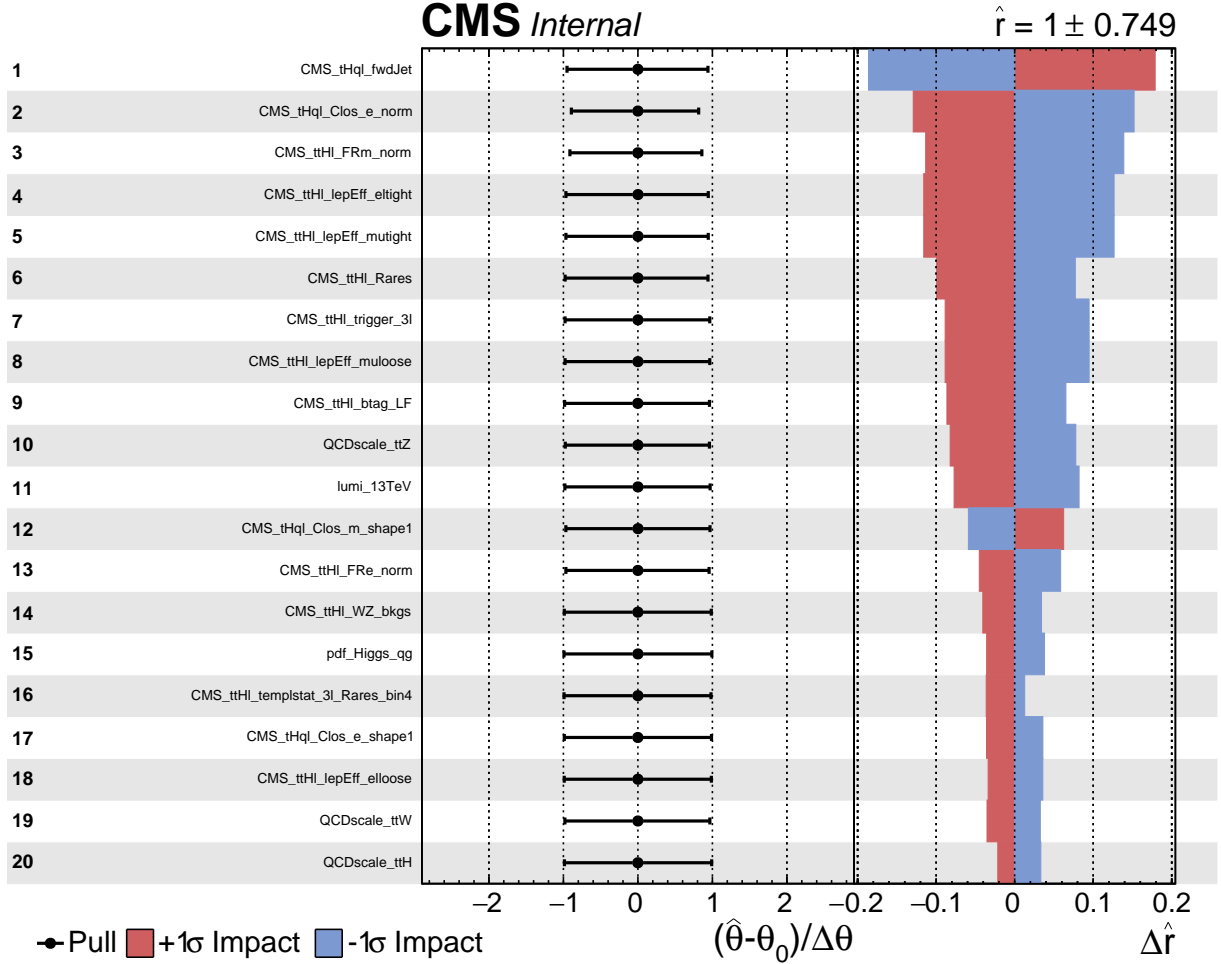


Figure 47: Post-fit pulls and impacts of the 20 nuisance parameters with  $p_T$  cut 25 GeV for the forward jet.

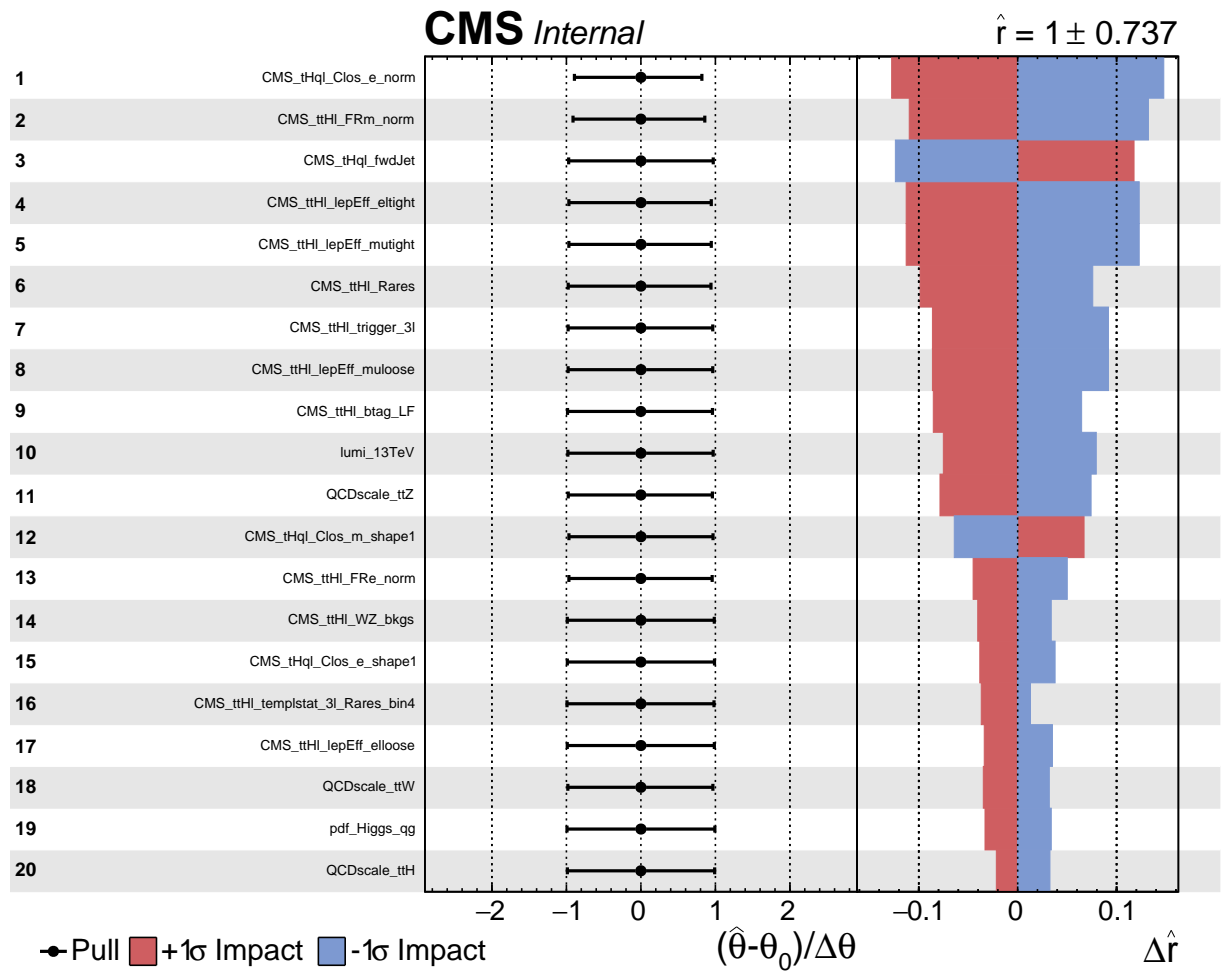


Figure 48: Post-fit pulls and impacts of the 20 nuisance parameters with  $p_T$  cut 30 GeV for the forward jet.

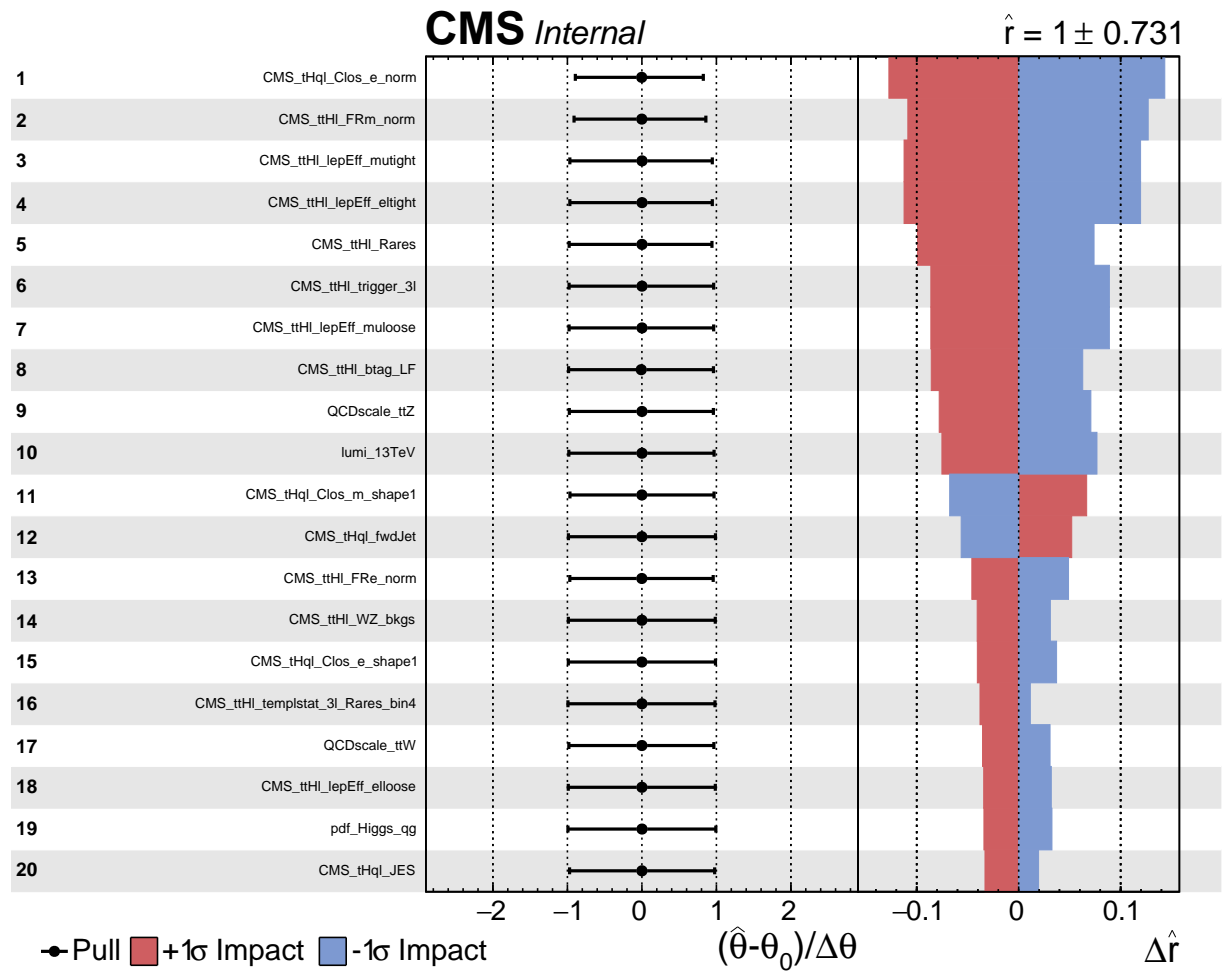


Figure 49: Post-fit pulls and impacts of the 20 nuisance parameters with  $p_T$  cut 40 GeV for the forward jet.

We study the change of BDT output shape when varying the  $\kappa_V/\kappa_t$  coupling scenario. Figure 50 shows the two BDT output shapes in the three lepton channel for five different values of  $\kappa_t$ , with  $\kappa_V$  fixed at 1.0.

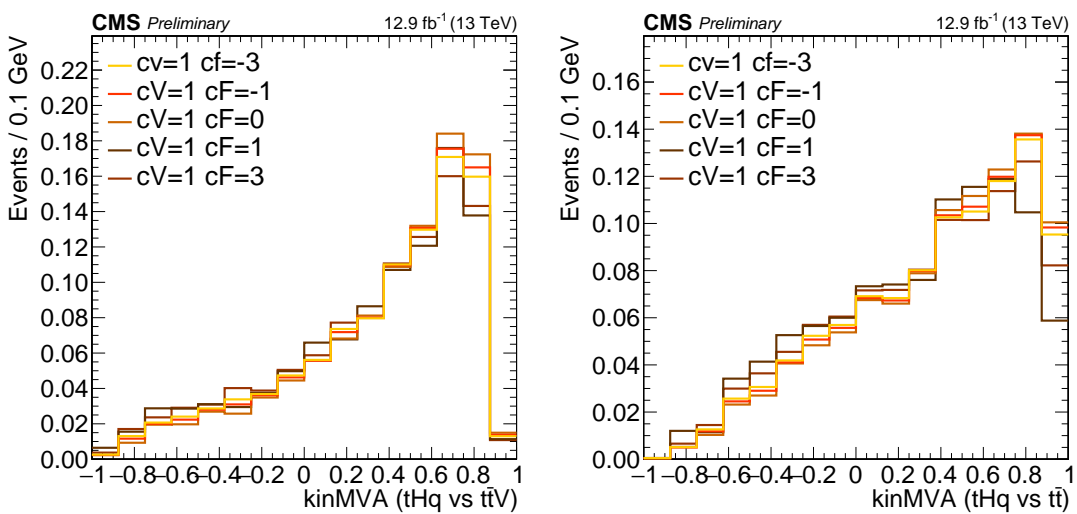


Figure 50: Change of BDT output when varying  $\kappa_t$  coupling ( $\kappa_V$  is fixed at 1.0). Training vs.  $t\bar{t}V$  (right) and vs.  $t\bar{t}$  (left).

## C Further channel categorization

Since electrons and muons have different selection efficiencies and fake-rates, the background spectrum in same-sign  $e^\pm \mu^\pm$  events is somewhat different in events where electrons or muons are the softer leg. Hence a splitting of the channel could potentially give an improvement in the limit. Similarly, for the three lepton channel, splitting into events with a pair of same-flavor, opposite-sign leptons (SFOS) or without (SFSS), changes the background composition somewhat, with a potential gain in sensitivity. We calculate the limits for each channel inclusively and compare with the limit obtained when combining the split categories, see Tab. 27.

In the case of same-sign dileptons channels, the limit improves from 2.18 (inclusive  $e^\pm \mu^\pm$  channel) to 2.12 after combining the exclusive channels. The three lepton channel improves from 1.96 (inclusive channel) to 1.90 when running SFSS and SFOS separately.

| Scenario          | Channel                                      | Exp. Limit (median) |
|-------------------|--|---------------------|
| $\kappa_V = 1.0$  | $e^\pm \mu^\pm$ (inclusive)                  | <b>2.18</b>         |
| $\kappa_t = -1.0$ | $e^\pm \mu^\pm$ (exclusive)                  | 2.59                |
|                   | $\mu^\pm e^\pm$ (exclusive)                  | 2.93                |
|                   | Combined ( $e^\pm \mu^\pm + \mu^\pm e^\pm$ ) | <b>2.12</b>         |
| <hr/>             |  |                     |
|                   | $lll$ (inclusive)                            | <b>1.96</b>         |
|                   | $lll$ (SFSS)                                 | 3.18                |
|                   | $lll$ (SFOS)                                 | 2.40                |
|                   | Combined (SFSS, SFOS)                        | <b>1.90</b>         |

Table 27: Expected limits (at 95% C.L.) on the combined tH production in the same-sign dilepton and three lepton channels, and for their combination, for a scenario with inverted couplings ( $\kappa_V = 1.0, \kappa_t = -1.0$ ). Numbers are for  $35.9 \text{ fb}^{-1}$ .

## D Cross section times BR scalings

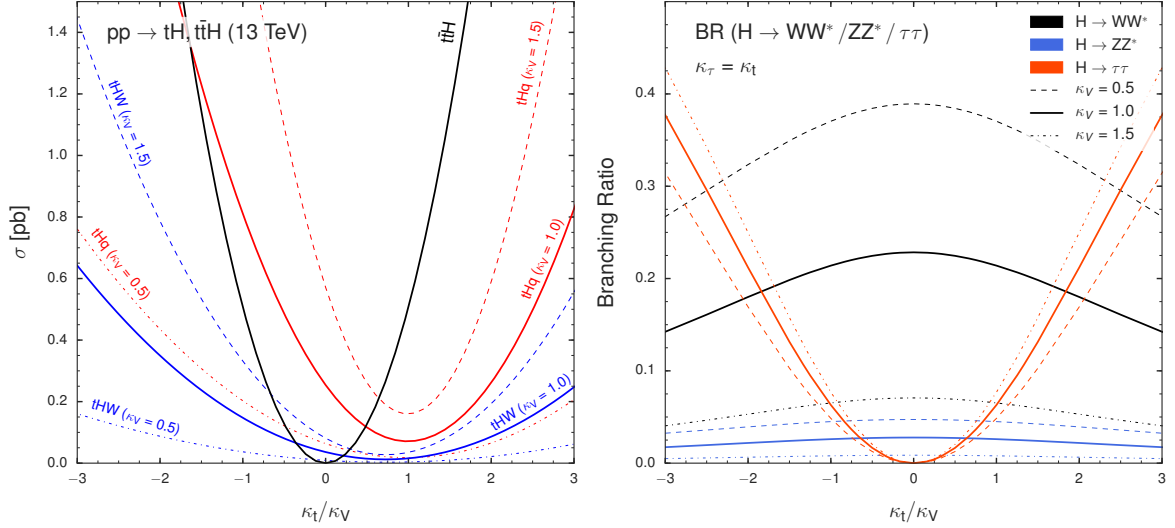


Figure 51: Scaling of the  $tHq$ ,  $tHW$ , and  $t\bar{t}H$  production cross sections (left) and of the  $H \rightarrow WW^*$ ,  $H \rightarrow \tau\tau$ , and  $H \rightarrow ZZ^*$  branching ratios (right), as a function of  $\kappa_t/\kappa_V$ , for three different values of  $\kappa_V$ .

| $\kappa_V$ | $\kappa_t$ | HWW    | HZZ    | H $\tau\tau$ | H $\mu\mu$ | Hbb    | Hcc    | H $\gamma\gamma$ | HZ $\gamma$ | Hgg    |
|------------|------------|--------|--------|--------------|------------|--------|--------|------------------|-------------|--------|
| 0.5        | -6.0       | 0.0827 | 0.0827 | 11.9098      | 11.9098    | 0.3308 | 0.3308 | 0.3308           | 0.3308      | 0.3308 |
| 0.5        | -4.0       | 0.1417 | 0.1417 | 9.0699       | 9.0699     | 0.5669 | 0.5669 | 0.5669           | 0.5669      | 0.5669 |
| 0.5        | -3.0       | 0.1889 | 0.1889 | 6.7999       | 6.7999     | 0.7555 | 0.7555 | 0.7555           | 0.7555      | 0.7555 |
| 0.5        | -2.5       | 0.2173 | 0.2173 | 5.4325       | 5.4325     | 0.8692 | 0.8692 | 0.8692           | 0.8692      | 0.8692 |
| 0.5        | -2.0       | 0.2478 | 0.2478 | 3.9647       | 3.9647     | 0.9912 | 0.9912 | 0.9912           | 0.9912      | 0.9912 |
| 0.5        | -1.5       | 0.2782 | 0.2782 | 2.5034       | 2.5034     | 1.1126 | 1.1126 | 1.1126           | 1.1126      | 1.1126 |
| 0.5        | -1.333     | 0.2877 | 0.2877 | 2.0448       | 2.0448     | 1.1508 | 1.1508 | 1.1508           | 1.1508      | 1.1508 |
| 0.5        | -1.25      | 0.2922 | 0.2922 | 1.8264       | 1.8264     | 1.1689 | 1.1689 | 1.1689           | 1.1689      | 1.1689 |
| 0.5        | -1.0       | 0.3048 | 0.3048 | 1.2194       | 1.2194     | 1.2194 | 1.2194 | 1.2194           | 1.2194      | 1.2194 |
| 0.5        | -0.833     | 0.3122 | 0.3122 | 0.8665       | 0.8665     | 1.2487 | 1.2487 | 1.2487           | 1.2487      | 1.2487 |
| 0.5        | -0.75      | 0.3154 | 0.3154 | 0.7097       | 0.7097     | 1.2617 | 1.2617 | 1.2617           | 1.2617      | 1.2617 |
| 0.5        | -0.667     | 0.3184 | 0.3184 | 0.5666       | 0.5666     | 1.2736 | 1.2736 | 1.2736           | 1.2736      | 1.2736 |
| 0.5        | -0.5       | 0.3235 | 0.3235 | 0.3235       | 0.3235     | 1.2938 | 1.2938 | 1.2938           | 1.2938      | 1.2938 |
| 0.5        | -0.333     | 0.3272 | 0.3272 | 0.1451       | 0.1451     | 1.3087 | 1.3087 | 1.3087           | 1.3087      | 1.3087 |
| 0.5        | -0.25      | 0.3285 | 0.3285 | 0.0821       | 0.0821     | 1.3139 | 1.3139 | 1.3139           | 1.3139      | 1.3139 |
| 0.5        | -0.167     | 0.3294 | 0.3294 | 0.0367       | 0.0367     | 1.3177 | 1.3177 | 1.3177           | 1.3177      | 1.3177 |
| 0.5        | 0.0        | 0.3302 | 0.3302 | 0.0000       | 0.0000     | 1.3207 | 1.3207 | 1.3207           | 1.3207      | 1.3207 |
| 0.5        | 0.167      | 0.3294 | 0.3294 | 0.0367       | 0.0367     | 1.3177 | 1.3177 | 1.3177           | 1.3177      | 1.3177 |
| 0.5        | 0.25       | 0.3285 | 0.3285 | 0.0821       | 0.0821     | 1.3139 | 1.3139 | 1.3139           | 1.3139      | 1.3139 |
| 0.5        | 0.333      | 0.3272 | 0.3272 | 0.1451       | 0.1451     | 1.3087 | 1.3087 | 1.3087           | 1.3087      | 1.3087 |
| 0.5        | 0.5        | 0.3235 | 0.3235 | 0.3235       | 0.3235     | 1.2938 | 1.2938 | 1.2938           | 1.2938      | 1.2938 |
| 0.5        | 0.667      | 0.3184 | 0.3184 | 0.5666       | 0.5666     | 1.2736 | 1.2736 | 1.2736           | 1.2736      | 1.2736 |
| 0.5        | 0.75       | 0.3154 | 0.3154 | 0.7097       | 0.7097     | 1.2617 | 1.2617 | 1.2617           | 1.2617      | 1.2617 |
| 0.5        | 0.833      | 0.3122 | 0.3122 | 0.8665       | 0.8665     | 1.2487 | 1.2487 | 1.2487           | 1.2487      | 1.2487 |
| 0.5        | 1.0        | 0.3048 | 0.3048 | 1.2194       | 1.2194     | 1.2194 | 1.2194 | 1.2194           | 1.2194      | 1.2194 |
| 0.5        | 1.25       | 0.2922 | 0.2922 | 1.8264       | 1.8264     | 1.1689 | 1.1689 | 1.1689           | 1.1689      | 1.1689 |
| 0.5        | 1.333      | 0.2877 | 0.2877 | 2.0448       | 2.0448     | 1.1508 | 1.1508 | 1.1508           | 1.1508      | 1.1508 |
| 0.5        | 1.5        | 0.2782 | 0.2782 | 2.5034       | 2.5034     | 1.1126 | 1.1126 | 1.1126           | 1.1126      | 1.1126 |
| 0.5        | 2.0        | 0.2478 | 0.2478 | 3.9647       | 3.9647     | 0.9912 | 0.9912 | 0.9912           | 0.9912      | 0.9912 |
| 0.5        | 2.5        | 0.2173 | 0.2173 | 5.4325       | 5.4325     | 0.8692 | 0.8692 | 0.8692           | 0.8692      | 0.8692 |
| 0.5        | 3.0        | 0.1889 | 0.1889 | 6.7999       | 6.7999     | 0.7555 | 0.7555 | 0.7555           | 0.7555      | 0.7555 |
| 0.5        | 4.0        | 0.1417 | 0.1417 | 9.0699       | 9.0699     | 0.5669 | 0.5669 | 0.5669           | 0.5669      | 0.5669 |
| 0.5        | 6.0        | 0.0827 | 0.0827 | 11.9098      | 11.9098    | 0.3308 | 0.3308 | 0.3308           | 0.3308      | 0.3308 |

Table 28: Scalings of Higgs decay branching ratios vs.  $\kappa_t$  and  $\kappa_V = 0.5$  for the resolved model.

| $\kappa_V$ | $\kappa_t$ | HWW    | HZZ    | H $\tau\tau$ | H $\mu\mu$ | Hbb    | Hcc    | H $\gamma\gamma$ | HZ $\gamma$ | Hgg    |
|------------|------------|--------|--------|--------------|------------|--------|--------|------------------|-------------|--------|
| 1.0        | -6.0       | 0.3122 | 0.3122 | 11.2408      | 11.2408    | 0.3122 | 0.3122 | 0.3122           | 0.3122      | 0.3122 |
| 1.0        | -4.0       | 0.5144 | 0.5144 | 8.2305       | 8.2305     | 0.5144 | 0.5144 | 0.5144           | 0.5144      | 0.5144 |
| 1.0        | -3.0       | 0.6651 | 0.6651 | 5.9862       | 5.9862     | 0.6651 | 0.6651 | 0.6651           | 0.6651      | 0.6651 |
| 1.0        | -2.5       | 0.7517 | 0.7517 | 4.6979       | 4.6979     | 0.7517 | 0.7517 | 0.7517           | 0.7517      | 0.7517 |
| 1.0        | -2.0       | 0.8412 | 0.8412 | 3.3647       | 3.3647     | 0.8412 | 0.8412 | 0.8412           | 0.8412      | 0.8412 |
| 1.0        | -1.5       | 0.9271 | 0.9271 | 2.0859       | 2.0859     | 0.9271 | 0.9271 | 0.9271           | 0.9271      | 0.9271 |
| 1.0        | -1.333     | 0.9534 | 0.9534 | 1.6941       | 1.6941     | 0.9534 | 0.9534 | 0.9534           | 0.9534      | 0.9534 |
| 1.0        | -1.25      | 0.9658 | 0.9658 | 1.5091       | 1.5091     | 0.9658 | 0.9658 | 0.9658           | 0.9658      | 0.9658 |
| 1.0        | -1.0       | 1.0000 | 1.0000 | 1.0000       | 1.0000     | 1.0000 | 1.0000 | 1.0000           | 1.0000      | 1.0000 |
| 1.0        | -0.833     | 1.0196 | 1.0196 | 0.7075       | 0.7075     | 1.0196 | 1.0196 | 1.0196           | 1.0196      | 1.0196 |
| 1.0        | -0.75      | 1.0283 | 1.0283 | 0.5784       | 0.5784     | 1.0283 | 1.0283 | 1.0283           | 1.0283      | 1.0283 |
| 1.0        | -0.667     | 1.0362 | 1.0362 | 0.4610       | 0.4610     | 1.0362 | 1.0362 | 1.0362           | 1.0362      | 1.0362 |
| 1.0        | -0.5       | 1.0495 | 1.0495 | 0.2624       | 0.2624     | 1.0495 | 1.0495 | 1.0495           | 1.0495      | 1.0495 |
| 1.0        | -0.333     | 1.0593 | 1.0593 | 0.1175       | 0.1175     | 1.0593 | 1.0593 | 1.0593           | 1.0593      | 1.0593 |
| 1.0        | -0.25      | 1.0627 | 1.0627 | 0.0664       | 0.0664     | 1.0627 | 1.0627 | 1.0627           | 1.0627      | 1.0627 |
| 1.0        | -0.167     | 1.0652 | 1.0652 | 0.0297       | 0.0297     | 1.0652 | 1.0652 | 1.0652           | 1.0652      | 1.0652 |
| 1.0        | 0.0        | 1.0672 | 1.0672 | 0.0000       | 0.0000     | 1.0672 | 1.0672 | 1.0672           | 1.0672      | 1.0672 |
| 1.0        | 0.167      | 1.0652 | 1.0652 | 0.0297       | 0.0297     | 1.0652 | 1.0652 | 1.0652           | 1.0652      | 1.0652 |
| 1.0        | 0.25       | 1.0627 | 1.0627 | 0.0664       | 0.0664     | 1.0627 | 1.0627 | 1.0627           | 1.0627      | 1.0627 |
| 1.0        | 0.333      | 1.0593 | 1.0593 | 0.1175       | 0.1175     | 1.0593 | 1.0593 | 1.0593           | 1.0593      | 1.0593 |
| 1.0        | 0.5        | 1.0495 | 1.0495 | 0.2624       | 0.2624     | 1.0495 | 1.0495 | 1.0495           | 1.0495      | 1.0495 |
| 1.0        | 0.667      | 1.0362 | 1.0362 | 0.4610       | 0.4610     | 1.0362 | 1.0362 | 1.0362           | 1.0362      | 1.0362 |
| 1.0        | 0.75       | 1.0283 | 1.0283 | 0.5784       | 0.5784     | 1.0283 | 1.0283 | 1.0283           | 1.0283      | 1.0283 |
| 1.0        | 0.833      | 1.0196 | 1.0196 | 0.7075       | 0.7075     | 1.0196 | 1.0196 | 1.0196           | 1.0196      | 1.0196 |
| 1.0        | 1.0        | 1.0000 | 1.0000 | 1.0000       | 1.0000     | 1.0000 | 1.0000 | 1.0000           | 1.0000      | 1.0000 |
| 1.0        | 1.25       | 0.9658 | 0.9658 | 1.5091       | 1.5091     | 0.9658 | 0.9658 | 0.9658           | 0.9658      | 0.9658 |
| 1.0        | 1.333      | 0.9534 | 0.9534 | 1.6941       | 1.6941     | 0.9534 | 0.9534 | 0.9534           | 0.9534      | 0.9534 |
| 1.0        | 1.5        | 0.9271 | 0.9271 | 2.0859       | 2.0859     | 0.9271 | 0.9271 | 0.9271           | 0.9271      | 0.9271 |
| 1.0        | 2.0        | 0.8412 | 0.8412 | 3.3647       | 3.3647     | 0.8412 | 0.8412 | 0.8412           | 0.8412      | 0.8412 |
| 1.0        | 2.5        | 0.7517 | 0.7517 | 4.6979       | 4.6979     | 0.7517 | 0.7517 | 0.7517           | 0.7517      | 0.7517 |
| 1.0        | 3.0        | 0.6651 | 0.6651 | 5.9862       | 5.9862     | 0.6651 | 0.6651 | 0.6651           | 0.6651      | 0.6651 |
| 1.0        | 4.0        | 0.5144 | 0.5144 | 8.2305       | 8.2305     | 0.5144 | 0.5144 | 0.5144           | 0.5144      | 0.5144 |
| 1.0        | 6.0        | 0.3122 | 0.3122 | 11.2408      | 11.2408    | 0.3122 | 0.3122 | 0.3122           | 0.3122      | 0.3122 |

Table 29: Scalings of Higgs decay branching ratios vs.  $\kappa_t$  and  $\kappa_V = 1.0$  for the resolved model.

| $\kappa_V$ | $\kappa_t$ | HWW    | HZZ    | H $\tau\tau$ | H $\mu\mu$ | Hbb    | Hcc    | H $\gamma\gamma$ | HZ $\gamma$ | Hgg    |
|------------|------------|--------|--------|--------------|------------|--------|--------|------------------|-------------|--------|
| 1.5        | -6.0       | 0.6424 | 0.6424 | 10.2785      | 10.2785    | 0.2855 | 0.2855 | 0.2855           | 0.2855      | 0.2855 |
| 1.5        | -4.0       | 1.0028 | 1.0028 | 7.1307       | 7.1307     | 0.4457 | 0.4457 | 0.4457           | 0.4457      | 0.4457 |
| 1.5        | -3.0       | 1.2477 | 1.2477 | 4.9909       | 4.9909     | 0.5545 | 0.5545 | 0.5545           | 0.5545      | 0.5545 |
| 1.5        | -2.5       | 1.3802 | 1.3802 | 3.8338       | 3.8338     | 0.6134 | 0.6134 | 0.6134           | 0.6134      | 0.6134 |
| 1.5        | -2.0       | 1.5115 | 1.5115 | 2.6870       | 2.6870     | 0.6718 | 0.6718 | 0.6718           | 0.6718      | 0.6718 |
| 1.5        | -1.5       | 1.6322 | 1.6322 | 1.6322       | 1.6322     | 0.7254 | 0.7254 | 0.7254           | 0.7254      | 0.7254 |
| 1.5        | -1.333     | 1.6682 | 1.6682 | 1.3175       | 1.3175     | 0.7414 | 0.7414 | 0.7414           | 0.7414      | 0.7414 |
| 1.5        | -1.25      | 1.6851 | 1.6851 | 1.1702       | 1.1702     | 0.7489 | 0.7489 | 0.7489           | 0.7489      | 0.7489 |
| 1.5        | -1.0       | 1.7310 | 1.7310 | 0.7693       | 0.7693     | 0.7693 | 0.7693 | 0.7693           | 0.7693      | 0.7693 |
| 1.5        | -0.833     | 1.7570 | 1.7570 | 0.5419       | 0.5419     | 0.7809 | 0.7809 | 0.7809           | 0.7809      | 0.7809 |
| 1.5        | -0.75      | 1.7684 | 1.7684 | 0.4421       | 0.4421     | 0.7860 | 0.7860 | 0.7860           | 0.7860      | 0.7860 |
| 1.5        | -0.667     | 1.7788 | 1.7788 | 0.3517       | 0.3517     | 0.7906 | 0.7906 | 0.7906           | 0.7906      | 0.7906 |
| 1.5        | -0.5       | 1.7962 | 1.7962 | 0.1996       | 0.1996     | 0.7983 | 0.7983 | 0.7983           | 0.7983      | 0.7983 |
| 1.5        | -0.333     | 1.8089 | 1.8089 | 0.0891       | 0.0891     | 0.8039 | 0.8039 | 0.8039           | 0.8039      | 0.8039 |
| 1.5        | -0.25      | 1.8133 | 1.8133 | 0.0504       | 0.0504     | 0.8059 | 0.8059 | 0.8059           | 0.8059      | 0.8059 |
| 1.5        | -0.167     | 1.8165 | 1.8165 | 0.0225       | 0.0225     | 0.8073 | 0.8073 | 0.8073           | 0.8073      | 0.8073 |
| 1.5        | 0.0        | 1.8191 | 1.8191 | 0.0000       | 0.0000     | 0.8085 | 0.8085 | 0.8085           | 0.8085      | 0.8085 |
| 1.5        | 0.167      | 1.8165 | 1.8165 | 0.0225       | 0.0225     | 0.8073 | 0.8073 | 0.8073           | 0.8073      | 0.8073 |
| 1.5        | 0.25       | 1.8133 | 1.8133 | 0.0504       | 0.0504     | 0.8059 | 0.8059 | 0.8059           | 0.8059      | 0.8059 |
| 1.5        | 0.333      | 1.8089 | 1.8089 | 0.0891       | 0.0891     | 0.8039 | 0.8039 | 0.8039           | 0.8039      | 0.8039 |
| 1.5        | 0.5        | 1.7962 | 1.7962 | 0.1996       | 0.1996     | 0.7983 | 0.7983 | 0.7983           | 0.7983      | 0.7983 |
| 1.5        | 0.667      | 1.7788 | 1.7788 | 0.3517       | 0.3517     | 0.7906 | 0.7906 | 0.7906           | 0.7906      | 0.7906 |
| 1.5        | 0.75       | 1.7684 | 1.7684 | 0.4421       | 0.4421     | 0.7860 | 0.7860 | 0.7860           | 0.7860      | 0.7860 |
| 1.5        | 0.833      | 1.7570 | 1.7570 | 0.5419       | 0.5419     | 0.7809 | 0.7809 | 0.7809           | 0.7809      | 0.7809 |
| 1.5        | 1.0        | 1.7310 | 1.7310 | 0.7693       | 0.7693     | 0.7693 | 0.7693 | 0.7693           | 0.7693      | 0.7693 |
| 1.5        | 1.25       | 1.6851 | 1.6851 | 1.1702       | 1.1702     | 0.7489 | 0.7489 | 0.7489           | 0.7489      | 0.7489 |
| 1.5        | 1.333      | 1.6682 | 1.6682 | 1.3175       | 1.3175     | 0.7414 | 0.7414 | 0.7414           | 0.7414      | 0.7414 |
| 1.5        | 1.5        | 1.6322 | 1.6322 | 1.6322       | 1.6322     | 0.7254 | 0.7254 | 0.7254           | 0.7254      | 0.7254 |
| 1.5        | 2.0        | 1.5115 | 1.5115 | 2.6870       | 2.6870     | 0.6718 | 0.6718 | 0.6718           | 0.6718      | 0.6718 |
| 1.5        | 2.5        | 1.3802 | 1.3802 | 3.8338       | 3.8338     | 0.6134 | 0.6134 | 0.6134           | 0.6134      | 0.6134 |
| 1.5        | 3.0        | 1.2477 | 1.2477 | 4.9909       | 4.9909     | 0.5545 | 0.5545 | 0.5545           | 0.5545      | 0.5545 |
| 1.5        | 4.0        | 1.0028 | 1.0028 | 7.1307       | 7.1307     | 0.4457 | 0.4457 | 0.4457           | 0.4457      | 0.4457 |
| 1.5        | 6.0        | 0.6424 | 0.6424 | 10.2785      | 10.2785    | 0.2855 | 0.2855 | 0.2855           | 0.2855      | 0.2855 |

Table 30: Scalings of Higgs decay branching ratios vs.  $\kappa_t$  and  $\kappa_V = 1.5$  for the resolved model.

| $\kappa_V$ | $\kappa_t$ | ttHWW  | ttHZZ  | ttH $\tau\tau$ | tHqWW  | tHqZZ  | tHq $\tau\tau$ | tHWWW  | tHWZZ  | tHW $\tau\tau$ |
|------------|------------|--------|--------|----------------|--------|--------|----------------|--------|--------|----------------|
| 0.5        | -6.0       | 2.9775 | 2.9775 | 428.7530       | 9.2066 | 9.2066 | 1325.7460      | 9.7660 | 9.7660 | 1406.3049      |
| 0.5        | -4.0       | 2.2675 | 2.2675 | 145.1182       | 7.5740 | 7.5740 | 484.7357       | 7.8819 | 7.8819 | 504.4411       |
| 0.5        | -3.0       | 1.7000 | 1.7000 | 61.1988        | 6.1214 | 6.1214 | 220.3702       | 6.2562 | 6.2562 | 225.2227       |
| 0.5        | -2.5       | 1.3581 | 1.3581 | 33.9529        | 5.1857 | 5.1857 | 129.6430       | 5.2277 | 5.2277 | 130.6931       |
| 0.5        | -2.0       | 0.9912 | 0.9912 | 15.8589        | 4.1227 | 4.1227 | 65.9633        | 4.0762 | 4.0762 | 65.2197        |
| 0.5        | -1.5       | 0.6259 | 0.6259 | 5.6327         | 2.9838 | 2.9838 | 26.8544        | 2.8645 | 2.8645 | 25.7805        |
| 0.5        | -1.333     | 0.5112 | 0.5112 | 3.6333         | 2.6025 | 2.6025 | 18.4974        | 2.4648 | 2.4648 | 17.5190        |
| 0.5        | -1.25      | 0.4566 | 0.4566 | 2.8538         | 2.4154 | 2.4154 | 15.0962        | 2.2700 | 2.2700 | 14.1878        |
| 0.5        | -1.0       | 0.3048 | 0.3048 | 1.2194         | 1.8696 | 1.8696 | 7.4784         | 1.7078 | 1.7078 | 6.8310         |
| 0.5        | -0.833     | 0.2166 | 0.2166 | 0.6012         | 1.5271 | 1.5271 | 4.2386         | 1.3605 | 1.3605 | 3.7760         |
| 0.5        | -0.75      | 0.1774 | 0.1774 | 0.3992         | 1.3657 | 1.3657 | 3.0729         | 1.1987 | 1.1987 | 2.6970         |
| 0.5        | -0.667     | 0.1417 | 0.1417 | 0.2521         | 1.2111 | 1.2111 | 2.1553         | 1.0451 | 1.0451 | 1.8598         |
| 0.5        | -0.5       | 0.0809 | 0.0809 | 0.0809         | 0.9236 | 0.9236 | 0.9236         | 0.7640 | 0.7640 | 0.7640         |
| 0.5        | -0.333     | 0.0363 | 0.0363 | 0.0161         | 0.6720 | 0.6720 | 0.2981         | 0.5249 | 0.5249 | 0.2328         |
| 0.5        | -0.25      | 0.0205 | 0.0205 | 0.0051         | 0.5618 | 0.5618 | 0.1405         | 0.4231 | 0.4231 | 0.1058         |
| 0.5        | -0.167     | 0.0092 | 0.0092 | 0.0010         | 0.4622 | 0.4622 | 0.0516         | 0.3334 | 0.3334 | 0.0372         |
| 0.5        | 0.0        | 0.0000 | 0.0000 | 0.0000         | 0.2953 | 0.2953 | 0.0000         | 0.1909 | 0.1909 | 0.0000         |
| 0.5        | 0.167      | 0.0092 | 0.0092 | 0.0010         | 0.1755 | 0.1755 | 0.0196         | 0.1010 | 0.1010 | 0.0113         |
| 0.5        | 0.25       | 0.0205 | 0.0205 | 0.0051         | 0.1339 | 0.1339 | 0.0335         | 0.0762 | 0.0762 | 0.0191         |
| 0.5        | 0.333      | 0.0363 | 0.0363 | 0.0161         | 0.1043 | 0.1043 | 0.0463         | 0.0647 | 0.0647 | 0.0287         |
| 0.5        | 0.5        | 0.0809 | 0.0809 | 0.0809         | 0.0809 | 0.0809 | 0.0809         | 0.0809 | 0.0809 | 0.0809         |
| 0.5        | 0.667      | 0.1417 | 0.1417 | 0.2521         | 0.1044 | 0.1044 | 0.1859         | 0.1480 | 0.1480 | 0.2634         |
| 0.5        | 0.75       | 0.1774 | 0.1774 | 0.3992         | 0.1329 | 0.1329 | 0.2991         | 0.1993 | 0.1993 | 0.4485         |
| 0.5        | 0.833      | 0.2166 | 0.2166 | 0.6012         | 0.1720 | 0.1720 | 0.4775         | 0.2620 | 0.2620 | 0.7272         |
| 0.5        | 1.0        | 0.3048 | 0.3048 | 1.2194         | 0.2811 | 0.2811 | 1.1243         | 0.4200 | 0.4200 | 1.6801         |
| 0.5        | 1.25       | 0.4566 | 0.4566 | 2.8538         | 0.5119 | 0.5119 | 3.1993         | 0.7270 | 0.7270 | 4.5438         |
| 0.5        | 1.333      | 0.5112 | 0.5112 | 3.6333         | 0.6041 | 0.6041 | 4.2939         | 0.8449 | 0.8449 | 6.0051         |
| 0.5        | 1.5        | 0.6259 | 0.6259 | 5.6327         | 0.8096 | 0.8096 | 7.2863         | 1.1020 | 1.1020 | 9.9179         |
| 0.5        | 2.0        | 0.9912 | 0.9912 | 15.8589        | 1.5402 | 1.5402 | 24.6428        | 1.9827 | 1.9827 | 31.7238        |
| 0.5        | 2.5        | 1.3581 | 1.3581 | 33.9529        | 2.3549 | 2.3549 | 58.8716        | 2.9329 | 2.9329 | 73.3233        |
| 0.5        | 3.0        | 1.7000 | 1.7000 | 61.1988        | 3.1686 | 3.1686 | 114.0678       | 3.8625 | 3.8625 | 139.0502       |
| 0.5        | 4.0        | 2.2675 | 2.2675 | 145.1182       | 4.6200 | 4.6200 | 295.6829       | 5.4873 | 5.4873 | 351.1881       |
| 0.5        | 6.0        | 2.9775 | 2.9775 | 428.7530       | 6.6207 | 6.6207 | 953.3740       | 7.6698 | 7.6698 | 1104.4467      |

Table 31: Scalings of cross section times BR for the resolved model, for the different  $t\bar{t}H$ ,  $tHq$ ,  $tHW$  signal components and  $\kappa_V = 0.5$ .

| $\kappa_V$ | $\kappa_t$ | ttHWW   | ttHZZ   | ttH $\tau\tau$ | tHqWW   | tHqZZ   | tHq $\tau\tau$ | tHWWW   | tHWZZ   | tHW $\tau\tau$ |
|------------|------------|---------|---------|----------------|---------|---------|----------------|---------|---------|----------------|
| 1.0        | -6.0       | 11.2408 | 11.2408 | 404.6686       | 40.4768 | 40.4768 | 1457.1666      | 41.3681 | 41.3681 | 1489.2533      |
| 1.0        | -4.0       | 8.2305  | 8.2305  | 131.6886       | 34.2339 | 34.2339 | 547.7422       | 33.8480 | 33.8480 | 541.5676       |
| 1.0        | -3.0       | 5.9862  | 5.9862  | 53.8759        | 28.5396 | 28.5396 | 256.8562       | 27.3983 | 27.3983 | 246.5850       |
| 1.0        | -2.5       | 4.6979  | 4.6979  | 29.3616        | 24.8511 | 24.8511 | 155.3195       | 23.3557 | 23.3557 | 145.9734       |
| 1.0        | -2.0       | 3.3647  | 3.3647  | 13.4590        | 20.6360 | 20.6360 | 82.5440        | 18.8497 | 18.8497 | 75.3987        |
| 1.0        | -1.5       | 2.0859  | 2.0859  | 4.6933         | 16.0557 | 16.0557 | 36.1254        | 14.0919 | 14.0919 | 31.7068        |
| 1.0        | -1.333     | 1.6941  | 1.6941  | 3.0102         | 14.4942 | 14.4942 | 25.7545        | 12.5059 | 12.5059 | 22.2216        |
| 1.0        | -1.25      | 1.5091  | 1.5091  | 2.3579         | 13.7201 | 13.7201 | 21.4377        | 11.7273 | 11.7273 | 18.3239        |
| 1.0        | -1.0       | 1.0000  | 1.0000  | 1.0000         | 11.4220 | 11.4220 | 11.4220        | 9.4484  | 9.4484  | 9.4484         |
| 1.0        | -0.833     | 0.7075  | 0.7075  | 0.4909         | 9.9372  | 9.9372  | 6.8953         | 8.0059  | 8.0059  | 5.5552         |
| 1.0        | -0.75      | 0.5784  | 0.5784  | 0.3254         | 9.2212  | 9.2212  | 5.1869         | 7.3200  | 7.3200  | 4.1175         |
| 1.0        | -0.667     | 0.4610  | 0.4610  | 0.2051         | 8.5229  | 8.5229  | 3.7917         | 6.6579  | 6.6579  | 2.9620         |
| 1.0        | -0.5       | 0.2624  | 0.2624  | 0.0656         | 7.1807  | 7.1807  | 1.7952         | 5.4076  | 5.4076  | 1.3519         |
| 1.0        | -0.333     | 0.1175  | 0.1175  | 0.0130         | 5.9375  | 5.9375  | 0.6584         | 4.2814  | 4.2814  | 0.4748         |
| 1.0        | -0.25      | 0.0664  | 0.0664  | 0.0042         | 5.3616  | 5.3616  | 0.3351         | 3.7730  | 3.7730  | 0.2358         |
| 1.0        | -0.167     | 0.0297  | 0.0297  | 0.0008         | 4.8163  | 4.8163  | 0.1343         | 3.3009  | 3.3009  | 0.0921         |
| 1.0        | 0.0        | 0.0000  | 0.0000  | 0.0000         | 3.8183  | 3.8183  | 0.0000         | 2.4676  | 2.4676  | 0.0000         |
| 1.0        | 0.167      | 0.0297  | 0.0297  | 0.0008         | 2.9624  | 2.9624  | 0.0826         | 1.7981  | 1.7981  | 0.0501         |
| 1.0        | 0.25       | 0.0664  | 0.0664  | 0.0042         | 2.5928  | 2.5928  | 0.1620         | 1.5284  | 1.5284  | 0.0955         |
| 1.0        | 0.333      | 0.1175  | 0.1175  | 0.0130         | 2.2612  | 2.2612  | 0.2507         | 1.3014  | 1.3014  | 0.1443         |
| 1.0        | 0.5        | 0.2624  | 0.2624  | 0.0656         | 1.7115  | 1.7115  | 0.4279         | 0.9742  | 0.9742  | 0.2435         |
| 1.0        | 0.667      | 0.4610  | 0.4610  | 0.2051         | 1.3198  | 1.3198  | 0.5871         | 0.8188  | 0.8188  | 0.3643         |
| 1.0        | 0.75       | 0.5784  | 0.5784  | 0.3254         | 1.1834  | 1.1834  | 0.6657         | 0.8042  | 0.8042  | 0.4524         |
| 1.0        | 0.833      | 0.7075  | 0.7075  | 0.4909         | 1.0852  | 1.0852  | 0.7530         | 0.8301  | 0.8301  | 0.5760         |
| 1.0        | 1.0        | 1.0000  | 1.0000  | 1.0000         | 1.0000  | 1.0000  | 1.0000         | 1.0000  | 1.0000  | 1.0000         |
| 1.0        | 1.25       | 1.5091  | 1.5091  | 2.3579         | 1.1380  | 1.1380  | 1.7782         | 1.5278  | 1.5278  | 2.3872         |
| 1.0        | 1.333      | 1.6941  | 1.6941  | 3.0102         | 1.2492  | 1.2492  | 2.2197         | 1.7691  | 1.7691  | 3.1434         |
| 1.0        | 1.5        | 2.0859  | 2.0859  | 4.6933         | 1.5628  | 1.5628  | 3.5163         | 2.3434  | 2.3434  | 5.2727         |
| 1.0        | 2.0        | 3.3647  | 3.3647  | 13.4590        | 3.1023  | 3.1023  | 12.4092        | 4.6362  | 4.6362  | 18.5449        |
| 1.0        | 2.5        | 4.6979  | 4.6979  | 29.3616        | 5.2667  | 5.2667  | 32.9167        | 7.4799  | 7.4799  | 46.7493        |
| 1.0        | 3.0        | 5.9862  | 5.9862  | 53.8759        | 7.7435  | 7.7435  | 69.6914        | 10.5403 | 10.5403 | 94.8625        |
| 1.0        | 4.0        | 8.2305  | 8.2305  | 131.6886       | 12.7892 | 12.7892 | 204.6276       | 16.4642 | 16.4642 | 263.4266       |
| 1.0        | 6.0        | 11.2408 | 11.2408 | 404.6686       | 20.9516 | 20.9516 | 754.2573       | 25.5403 | 25.5403 | 919.4497       |

Table 32: Scalings of cross section times BR for the resolved model, for the different  $t\bar{t}H$ , tHq, tHW signal components and  $\kappa_V = 1.0$ .

| $\kappa_V$ | $\kappa_t$ | ttHWW   | ttHZZ   | ttH $\tau\tau$ | tHqWW   | tHqZZ   | tHq $\tau\tau$ | tHWWW   | tHWZZ   | tHW $\tau\tau$ |
|------------|------------|---------|---------|----------------|---------|---------|----------------|---------|---------|----------------|
| 1.5        | -6.0       | 23.1266 | 23.1266 | 370.0260       | 96.1923 | 96.1923 | 1539.0768      | 95.1080 | 95.1080 | 1521.7272      |
| 1.5        | -4.0       | 16.0441 | 16.0441 | 114.0913       | 81.6690 | 81.6690 | 580.7570       | 77.3512 | 77.3512 | 550.0531       |
| 1.5        | -3.0       | 11.2295 | 11.2295 | 44.9178        | 68.8703 | 68.8703 | 275.4812       | 62.9086 | 62.9086 | 251.6344       |
| 1.5        | -2.5       | 8.6261  | 8.6261  | 23.9614        | 60.7939 | 60.7939 | 168.8720       | 54.1622 | 54.1622 | 150.4505       |
| 1.5        | -2.0       | 6.0458  | 6.0458  | 10.7481        | 51.7152 | 51.7152 | 91.9381        | 44.6227 | 44.6227 | 79.3293        |
| 1.5        | -1.5       | 3.6725  | 3.6725  | 3.6725         | 41.9469 | 41.9469 | 41.9469        | 34.6991 | 34.6991 | 34.6991        |
| 1.5        | -1.333     | 2.9643  | 2.9643  | 2.3410         | 38.6171 | 38.6171 | 30.4971        | 31.4016 | 31.4016 | 24.7987        |
| 1.5        | -1.25      | 2.6330  | 2.6330  | 1.8284         | 36.9629 | 36.9629 | 25.6687        | 29.7807 | 29.7807 | 20.6810        |
| 1.5        | -1.0       | 1.7310  | 1.7310  | 0.7693         | 32.0233 | 32.0233 | 14.2326        | 25.0144 | 25.0144 | 11.1175        |
| 1.5        | -0.833     | 1.2192  | 1.2192  | 0.3760         | 28.7953 | 28.7953 | 8.8803         | 21.9653 | 21.9653 | 6.7740         |
| 1.5        | -0.75      | 0.9948  | 0.9948  | 0.2487         | 27.2234 | 27.2234 | 6.8058         | 20.5014 | 20.5014 | 5.1254         |
| 1.5        | -0.667     | 0.7914  | 0.7914  | 0.1565         | 25.6778 | 25.6778 | 5.0772         | 19.0767 | 19.0767 | 3.7720         |
| 1.5        | -0.5       | 0.4491  | 0.4491  | 0.0499         | 22.6628 | 22.6628 | 2.5181         | 16.3435 | 16.3435 | 1.8159         |
| 1.5        | -0.333     | 0.2006  | 0.2006  | 0.0099         | 19.7986 | 19.7986 | 0.9758         | 13.8117 | 13.8117 | 0.6807         |
| 1.5        | -0.25      | 0.1133  | 0.1133  | 0.0031         | 18.4397 | 18.4397 | 0.5122         | 12.6364 | 12.6364 | 0.3510         |
| 1.5        | -0.167     | 0.0507  | 0.0507  | 0.0006         | 17.1281 | 17.1281 | 0.2123         | 11.5203 | 11.5203 | 0.1428         |
| 1.5        | 0.0        | 0.0000  | 0.0000  | 0.0000         | 14.6443 | 14.6443 | 0.0000         | 9.4640  | 9.4640  | 0.0000         |
| 1.5        | 0.167      | 0.0507  | 0.0507  | 0.0006         | 12.3858 | 12.3858 | 0.1535         | 7.6760  | 7.6760  | 0.0951         |
| 1.5        | 0.25       | 0.1133  | 0.1133  | 0.0031         | 11.3529 | 11.3529 | 0.3154         | 6.8916  | 6.8916  | 0.1914         |
| 1.5        | 0.333      | 0.2006  | 0.2006  | 0.0099         | 10.3820 | 10.3820 | 0.5117         | 6.1783  | 6.1783  | 0.3045         |
| 1.5        | 0.5        | 0.4491  | 0.4491  | 0.0499         | 8.6227  | 8.6227  | 0.9581         | 4.9621  | 4.9621  | 0.5513         |
| 1.5        | 0.667      | 0.7914  | 0.7914  | 0.1565         | 7.1299  | 7.1299  | 1.4098         | 4.0411  | 4.0411  | 0.7990         |
| 1.5        | 0.75       | 0.9948  | 0.9948  | 0.2487         | 6.4888  | 6.4888  | 1.6222         | 3.6932  | 3.6932  | 0.9233         |
| 1.5        | 0.833      | 1.2192  | 1.2192  | 0.3760         | 5.9148  | 5.9148  | 1.8241         | 3.4176  | 3.4176  | 1.0540         |
| 1.5        | 1.0        | 1.7310  | 1.7310  | 0.7693         | 4.9627  | 4.9627  | 2.2057         | 3.0782  | 3.0782  | 1.3681         |
| 1.5        | 1.25       | 2.6330  | 2.6330  | 1.8284         | 4.0340  | 4.0340  | 2.8014         | 3.0873  | 3.0873  | 2.1440         |
| 1.5        | 1.333      | 2.9643  | 2.9643  | 2.3410         | 3.8531  | 3.8531  | 3.0429         | 3.2206  | 3.2206  | 2.5434         |
| 1.5        | 1.5        | 3.6725  | 3.6725  | 3.6725         | 3.6725  | 3.6725  | 3.6725         | 3.6725  | 3.6725  | 3.6725         |
| 1.5        | 2.0        | 6.0458  | 6.0458  | 10.7481        | 4.4580  | 4.4580  | 7.9254         | 6.3144  | 6.3144  | 11.2255        |
| 1.5        | 2.5        | 8.6261  | 8.6261  | 23.9614        | 6.8533  | 6.8533  | 19.0368        | 10.4359 | 10.4359 | 28.9887        |
| 1.5        | 3.0        | 11.2295 | 11.2295 | 44.9178        | 10.3536 | 10.3536 | 41.4143        | 15.4728 | 15.4728 | 61.8913        |
| 1.5        | 4.0        | 16.0441 | 16.0441 | 114.0913       | 18.9646 | 18.9646 | 134.8595       | 26.5208 | 26.5208 | 188.5926       |
| 1.5        | 6.0        | 23.1266 | 23.1266 | 370.0260       | 35.9359 | 35.9359 | 574.9741       | 46.2619 | 46.2619 | 740.1909       |

Table 33: Scalings of cross section times BR for the resolved model, for the different ttH, tHq, tHW signal components and  $\kappa_V = 1.5$ .

## E tHq-ttH overlap

This section provides a quick overview of the differences and commonalities in event selections between this analysis and the ttH multilepton search [6]. The object selections of the two analysis are perfectly synchronized due to shared frameworks and ROOT trees. The only exception is the usage of forward jets ( $|\eta| > 2.4, p_T > 40 \text{ GeV}$ ) in this analysis. Such jets are not considered in the ttH analysis.

Table 34 gives an overview of the main differences in the event selections. Here,  $E_T^{\text{miss, LD}}$  is defined as  $E_T^{\text{miss}} \times 0.00397 + H_T^{\text{miss}} \times 0.00265$ . Un-tagged jets in the tHq analysis are jets that do not pass the CSV loose working point and are either central ( $|\eta| < 2.4, p_T > 25 \text{ GeV}$ ) or forward ( $|\eta| < 2.4, p_T > 40 \text{ GeV}$ ). All jets in the ttH analysis are selected with  $p_T > 25 \text{ GeV}$ . Lepton  $p_T$  cuts and the trigger selections are identical.

| Channel | tHq   | ttH  |
|---------|---|--|
| 3l      | Z veto, 15 GeV<br>$N_{\text{jets}}^{\text{b, med.}} \geq 1$<br>$\geq 1$ un-tagged jet | Z veto, 10 GeV<br>$N_{\text{jets}}^{\text{b, med.}} \geq 1$ OR $N_{\text{jets}}^{\text{b, loose}} \geq 2$<br>$E_T^{\text{miss, LD}} > 0.2$ OR $N_{\text{jets}}^{\text{central.}} \geq 4$ |
|         | $N_{\text{jets}}^{\text{b, med.}} \geq 1$<br>$\geq 1$ un-tagged jet                   | $N_{\text{jets}}^{\text{b, med.}} \geq 1$ OR $N_{\text{jets}}^{\text{b, loose}} \geq 2$<br>$N_{\text{jets}}^{\text{central}} \geq 4$   |
| 2lss    | $N_{\text{jets}}^{\text{b, med.}} \geq 1$<br>$\geq 1$ un-tagged jet                   | $N_{\text{jets}}^{\text{b, med.}} \geq 1$ OR $N_{\text{jets}}^{\text{b, loose}} \geq 2$<br>$N_{\text{jets}}^{\text{central}} \geq 4$   |
|         |   |  |

Table 34: Differences in event selection between this analysis and the ttH multilepton analysis.

Table 35 shows the total events yields in the individual channels, and the yield of shared events between each channel, for the tHq signal sample, the ttH signal sample, and the data. In the data, for the three lepton channel, about 80% of events passing the tHq selection also pass the ttH selection, constituting about 70% of that channel. In the same-sign dilepton channel, about 50% of data events passing the tHq selection also pass the ttH selection, but these events constitute almost 90% of the ttH selection in those channels. Similar overlaps are also seen in the tHq and ttH signal samples.

There is no migration between different channels and different selections, i.e. no events passing the selection of a given tHq channel pass the selection of any other channels of ttH and vice versa.

| <b>tHq sample</b> | tHq   | ttH  | Common | (% tHq) | (% ttH) |
|-------------------|-------|------|--------|---------|---------|
| $\mu^\pm\mu^\pm$  | 7400  | 2353 | 2166   | 29.3    | 92.1    |
| $e^\pm\mu^\pm$    | 11158 | 3600 | 3321   | 29.8    | 92.2    |
| $e^\pm e^\pm$     | 3550  | 1106 | 1025   | 28.9    | 92.7    |
| $\ell\ell\ell$    | 3115  | 2923 | 2347   | 75.3    | 80.3    |

| <b>ttH sample</b> | tHq   | ttH   | Common | (% tHq) | (% ttH) |
|-------------------|-------|-------|--------|---------|---------|
| $\mu^\pm\mu^\pm$  | 32612 | 28703 | 26547  | 81.4    | 92.5    |
| $e^\pm\mu^\pm$    | 48088 | 42521 | 39164  | 81.4    | 92.1    |
| $e^\pm e^\pm$     | 15476 | 12869 | 11896  | 76.9    | 92.4    |
| $\ell\ell\ell$    | 26627 | 30598 | 25288  | 95.0    | 82.6    |

| <b>Data</b>      | tHq | ttH | Common | (% tHq) | (% ttH) |
|------------------|-----|-----|--------|---------|---------|
| $\mu^\pm\mu^\pm$ | 280 | 160 | 140    | 50.0    | 87.5    |
| $e^\pm\mu^\pm$   | 525 | 280 | 242    | 46.1    | 86.4    |
| $e^\pm e^\pm$    | 208 | 90  | 79     | 38.0    | 87.8    |
| $\ell\ell\ell$   | 126 | 154 | 104    | 82.5    | 67.5    |

Table 35: Individual and shared event yields between this analysis (tHq) and ttH multilepton selections.

## References

- [1] CMS Collaboration, "Search for the associated production of a Higgs boson with a single top quark in proton-proton collisions at  $\sqrt{s} = 8$  TeV", *JHEP* **06** (2016) 177, doi:10.1007/JHEP06(2016)177, arXiv:1509.08159.
- [2] B. Stieger, C. Jorda Lope et al., "Search for Associated Production of a Single Top Quark and a Higgs Boson in Leptonic Channels", CMS Analysis Note CMS AN-14-140, 2014.
- [3] M. Peruzzi, C. Mueller, B. Stieger et al., "Search for  $t\bar{t}H$  in multilepton final states at 13 TeV", CMS Analysis Note CMS AN-16-211, 2016.
- [4] CMS Collaboration, "Search for H to bbar in association with a single top quark as a test of Higgs boson couplings at 13 TeV", CMS Physics Analysis Summary CMS-PAS-HIG-16-019, 2016.
- [5] B. Maier, "SingleTopHiggProduction13TeV", February, 2016. <https://twiki.cern.ch/twiki/bin/viewauth/CMS/SingleTopHiggsGeneration13TeV>.
- [6] M. Peruzzi, F. Romeo, B. Stieger et al., "Search for  $t\bar{t}H$  in multilepton final1 states at 13 TeV", CMS Analysis Note CMS AN-17-029, 2017.
- [7] B. WG, "BtagRecommendation80XReReco", February, 2017. <https://twiki.cern.ch/twiki/bin/view/CMS/BtagRecommendation80XReReco>.